ANALYTICAL AND EXPERIMENTAL STUDY OF THE TRANSIENT BASE PRESSURES RESULTING WHEN AN AXI-SYMMETRIC SUPERSONIC MISSILE FLIES HEAD-ON THROUGH A BLAST WAVE

By
HOMER HO TANG
Bachelor of Science
Taiwan Provincial Cheng-Kung University
Tainan, Taiwan, Free China
June, 1956

Master of Science
Oklahoma State University
Stillwater, Oklahoma
August, 1961

Submitted to the Faculty of the Graduate School of
the Oklahoma State University
in partial fulfillment of the requirements
for the degree of
DOCTOR OF PHILOSOPHY
May, 1964

ANALYTICAL AND EXPERIMENTAL STUDY OF THE TRANSIENT BASE PRESSURES RESULTING WHEN AN AXI-SYMMETRIC SUPERSONIC MISSILE FLIES HEAD-ON THROUGH A BLAST WAVE

Thesis Approved:

G. W. Zumwalt
Thesis Adviser

J. A. Wiebelt

O. H. Hamilton

Ladislaus J. Fila

J. H. Boggs
Dean of the Graduate School

PREFACE

Sincere appreciation is expressed to Dr. Glen W. Zumwalt, Associate Professor of Aerospace Engineering at Oklahoma State University, as my thesis adviser, research supervisor, and instructor. I am indebted to him for giving me a great deal of his time and effort to direct my study. Without him, this work could not have been done.

The educational opportunity and guidance provided by Dr. J. H. Boggs, Head of the School of Mechanical Engineering and the instructive assistance of my Ph.D. committee members, Professor L. J. Fila, Dr. O. H. Hamilton, Dr. M. K. Jovanovic and Dr. J. A. Wiebelt contributed to the success of the whole program. I give them my heartfelt gratitude.

Thanks is also extended to the Sandia Corporation, and especially Mr. H. R. Vaughn, for sponsoring a research project at Oklahoma State University from 1960 to 1964. The major portion of the experimental work was carried out by Mr. E. J. Meyer and Mr. J. F. Reed of Sandia's Experimental Aerodynamics Division. Their efforts and skill are greatly appreciated.

The information on jet spreading parameter provided by Mr. R. C. Maydew of Sandia Corporation and Mr. C. C. Chrisman of OSU, the help in computing the auxiliary curves by Mr. K. R. Royer, the aid in investigating the effective pumping surface by Mr. W. J. Young, the proof reading of the manuscript by Mr. W. F. Walker and Mrs. Claudine King, have contributed in one way or another to the completion of this dissertation.

I wish to thank them for their help. The patience and skill of Mrs. Claudine King in typing these long and difficult equations and symbols are particularly acknowledged.

To my parents, who have supplied me hope and faith for a long time, I acknowledge my indebtedness.

Finally, my special thanks goes to my wife, May Shu-I, whose encouragement, constant care for our infant son, and willingness to delay her own graduate study, made the writing of this thesis possible.

TABLE OF CONTENTS

LIST OF FIGURES

Figure Page

LIST OF TABLES

LIST OF SYMBOLS

A	Area
a	Velocity of sound
B	Dimensionless group defined on page 13
b	A separation variable defined on page 80
C	Crocco number $= \frac{u}{u_{max}} = \left(\frac{M^2}{\frac{2}{k-1} + M^2} \right)^{\frac{1}{2}}$
C_p	Pressure coefficient
c	A constant in the eddy viscosity expression
erf	Error function; erf $\eta = \frac{2}{\sqrt{\pi}} \int_0^{\eta} e^{-\beta^2} d\beta$
F_x	Field forces in x direction
f( )	Function of some variables
G_d	Mass rate per unit base area added to the dead-air region by a jet mixing stream
g	Gravitational constant
I_1	Integral associated with mass transport for plane flow (defined on page 13)
I_2	Integral associated with momentum transport for plane flow (defined on page 14)
J_1	Integral associated with mass transport for axi-symmetric flow (defined on page 14)
J_2	Integral associated with momentum transport for axi-symmetric flow (defined on page 14)
K	A constant defined on page 82
K	A parameter defined on page 18

k	Ratio of specific heats
ΔL	Elemental length on a circular cylinder
ℓ	Length of jet mixing layer in the axial direction (page 30), or $\ell(\xi)$ defined on page 80
ℓn	Napierian logarithmic value
M	Mach number
m	Mass in the base region
$\dot{m}$	Mass bleeding rate to or from the base region
n	Exponent of velocity profile within boundary layer (page 87)
p	Absolute pressure
Q	An integral defined on page 81
R	Radius of body
$\bar{R}$	Radius of the reference system of coordinates in axi-symmetric flow
$\mathbb{R}$	Reference streamline near but outside the mixing region
$\mathfrak{R}$	Gas Constant
r	Axi-symmetric radial coordinate
T	Absolute temperature
t	Time
t^+	Positive over-pressure time for a blast wave (page 29)
u	Velocity in x or X direction
V	Volume of the dead-air region
v	Velocity in y or Y direction
x, y	Coordinates of the intrinsic (viscous) coordinate system
X, Y	Coordinates of the reference (inviscid) coordinate system
y_o	Defined on page 86
y_T	Defined on page 86
y'	Defined on page 86

β	Variable in error function; or stagnation temperature ratio, page 56
γ	Compressible divergence factor (page 85)
Δ	Difference between two quantities
δ	Boundary layer thickness
ϵ	Eddy viscosity
ζ	Dimensionless y-coordinate (page 8)
$\mathcal{K}$	Non-dimensional bleed number (page 19)
$\eta = \sigma \frac{y}{x}$	Dimensionless coordinate for a jet mixing profile
η_p	Position parameter (page 9)
θ	Streamline angle
θ_w	Conical shock wave angle
λ	Separation constant (page 80)
υ	Prandtl-Meyer turning angle
ξ	x-coordinate in the integral transformation (page 9)
ρ	Density
σ	Similarity parameter of the homogeneous coordinate y/x (also called the free jet spreading parameter)
σ_x	Normal stress in x direction
τ_{yx}	Shearing stress in x direction
$\varphi = \frac{u}{u_a}$	Dimensionless velocity
ψ	Dimensionless x-coordinate (page 8)

Subscripts

1, 2, 3, 4	Conditions at cross sections indicated in Figure 2
a	Condition of the flow in the isentropic stream adjacent to the dissipative region

b	Condition at the base of the sudden expansion
c	Condition on cone surface
d	Streamline whose kinetic energy is just sufficient to enter the recompression region
incomp.	Incompressible flow
j	Condition along the jet boundary separating streamline
m	Coordinate shift in the mixing theory due to the momentum integral
max.	Maximum value
noz.	Condition at nozzle exit
o	Stagnation condition or condition at metering orifice
"prime"	Condition in the blast wave transformed plane (page 98), or perturbation terms (page 7), or y' defined on page 86
$\mathbb{R}$	Condition along the $\mathbb{R}$ streamline
s	"Stable solution" of base pressure
sh	Moving shock wave
t	Condition at the time, t
w	Conical shock wave
x	Condition just before the blast wave intersection occurs
y	Condition just after the blast wave intersection has occurred
∞	Freestream condition

CHAPTER I

INTRODUCTION

With the advent of supersonic flight of airplanes, re-entering missiles, and targeting projectiles in the atmosphere, the pressure distribution on flying vehicles under transient conditions has become significant for technological developments, such as for calculation of drag and for designing the guidance system. Also, the base pressure, which is due to the separation of the flow field, is particularly important information for many practical cases, such as the base pressure behind a ram-jet engine, an airfoil, a rocket, or an axi-symmetric body.

In this thesis, the study deals with one specific problem which has shown its significance in the fields of rocketry and missile development. This is the blast wave effect on missile base pressure. The scope of the problem is defined by the following limitations:

1. Supersonic missile speeds, $1.2 \leq M_1 \leq 5$.
2. Plane blast waves approaching the vehicle from axial (front) direction.
3. Slender, axi-symmetric missile configurations.
4. Turbulent flows in the separated boundary layer.
5. Various flight conditions, such as altitudes, semi-apex nose angles, and maximum over-pressures of blast wave, but not including extremes of conditions which would cause dissociation of the air behind an attached conical nose shock.

Since this is a highly transient base pressure problem, the main objectives are to develop methods of computing the sudden pressure

increase occurring as the blast wave passes the base, and the base pressure-time history during the transient period which results from the decaying of the blast wave.

The basic knowledge needed for base pressure calculation is a jet mixing theory with a proper flow model associated. There are several existing mixing theories, such as Korst (1)[1], Chapman (2), Pai (3)(4), Crane (5), etc. Their approaches are different from one another, so the theories differ in their applicable cases. In this thesis, Korst's mixing theory imposed on Zumwalt's (6) conical flow model analysis is chosen, since it meets the conditions imposed, and is discussed briefly in Chapter II.

By reviewing Zumwalt's analysis, it is seen that he evaluated the base pressure only for steady, non-bleed cases. Thus, to take into account mass bleed cases, his analysis should be extended; also a graphical technique may be desirable in order to lessen the mathematical complexities for solving his non-linear integral equation explicitly. The theoretical analyses for steady mass-bleed cases are described in Chapter III, and transient cases in Chapter VI.

Chapters IV and V present the information for experimental verification of steady and transient mass-bleed base pressures, respectively. The detailed discussion is given in Chapter VI for the transient conditions which are generated due to a passing blast wave on an axi-symmetric missile.

Various detailed computing procedures and supporting information are included in Appendices, Figures, and Tables. Finally, a summary

---

[1] Refers to Selected Bibliography.

of conclusions and suggestions for continuing investigations are given in Chapter VII.

CHAPTER II

KORST'S MIXING THEORY AND ZUMWALT'S CONICAL FLOW MODEL ANALYSIS

In separated flows, any analytical method must consist of two parts. One part is a flow model, the other is a jet mixing theory. Jet mixing occurs due to fluid viscosity, either as a laminar or a turbulent mixing layer. The jet may be one high velocity gas which is immersed externally into a quiescent gas, or two gases differing in fluid properties and flow conditions mixed internally inside, as in a ram-jet engine, or two gases differing in fluid properties and flow conditions mixed externally to a body.

It has been known that Korst's two-dimensional jet theory, having unusual generality, is not only capable of treating plane jet mixing involving

1. compressible flow,
2. mass transfer across the mixing region,
3. heat transfer across the mixing region,
4. the reattachment of a jet to a wall,
5. the interaction of the jet of differing chemical and thermodynamic properties,
6. influence of the oncoming boundary layer,
7. two-stream mixing,

but also has been successfully extended for axi-symmetric configuration by using Zumwalt's conical flow model analysis. This is the reason the

author has chosen to adapt Zumwalt's model and Korst's mixing theory to develop an analysis for solving axi-symmetric, highly transient, base pressure problems.

The Korst mixing theory and Zumwalt's conical flow model are discussed briefly.

Korst's Mixing Theory

Coordinates

In Figure 1 (a) and (b) are shown inviscid and viscous jets having identical conditions in the flow adjacent to the mixing region. The jet boundary of the "corresponding inviscid jet" forms the coordinate system (X, Y). For the viscous jet mixing region, a second set of coordinates (x, y), the "intrinsic coordinates," are defined. These are aligned with the center of the mixing region, that is, y = 0 at $u = \frac{1}{2} u_{2a}$. Thus,

$$X \cong x$$

$$Y \cong y - y_m(x) \; ; \qquad y_m(0) = 0.$$

The coordinate shift $y_m'(x)$ will be found by the use of the streamwise momentum equation.

Equation of Motion

For plane-flow, the equation of motion in the x direction is

$$\frac{du}{dt} = F_x + \frac{1}{\rho}\frac{\partial \sigma_x}{\partial x} + \frac{1}{\rho}\frac{\partial \tau_{yx}}{\partial y} \qquad [1]$$

where F_x = field forces in x direction

σ_x = normal stress in x direction

τ_{yx} = shearing stress in x direction.

J. Boussinesq (and many others) suggests that the stress terms be expressed as

$$\tau_{yx} = \rho\ \epsilon \left(\frac{\partial v}{\partial x} + \frac{\partial u}{\partial y}\right)$$

$$\sigma_x = -p - \frac{2}{3}\rho\epsilon\left(\frac{\partial u}{\partial x} + \frac{\partial v}{\partial y}\right) + 2\rho\epsilon\frac{\partial u}{\partial x}$$

where ϵ is the apparent kinematic viscosity. (ϵ is independent of y for small wake referent velocity, i.e., $\frac{u_b}{u_a} \to 0$.)

Substituting these:

$$\frac{du}{dt} = F_x + \frac{1}{\rho}\left[-\frac{\partial p}{\partial x} - \frac{2}{3}\frac{\partial(\rho\epsilon)}{\partial x}\left(\frac{\partial u}{\partial x} + \frac{\partial v}{\partial y}\right)\right.$$

$$-\frac{2}{3}\rho\epsilon\left(\frac{\partial^2 u}{\partial x^2} + \frac{\partial^2 v}{\partial y \partial x}\right) + 2\frac{\partial(\rho\epsilon)}{\partial x}\frac{\partial u}{\partial x} + 2\rho\epsilon\frac{\partial^2 u}{\partial x^2}$$

$$\left. + \frac{\partial(\rho\epsilon)}{\partial y}\left(\frac{\partial v}{\partial x} + \frac{\partial u}{\partial y}\right) + \rho\epsilon\left(\frac{\partial^2 v}{\partial x \partial y} + \frac{\partial^2 u}{\partial y^2}\right)\right].$$

Rearranging:

$$\rho\frac{du}{dt} = \rho F_x - \frac{\partial p}{\partial x} + \frac{4}{3}\frac{\partial(\rho\epsilon)}{\partial x}\left(\frac{\partial u}{\partial x} - \frac{1}{2}\frac{\partial v}{\partial y}\right)$$

$$+ \frac{4}{3}\rho\epsilon\frac{\partial}{\partial x}\left(\frac{\partial u}{\partial x} + \frac{1}{4}\frac{\partial v}{\partial y}\right) + \frac{\partial(\rho\epsilon)}{\partial y}\left(\frac{\partial v}{\partial x} + \frac{\partial u}{\partial y}\right) + \rho\epsilon\frac{\partial^2 u}{\partial y^2}.$$

Since $u = u(x, y, t)$, $du \equiv \frac{\partial u}{\partial x}dx + \frac{\partial u}{\partial y}dy + \frac{\partial u}{\partial t}dt$.

Thus, for the left side of the equation of motion, dividing the du equation by dt gives:

$$\frac{du}{dt} = u\frac{\partial u}{\partial x} + v\frac{\partial u}{\partial y} + \frac{\partial u}{\partial t}.$$

Simplifications

Simplifications which are applicable to the jet mixing region are:

1. steady flow: $\frac{\partial u}{\partial t} = 0$
2. constant pressure: $\frac{\partial p}{\partial x} = 0$
3. negligible field forces: $F_x = 0$
4. $\frac{\partial v}{\partial x} \ll \frac{\partial u}{\partial y}$
5. $\frac{\partial v}{\partial y} \ll \frac{\partial u}{\partial x}$.

The equation of motion now becomes:

$$\rho\left(u\frac{\partial u}{\partial x} + v\frac{\partial u}{\partial y}\right) = \frac{4}{3}\frac{\partial(\rho\epsilon)}{\partial x}\frac{\partial u}{\partial x} + \frac{4}{3}\rho\epsilon\frac{\partial^2 u}{\partial x^2} + \frac{\partial(\rho\epsilon)}{\partial y}\frac{\partial u}{\partial y} + \rho\epsilon\frac{\partial^2 u}{\partial y^2} .$$

Another simplification is generally justifiable:

$$\rho\epsilon\frac{\partial^2 u}{\partial y^2} \gg \left[\frac{4}{3}\frac{\partial(\rho\epsilon)}{\partial x}\frac{\partial u}{\partial x} + \frac{4}{3}\rho\epsilon\frac{\partial^2 u}{\partial x^2} + \frac{\partial(\rho\epsilon)}{\partial y}\frac{\partial u}{\partial y}\right].$$

With this inserted:

$$u\frac{\partial u}{\partial x} + v\frac{\partial u}{\partial y} = \epsilon\frac{\partial^2 u}{\partial y^2} .$$

Following the method of S. I. Pai, the velocities can be written in terms of the free-stream velocity plus perturbations u' and v',

$$u = u_{2a} + u' \quad ; \quad \frac{\partial u}{\partial(\ )} = \frac{\partial u'}{\partial(\ )} \quad ; \quad v = v'$$

$$u'\frac{\partial u}{\partial x} + v\frac{\partial u}{\partial y} = \epsilon\frac{\partial^2 u}{\partial y^2} - u_{2a}\frac{\partial u}{\partial x}$$

$$\frac{u'}{u_{2a}}\frac{\partial u}{\partial x} + \frac{v}{u_{2a}}\frac{\partial u}{\partial y} = \frac{\epsilon}{u_{2a}}\frac{\partial^2 u}{\partial y^2} - \frac{\partial u}{\partial x} .$$

In this equation, all terms are equal to zero at y = 0, and approach zero for a y approaching either positive or negative infinity. On the left hand side of the equation, the first term is very small except for moderate negative values of y, and the second term is very small except for both positive and negative moderate values of y. On the right hand side of the equation, the first term is large for both moderate positive and negative values of y. By this reasoning, it can now be shown that the left side of this equation is much smaller than the right (absolute values) for most values of y, giving, finally:

$$\frac{\partial u}{\partial x} = \frac{\varepsilon}{u_{2a}} \frac{\partial^2 u}{\partial y^2} \qquad [2]$$

The two neglected terms are of most significance at moderate values of -y. These terms then have the same signs (positive), and would increase the absolute value of the left side of the above equation. Omitting these terms will, therefore, be expected to underestimate the velocity for these y values. Comparison with experiment verifies this deviation (7).

Transformation

Introducing dimensionless variables for Equation 2

$$\varphi = \frac{u}{u_{2a}}, \qquad \psi = \frac{x}{\delta_2}, \qquad \zeta = \frac{y}{\delta_2}$$

where δ_2 is the thickness of the mixing region at section 2, one obtains

$$\frac{\partial \varphi}{\partial \psi} = \frac{\varepsilon}{u_{2a}\delta_2} \frac{\partial^2 \varphi}{\partial \zeta^2} . \qquad [3]$$

The functional relation for the variation of ϵ with x for jet mixing is, according to H. Görtler (8), $\epsilon \cong u_{2a}x$, if a semi-infinite uniform stream mixes with a quiesent fluid. Then, $\epsilon = c\, u_{2a}x = c\, u_{2a}\psi\delta_2$. Equation 3 becomes:

$$\frac{\partial\varphi}{\partial\psi} = c\ \psi\ \frac{\partial^2\varphi}{\partial\zeta^2} \qquad [4]$$

A new variable, ξ, is defined by

$$c\psi = \frac{d\xi}{d\psi}$$

$$\xi \equiv \xi\ (\psi) = c \int_o^{\psi} \psi\ d\psi = \frac{1}{2}\ c\psi^2 . \qquad [5]$$

This transformation simplifies Equation 4 to become:

$$\frac{\partial\varphi}{\partial\xi} = \frac{\partial^2\varphi}{\partial\zeta^2} . \qquad [6]$$

For Equation 6 and the pertinent initial and boundary conditions, the velocity profile solution (see Appendix A for details) is:

$$\varphi = \frac{1}{2}\left[1 + \text{erf}\ (\eta-\eta_p)\right] + \frac{1}{\sqrt{\pi}} \int_{\eta-\eta_p}^{\eta} \left[\varphi_2\left(\frac{\eta-\beta}{\eta_p}\right)\right] e^{-\beta^2}\, d\beta \qquad [7]$$

where

$$\eta_p = \frac{1}{2\sqrt{\xi}}$$

and

$$\eta = \zeta\ \eta_p ,$$

Restriction to Thin Boundary Layers

We may note that for positions far downstream of the separation corner, or for very thin upstream boundary layers,

$$\frac{x}{\delta^2} \to \infty ; \qquad \psi \to \infty ;$$

thus,

$$\xi \to \infty \quad \text{and} \quad \eta_p \to 0.$$

This is called the restriction of the theory for thin approaching boundary layers.

$$\eta = \zeta \eta_p = \zeta \frac{1}{2\sqrt{\xi}} = \frac{1}{\sqrt{2c}\psi} \zeta .$$

$$\eta = \frac{1}{\sqrt{2c}} \frac{\zeta}{\psi} = \frac{1}{\sqrt{2c}} \frac{y}{x}$$

$$\eta = \sigma \frac{y}{x} , \text{ where } \sigma = \frac{1}{\sqrt{2c}} .$$

Also $$\varphi = \tfrac{1}{2} (1 + \operatorname{erf} \eta). \qquad [8]$$

Experimental data verify that the velocity profile for large x becomes "fully developed," i.e., unchanging in shape with further increase in x. The constant σ was suggested by Görtler as a "spreading rate parameter" for the mixing region. It is a function of the compressibility (e.g., Mach number); a detailed discussion is given in Appendix B. Korst (1) expressed the subsequent results with η_p included, i.e., effect of initial boundary layer. But results have generally been obtainable only for $\eta_p = 0$, the fully developed profile. We shall therefore restrict this treatment to these cases.

Zumwalt's Conical Wake Analysis

Flow Model

Korst's theory has been used to obtain the analytical base pressure solutions for most of the important two-dimensional applications with success. But many of the occurrences of base pressures involve axially-symmetrical flows, e.g., flow past a fuselage or a missile having a blunt base; ram-jet engine having an ejector in the tail section; etc. The axi-symmetric effect must be taken into additional consideration. Zumwalt (6) investigated these problems by using a conical flow model (Figure 2) and carefully re-examining the fundamental concepts of Korst and Chapman. He concluded that different treatments must be employed for external and internal axi-symmetric base pressure problems. He showed that the mathematical difficulties of axi-symmetric external jet flow can be avoided by establishing a second reduced, concentric, cylindrical sting added to the base of the body. Basically, the plane jet mixing analysis is superimposed upon an axi-symmetric flow field. Referring to Figure 2, the flow model involves the following components:

1. The use of two-dimensional expansion at the separation corner is satisfactory, unless boundary layer thickness is appreciable.
2. The assumption of constant pressure mixing cannot be maintained, as may be seen from results obtained using that assumption. Instead, the potential flow past a cone is utilized for defining the pressure field impressed on the mixing region.

This conclusion is due to two substantiating types of evidence. One, schlieren pictures from many sources show cone-like streamlines after suddenly-terminated bodies of revolution. And two, E. S. Love (9) measured the pressure in the wake at axial locations and found these to be very similar to the pressures on a cone-tail.

3. The cone, as utilized in 2 above, also serves as the "corresponding inviscid jet boundary." Since a pressure gradient exists along the streamlines, further modification of the flow can be expected. These effects have been evaluated in Chapter III.

4. The use of the error function velocity profile proved advantageous. Area (radius) effects due to axially-symmetric flow are considerable and were determined by analytical means. Some detailed descriptions are presented in the next section, Analysis.

5. The oblique shock recompression was used in calculations in conjunction with the procedures outlined above. Referring to Figure 2, a streamline, j, can be identified which divides the amount of mass passing over the corner at ① from that mass flow entrained by the viscous action of the free jet. A second streamline, d, can be identified which has just sufficient kinetic energy at ③ to penetrate the pressure rise to ④. Streamlines above this one have higher kinetic energies and enter the recompression zone ④ with a remaining velocity. Streamlines below have lower kinetic energies and are unable to escape through the recompression, but are turned back to recirculate in the (nearly)dead-air space. If there is no secondary flow, the conservation of mass in the dead-air region requires that the j and d streamlines be identical.

Agreement with published experimental data (10) on sting-supported cylinders was satisfactory and showed marked improvement over the previous attempts to apply two-dimensional jet mixing theory directly.

Analysis

Defining the coordinate systems in the same way as Korst, Zumwalt added two more considerations in his analysis of the jet mixing region with pressure rise. One, the pressure change along the mixing region is the same as that along a conical surface coinciding with the "corresponding inviscid jet boundary," and the pressure gradient normal to the "corresponding inviscid jet boundary" is zero within, and in the vicinity of, the mixing region. And two, the velocity of the jet adjacent to the mixing region is that which would prevail along the conical "corresponding jet boundary." For plane jet mixing, the continuity

and momentum equations of the intrinsic coordinates are sufficient to locate the j streamline as well as the momentum shift η_m. For axi-symmetric jet mixing, the reference streamline $\eta_{\mathbb{R}}$ is no longer parallel with the inviscid X axis. Thus, an equation is needed to locate the $\mathbb{R}$ streamline. This equation is the continuity equation in inviscid coordinates. Taking into account the axi-symmetric effect, Zumwalt wrote the momentum equation in the axial direction with some geometrical and reference coordinate transformations. He solved this simultaneously with the combined viscous and inviscid continuity equations between the separation corner cross section, section ②, and a downstream flow cross section ③, for the mass passing along the annular stream tube bounded by a streamline j and a streamline $\mathbb{R}$ outside the mixing region. For $\mathbb{R}$, he found $\eta_{\mathbb{R}} = 3$ to be sufficiently large. Finally, he obtained the the following governing equation which allows one to locate the j streamline at the recompression point ③,

$$(B-3)^2 + 2(1-C_{3a}^2)\left[I_1\Big|_{-\infty}^{3} - I_1\Big|_{-\infty}^{\varphi_j}\right]B - 2(1-C_{3a}^2)\left[J_1\Big|_{-\infty}^{3} - J_1\Big|_{-\infty}^{\varphi_j}\right] = \left(\frac{\sigma \bar{R}}{x\cos\theta}\right)_3^2 \qquad [9]$$

where the integral limits refer to η values, and

$$B = \frac{J_1\Big|_{-\infty}^{\varphi_j}\left(1-\frac{C_{3a}}{C_{2a}}\right) J_1\Big|_{-\infty}^{3} - \frac{C_{3a}}{C_{2a}}\left(J_1-J_2\right)\Big|_{-\infty}^{3}}{I_1\Big|_{-\infty}^{\varphi_j}\left(1-\frac{C_{3a}}{C_{2a}}\right) I_1\Big|_{-\infty}^{3} - \frac{C_{3a}}{C_{2a}}\left(I_1-I_2\right)\Big|_{-\infty}^{3} + \frac{k-1}{k}\frac{3}{C_{2a}C_{3a}}\left(1-\frac{p_2}{p_3}\right)} \qquad [10]$$

and

$I_1 = \int_{-\infty}^{\eta} \frac{\varphi\, d\eta}{1-C_{3a}^2\varphi^2}$ mass flux integral for plane jet mixing.

$$I_2 = \int_{-\infty}^{\eta} \frac{\varphi^2 \, d\eta}{1-C_{3a}^2\varphi^2}$$ momentum integral for plane jet mixing.

$$J_1 = \int_{-\infty}^{\eta} \frac{\varphi \, \eta \, d\eta}{1-C_{3a}^2\varphi^2}$$ additional mass flux integral due to axi-symmetric jet mixing.

$$J_2 = \int_{-\infty}^{\eta} \frac{\varphi^2 \eta \, d\eta}{1-C_{3a}^2\varphi^2}$$ additional momentum integral due to axi-symmetric jet mixing.

These four integrals are functions of C_{3a}, and the necessary working curves of these were plotted in Reference 6. The subscript ,a, represents flow adjacent to the mixing region for a base with the conical pressure rise condition. Also, note that $\bar{R}$ is the radius of the mixing region center and thus introduces the axi-symmetric aspect into the solution. If $\bar{R}/x$ approaches infinity, this reduces to the two-dimensional solution. In order to obtain an explicit solution of the above non-linear integral equation which contains implicitly four parameters, namely, C_{2a}, C_{3a}, φ_{j3}, and θ_{3-4}, a graphical representation has been constructed. This is discussed in Chapter III.

CHAPTER III

STEADY MASS-BLEED BASE PRESSURE ANALYSIS

Further Extension of the Conical Wake Analysis

Superimposing Zumwalt's conical flow model into Korst's mixing theory enables one to evaluate steady, non-bleed, base pressure for a axi-symmetric body. However, for base pressures both with and without mass-bleed, some empirical formulations are helpful in performing computations; and the computation complexity of the analysis can be reduced by the provision of auxiliary curves.

Corresponding Inviscid Jet Boundary

Properties on a boattail cone which serves as the "corresponding inviscid jet boundary" are required to obtain the local Mach number at a recompression point. This Mach number provides the necessary information for base pressure calculation.

Digital computer solutions of the conical wake flow can be found using the method of characteristics. Data of 64 combinations of approaching Mach number and cone angles were ordered and provided from the Chance-Vought Aircraft Company computing center which utilized the digital computer solution of the method of characteristics.

These solutions cross plotted on semi-log paper show that the downstream Mach number M_{3a} is approximately a function of position $\tilde{R}/R$, and Mach number M_{2a} (the Mach number when the Prandtl-Meyer expansion has been completed) is as follows:

$$M_{3a} = M_{2a}\, e^{-0.209(1-\bar{R}/R)} \qquad [11]$$

This equation provides a means to calculate M_{3a} values within 2% for the moderate Mach number range at any position of $\bar{R}/R$ when an initial M_1 is given and a flow turning angle Θ is chosen. Typical curves are given in Figure 26.

Auxiliary Curves

Equations 9 and 10 contain four parameters: C_{3a}, C_{2a}, Θ, and φ_j. Tedious calculations to obtain a proper combination of these parameters by trial and error can be reduced greatly if two sets of auxiliary curves are used. For each $C_{3\bar{a}}^2$ from 0.4 up to 0.92, random values of C_{3a}/C_{2a} and φ_j have been chosen, thus allowing one to obtain B and φ_j for each combination of cases. This constitutes a graphical solution of Equations 9 and 10. Two sets of curves for B and $\left(\frac{\sigma \bar{R}}{x\cos\Theta}\right)^2$ versus φ_j for various $C_{3\bar{a}}^2$, with C_{3a}/C_{2a} as a parameter are plotted in Figures 3 to 15. (Non-numbered curves are obtained by linear interpolation.)

Jet Spreading Parameter

The detailed discussion of jet spreading parameter, σ, is given in Appendix B. In the case of isoenergetic jet mixing, an experimental approximate formula is suggested as follows:

$$\sigma_{3a} = 47.1\, C_{3\bar{a}}^2 \quad (\text{for } C_{3\bar{a}}^2 > 0.22) \qquad [12]$$

where C_{3a} is the value of Crocco number for the adjacent stream at position ③, the position where the recompression is supposed to take place. Note that for very high Mach numbers, σ has an asymptotical value of 47.1, which is in good agreement with the prediction by Channapragada (11).

Steady Mass-Bleed Base Pressure Analysis

Mass Transfer

For steady mass bleeding cases, some amount of mass will be pumped in or out through the mixing region such that a stable condition is reached. The mass transfer, G_d, which flows between streamlines j and d can be evaluated as follows:

$$G_d \equiv \int_{Y_j}^{Y_d} \rho u 2\pi r dY \qquad [13]$$

From geometry, one has $r = \bar{R} + Y \cos\Theta$. Using the corresponding intrinsic system of coordinates, one obtains

$$y = Y + y_m, \quad y = \frac{x}{\sigma}\eta, \quad \text{and} \quad y_m = \frac{x}{\sigma}\eta_m$$

or $$\frac{x}{\sigma}\eta = Y + \frac{x}{\sigma}\eta_m, \quad Y = \frac{x}{\sigma}(\eta-\eta_m), \text{ thus } dY = \frac{x}{\sigma}d\eta,$$

and $$r = \bar{R} + Y\cos\Theta = \bar{R} + \frac{x}{\sigma}(\eta-\eta_m)\cos\Theta,$$

$$\therefore \quad G_d = 2\pi\int_{\eta_j}^{\eta_d} \rho u \left[\bar{R} + \frac{x}{\sigma}(\eta-\eta_m)\cos\Theta\right]\frac{x}{\sigma}d\eta$$

$$= 2\pi\bar{R}\frac{x}{\sigma}\int_{\eta_j}^{\eta_d}\rho u d\eta + 2\pi\cos\Theta\left(\frac{x}{\sigma}\right)^2\left[\int_{\eta_j}^{\eta_d}\rho u\eta d\eta - \int_{\eta_j}^{\eta_d}\rho u\eta_m d\eta\right]$$

By selecting a proper reference section, e.g., (3a), where the recompression will take place, and with constant pressure prevailing across the mixing region at a given x location,

$$\frac{\rho}{\rho_{3a}} = \frac{1-C_{3a}^2}{1-C_{3a}\varphi^2} \text{ , where } \varphi = \frac{u}{u_{3a}} .$$

Introducing $I_1 = \int_{-\infty}^{\eta} \frac{\varphi\, d\eta}{1-C_{3a}^2\varphi^2}$, $J_1 = \int_{-\infty}^{\eta} \frac{\varphi\,\eta\, d\eta}{1-C_{3a}^2\varphi^2}$,

and, from Ref. 6

$$\eta_m = B + \left(\frac{\bar{R}\,\sigma}{x\cos\Theta}\right) = B + \left[\frac{\sigma\tan\Theta}{\frac{1}{\bar{R}/R} - 1}\right]$$ for external jet, the above

equation becomes,

$$G_d = 2\pi\left\{\frac{x^2}{\sigma^2}\rho u(1-C^2)\cos\Theta\left[(J_{1d}-J_{1j}) - B(I_{1d}-I_{1j})\right]\right\}_{3a}.$$

Noting that $(\rho u)_{3a} = \sqrt{\frac{kg}{R}}\ \frac{p_o}{\sqrt{T_o}}\left(\frac{p_{3a}}{p_o}\right)\sqrt{\frac{T_o}{T_{3a}}}\ M_{3a}$,

$$x_{3a}^2 = \left(\frac{R-\bar{R}}{\sin\Theta}\right)^2_{3a}$$

and defining

$$\mathbb{K} = \frac{8\left(\frac{2}{k+1}\right)^{\frac{k+1}{2(k-1)}}(1-C_{3a}^2)}{\frac{A_{3a}}{A^*}\sqrt{\frac{R}{gk}}} = \frac{4.25(1-C_{3a}^2)}{\left(\frac{A}{A^*}\right)_{3a}} \quad \text{for air} \qquad [14]_a$$

then

$$G_d = \frac{\pi R^2}{4}\ \frac{\mathbb{K}\, p_o \cot\Theta}{\sigma_{3a}^2\sqrt{T_o}\sin\Theta}\left(1-\frac{\bar{R}}{R}\right)^2_{3a}\left[(J_{1d}-J_{1j}) - B(I_{1d}-I_{1j})\right]_{3a} . \qquad [14]_b$$

$\mathbb{K}$ versus C_{3a} is plotted in Figure 24.

Non-dimensional Bleed Number, $\mathcal{K}$

A non-dimensional bleed number, $\mathcal{K}$, was introduced by Korst in his two-dimensional base pressure analysis with mass-bleed as

$$\mathcal{K} = \frac{-G_d\sqrt{T_{oa}}}{H\, p_{oa}}\sqrt{\frac{\mathcal{R}}{gk}},$$

where T_{oa} and p_{oa} are free stream stagnation temperature and pressure, respectively; and H is the height of the step. G_d is the mass flow rate per unit width of gas added externally to the wake through the mixing region. Also, g is the gravitational constant, k is the specific heat ratio, and $\mathcal{R}$ is the gas constant. Noting that the mass flow function has the relation

$$\frac{\dot{m}\sqrt{T_o}}{A\, p_o} = M\sqrt{\frac{gk}{\mathcal{R}}}\left(1 + \frac{k-1}{2}M^2\right)^{-\frac{k+1}{2(k-1)}},$$

it can be seen that $\mathcal{K}$ links the mass bleed rate of the base with free stream properties by giving $\mathcal{K}$ proportional to the ratio of mass fluxes in the base and in the free stream for a given M_1 and k.

For axi-symmetric cases, the same idea is used except H is replaced by A_b, the base area. Thus, one has

$$\mathcal{K} = \frac{-G_d\sqrt{T_o}}{A_b\, p_o}\sqrt{\frac{\mathcal{R}}{gk}}. \qquad [15]$$

It should be noted that G_d for axi-symmetric analysis has the unit of mass rate per unit area, while for plane flow analysis the unit is mass rate per unit width.

CHAPTER IV

STEADY MASS-BLEED BASE PRESSURE TESTS

The preliminary program of a blow-down wind tunnel test to verify the conical wake analysis was planned by the author under his adviser's supervision. This included a general list of needed apparatus with their specifications, a detailed design of a Mach 2 annular nozzle, and an outline of testing procedure. The over-all design and experimental work were carried out by Mr. E. J. Meyer and Mr. R. C. Maydew and other personnel of Sandia Corporation, the sponsor of this research project. In this chapter, only calibration and steady mass-bleed testings, termed phase I and II, have been presented. The phase III, transient base pressure testing, is described in Chapter V.

Equipment

The test facility and installation diagram is shown schematically in Figure 16. The high pressure air, which is supplied by a storage tank, flows through an annular nozzle, but outside a center tube which is concentric with the nozzle. This tube simulates the aft end of a slender flight vehicle flying at Mach 2. Mass bleed into or out of the base region is controlled by a quick opening valve vented through a chosen metering nozzle to the atmosphere or to a vacuum source. Apparatus developed by Division 7423, Sandia Corporation, was specified as follows:

1. A settling chamber for the primary flow (to the annular nozzle) inside of which was a second chamber, of 685.8 cubic inches inside volume, connected to the center tube.

2. A Mach 2 annular nozzle in which was mounted a 2.123 inch O.D. center tube (1.769 inches I.D. and 10.75 inches in length) connected to the inner chamber.

3. The metering nozzle used to vent to atmosphere or a vacuum source had a size range of 0.625, 0.825, 1.00, 1.25 inches in diameter. Also two plates, with 0.500 and 0.375 inch diameter holes, were used to get smaller flow rate control. The plate was installed upstream of the orifice metering nozzle and control valve. This nozzle was in a pipe extending from the inner chamber.

4. A diffuser was provided downstream of the nozzle to enable the tunnel exhausting to the atmosphere to operate at Mach 2 using lower stagnation pressures and thereby gaining longer run times.

Test Program

Phase I was calibration of the M=2 nozzle. A static pressure port, numbered ③ in Figure 16, at the nozzle exit, and a rake with four pitot probes, numbered ④ , ⑤ , ⑥ , ⑦ , were used to determine the Mach number distribution across the nozzle. Base pressure was measured by a pressure transducer located in the sealed tank chamber.

Phase II determined the effect on base pressure of metered flows bled steadily into or out of the base tube. The bleed-out, in which the tank chamber was vented to a vacuum source through metering nozzles of various sizes, simulates the mass pumping by the jet into the wake. This phenomenon corresponds to the rising base pressure transient period which takes place just after the sudden compression due to a blast wave rapidly passing the base region. The results of these testing data allow one to evaluate the effective pumping surface of the jet. The analytical prediction, assuming quasi-steady state exists at each infinitesimal instant of time, can be performed and checked with the experimental data obtained in Phase III. The bleed-in, in which the tank

chamber was vented to ambient pressure (approximately 12 psia) through similar metering nozzles, simulated the mass pumping by the jet out from the wake. The phenomenon corresponds to the decaying base pressure period in which mass flows out from the wake and the base pressure approaches asymptotically its stable (quasi-steady) solution. The accuracy of the analytical calculation for high bleed-in rates versus base pressure is poor due to the base pressure's insensitivity to mass bleed, however, the bleed-out cases are those of interest for the present purpose.

Test Data Analysis and Result

Phase I

This phase was for calibration of a Mach 2 annular nozzle. Eighteen runs were made. Three typical runs have been tabulated in Table 1. The Mach number distributions extracted from Table 1 are:

Position	Local Mach Number		
③	2.014	2.023	1.985
④	2.016	2.014	2.002
⑤	2.017	2.015	2.008
⑥	2.007	2.005	1.997
⑦	2.004	2.005	2.001

where position number ③ was at the nozzle inside wall and ④ through ⑦ equally spaced across the flow passage from the outside wall to the center tube. Since values of positions ⑥ and ⑦ indicate the condition adjacent to the base, their average value of $M_1 = 2.003$, which yields $p_1/p_{o1} = 1.027$, will be used in the data analyses.

Phase II

This phase was for steady mass-bleed testings. It included two parts. One was mass bleeding to the wake by venting the air into the base region from the atmosphere; thus, $\mathring{m}$ was positive. The other was by venting to

a vacuum source, and $\dot{m}$ was a negative because mass was bled out from the base region. Each part has four runs with different sizes of metering nozzles in the vent line. Each run had a recorded base pressure and a corresponding $\mathcal{K}$ value. The $\mathcal{K}$ value can be computed as follows:

$$\mathcal{K} \equiv \frac{\dot{m}\sqrt{T_o}}{A_b p_o}\sqrt{\frac{\mathcal{R}}{gk}},$$

where: $\dot{m}$ - mass bleeding rate; lb_m/sec

T_o - stagnation temperature of flow; °R

p_o - stagnation pressure of flow; psia

A_b - area of base; $\frac{\pi}{4}(1.769)^2 = 2.4565\ in^2$

$\mathcal{R}$ - gas constant; $53.35\ \frac{lb_f\text{-}ft}{lb_m\text{-}°F}$ for air

g - conversion constant; $32.16\ \frac{lb_m\text{-}ft}{lb_f\text{-}sec^2}$ in English units

k - specific heat ratio; 1.4 for air.

The mass flow equation for a metering nozzle with critical flow is

$$\dot{m} = \frac{0.532 p_b A_{noz}}{\sqrt{T_o}}$$ for a discharge coefficient of unity, one

then has

$$\mathcal{K} = \frac{\dot{m}\sqrt{T_o}}{p_o A_b}\sqrt{\frac{\mathcal{R}}{gk}} = \frac{0.532 p_b A_{noz}}{\sqrt{T_o}}\ \frac{\sqrt{T_o}}{p_o A_b}\sqrt{\frac{\mathcal{R}}{gk}}$$

or $$\mathcal{K} = 0.2356\ \frac{A_{noz} p_b}{p_o}.$$

Thus, $\mathcal{K}$ versus p_b/p_1 for each run was obtained, and the data are tabulated in Table 2 and plotted in Figure 17. This curve yields $p_b/p_1 = 0.537$ at $\mathcal{K} = 0$, agreeing quite well with the data for the non-bleed base pressures obtained in other investigations.

Effective Pumping Surface

Combining Equations 14 and 15, one obtains for air:

$$\mathcal{K} = \frac{-1.088\,\mathbb{K}}{\sigma_{3a}^2}\,\frac{\cot\Theta}{\sin\Theta}\left(1-\frac{\bar{R}}{R}\right)_{3a}^{2}\left[(J_{1d}-J_{1j})-B(I_{1d}-I_{1j})\right]_{3a}. \qquad [16]$$

This equation will allow one to obtain values of effective pumping surface, as represented by $\bar{R}/R$, for the test conditions. Knowing $\mathcal{K}$ versus p_b/p_1 for $M_1 = 2$, a trial and error procedure can be performed to obtain a corresponding $\bar{R}/R$ value such that Equation 16 is satisfied. A detailed discussion is given in Appendix D. The result yields a relation between $\mathcal{K}$ and $\bar{R}/R$.

This relation is significant because it seems likely that it may be a general relation which is valid for other Mach numbers. The argument for this is based on the fact that $\mathcal{K}$ is a combination parameter which includes p_o, T_o, gas properties, geometry of the base, and a given mass flow rate, but it is not specified to any Mach number. Thus, its corresponding $\bar{R}/R$ value should have the same nature, i.e., be independent of Mach number. This relation becomes very useful in predicting $\mathcal{K}$ versus p_b/p_1 for any other Mach number. A moderate range of Mach numbers has been chosen and the result of calculations is given in Figure 18. It will be later referred to as "$\mathcal{K}$ curves."

CHAPTER V

TRANSIENT BASE PRESSURE TESTS

In order to check the reliability of the $\mathcal{K}$ curves, which will be used in the transient base pressure analysis, a series of tests were performed. These tests are designated as Phase III in the test program.

Test Program in Phase III

For this phase, a Mylar diaphragm, on which was deposited a very thin, high resistance, burn-out wire, was placed across the center tube interior, 0.708 inches from the tube base. The inner chamber was then evacuated to about 1 to 3 psia. When Mach 2 flow conditions were established around the base tube, a high current was sent through the burn-out wire, causing the diaphragm to rupture, and thus allowing the base region gas to flow into the chamber with subsequent lowering of the pressure at the tube base. Since the base pressure was not the stable value, mass would enter the base region through the jet mixing surface to raise the pressure, until the stable condition was reached. Thus, a transient base pressure situation was created.

All pressure changes were measured by a wafer gage, a very sensitive differential pressure sensing device, and recorded by a high speed strip-chart recorder. A sample of the recorder chart is given in Figure 20.

Data Analyses

The test data have been reduced to graphical form. Figure 19 shows the pressure-time histories for each run. Table IV gives these data in tabular form, listing base pressure for various times. Also, their corresponding $\mathcal{K}$ or $\dot{m}$ values, which were read from the "$\mathcal{K}$ curves," are listed in the same table. These data were then compared with the analytically predicted results.

In order to use the $\mathcal{K}$ curves to predict the pressure-time histories for this experimental set-up, some simple approximations were needed in order to obtain the first order values.

There are three basic approximations which have been used. These are:

1. When the diaphragm is suddenly burned out, a moving pressure wave is expected. This wave with its reflections will disturb the uniform properties of the air inside the chamber. For simplicity, it is assumed that air inside the chamber has reached its equilibrium state at any instant of time, i.e., the air in the chamber has uniform temperature and pressure properties at any time.

2. The temperature of the air inside the chamber increases according to the adiabatic compression relations.

3. A quasi-steady assumption is made, i.e., a steady condition prevails during an infinitesimal interval of time.

To obtain the mass and the over-all average value of the air temperature inside the evacuated chamber, two data points, at $t = 0.01$ and 0.02 seconds immediately after the diaphragm was burst, were chosen. Equations of state for these two instants allow one to solve the two unknowns, m_c and T_c, simultaneously. It is found that the solutions agree with the m_c from the equation of state for air inside the chamber just before the diaphragm is burst within three per cent for all runs.

The three assumptions listed provide a means for constructing pressure-time analytical predictions to be compared with the experimental data. At any time, t, temperature is obtained by $T = T_c(p_b/p_c)^{\frac{k-1}{k}}$, $\Delta m = \dot{m}\Delta t$, where $\dot{m}$ is read from $\mathcal{H}$ curves, and the equation of state yields a new pressure value at $t + \Delta t$. The results of these step-by-step calculations are plotted as dashed lines in Figure 19 for comparison with the solid lines for test data. The agreement is seen to be very good.

In this quasi-steady analysis, $\dot{m}$ has been overestimated while the temperature T has been underestimated for each step. These seem to compensate well in the most transient period, but less well in the nearly stable region due to the insensitivity to time, i.e., a very slight increase of pressure covers a considerable length of time in that region.

These tests thus showed that the $\mathcal{H}$ curves can be used as a basis to evaluate the transient base pressure problems which are generated by blast wave passage. The detailed discussion of this use is given in the next chapter.

CHAPTER VI

TRANSIENT BASE PRESSURE ANALYSIS

To deal with the highly transient base pressure problem due to a blast wave passing axially over an axi-symmetric missile, there are several things which need to be discussed before a computation method is outlined.

Transformation of Moving Blast Wave

It is rather convenient to employ a relative moving coordinate system, in which a blast wave becomes stationary, and the stationary normal shock relations are then applicable to the fluid properties in this coordinate system. The same result is true, to a very good approximation, even when the shock strength is changing with time or when the shock speed is not constant. This is true because the shock thickness is minute, from which it follows that the time rates of change of mass, momentum, and energy within a control surface surrounding the shock are negligible compared with the changes in the respective fluxes of these quantities passing through the control surface. In this transformation, the blast wave is considered as a normal shock wave and properties termed as the "prime" condition. The computing procedure for the shock conditions in the transformed plane is given in Appendix E. Note that in this transformation, stream thermodynamic properties are invariant, but stagnation properties are changed.

Decaying Over-Pressure

The transient period is influenced by the decaying over-pressure, which is a function of time, the type of explosion, and the distance from the blast center. For a spherical blast wave, it is suggested by Sandia Corporation to be approximated as follows:

$$\Delta p_t = \Delta p_{max}\left(1 - \frac{t}{t^+}\right) e^{-\frac{t}{t^+}} \qquad [17]$$

where t^+ is shown on the following drawing, and can be obtained from Sandia Corporation publications (12). This drawing shows the pressure change with time for a blast wave passing a stationary point.

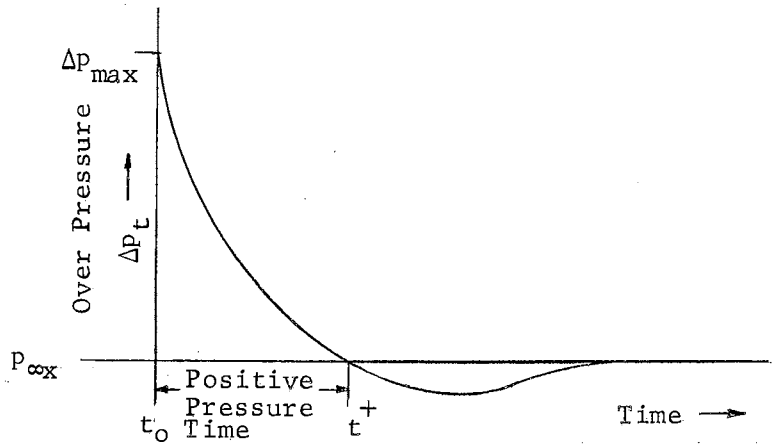

Thus $p_{\infty t} = p_{\infty x} + \Delta p_t$. [18]

This equation is used in Appendix E.

The Quasi-Steady Concept

A transient flow can be treated as a finite number of time steps with steady flow conditions prevailing during each increment of time. The magnitude of the time increment depends entirely upon the accuracy

required. This quasi-steady technique permits a good prediction of the value of the conditions at the next step, and the process may be continued in the same manner as long as desired.

During each quasi-steady step duration, mass transfer must occur in order to adjust the flow field toward a new equilibrium state until a stable condition is asymptotically reached.

Conditions Just Before (subscript x) and After (subscript y) the Shock Front Passes

Generally, a blast wave will encounter a flying missile with a very high relative speed. The length of time for the shock front to pass the base region then becomes practically negligible. Practically speaking, the mass inside the mixing region is subject to a sudden, almost isentropic, compression without any mass transport. Knowing from the experiment by Love (9) that the base pressure is almost constant for most of the conical wake volume, one has, by geometry:

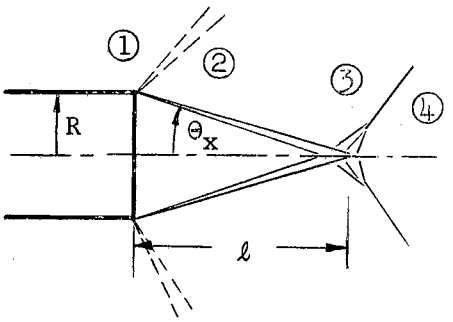

$$\ell = \frac{R}{\tan\theta_x}$$

$$m_{bx} = \rho V_{bx} = \frac{p_{bx}}{\mathcal{R}T_{bx}} \frac{\pi R^3}{\tan\theta_x}$$

By isentropic compression of the mass inside the wake: $m_{bx} = m_{by}$, then

$$\frac{p_{bx}\pi R^3}{\mathcal{R}T_{bx}\tan\theta_x} = \frac{p_{by}\pi R^3}{\mathcal{R}T_{by}\tan\theta_y},$$

or

$$\frac{T_{bx}}{T_{by}} \frac{p_{by}}{p_{bx}} = \frac{\tan\theta_y}{\tan\theta_x};$$

but $$\frac{T_{bx}}{T_{by}} = \left(\frac{p_{bx}}{p_{by}} \right)^{\frac{k-1}{k}}$$ by isentropic relation;

thus, one obtains

$$p_{by} = p_{bx}\left(\frac{\tan\theta_y}{\tan\theta_x} \right)^k \quad . \qquad [19]$$

For condition "y", the pressures across the mixing region are assumed to have equalized:

$$p_{by} = p_{2y} \quad .$$

By adjusting θ_y values, such that p_{2y} obtained by Prandtl-Meyer turn is equal to p_{by} from the above equation, a "y" condition solution can be found.

Base Pressure Solutions During the Transient Period

The mass in the base at any instant of time during the transient period is

$$m_t = (\rho_b V_b)_t = \frac{p_{bt} \pi R^3 \cot\theta_t}{\mathcal{R} T_{ot}} \quad . \qquad [20]$$

By assuming an isoenergetic jet mixing condition*, i.e., the gas in the base region will have the same stagnation temperature as the adjacent stream, and using the quasi-steady concept, the mass in the base at time, $t + \Delta t$, will be

*This assumption is justified by the argument given in Appendix F,

$$m_{(t+\Delta t)} = m_t + \dot{m}\Delta t$$

where $\dot{m}$ can be calculated from the $\mathcal{K}$ curves. Note that p_o and T_o are not constants; their values can be determined by knowing the decaying external flow field conditions as specified on page 99.

Knowing $m_{t+\Delta t}$ value, one can iterate $\theta_{t+\Delta t}$ such that $p_{b(t+\Delta t)}$, obtained by Equation 20, is equal to $p_{2(t+\Delta t)}$ which is calculated by the Prandtl-Meyer relation. Successive conditions can be continued in the same manner until the solution agrees with the stable solution. A complete outline of this procedure is also given in Appendix E.

CHAPTER VII

CONCLUSIONS AND RECOMMENDATIONS

Conclusions

The analysis, undertaken to develop an analytical method for computing the highly transient base pressure on an axi-symmetric supersonic missile resulting from a head-on passing blast wave, has been completed and verified to be an acceptable method. Consequently, the following observations are summarized:

1. The use of Korst's mixing theory is advisable.
2. The use of Zumwalt's conical flow model analysis provides a satisfactory physical model.
3. The extension of the mass transfer consideration, imposed on Zumwalt's non-bleed base pressure analysis, enables one to use the quasi-steady concept for transient base pressure evaluation.
4. The jet spreading parameter, which originally was used for steady flow, is usable for quasi-steady flow as well.
5. The transformation of a moving blast wave into a relative stationary plane has been shown to be advantageous for simplicity.
6. The graphical technique to solve the governing non-linear integral equation permits construction of the $\mathcal{K}$ curves with reasonable effort.
7. The $\mathcal{K}$ curves, formed by knowing the effective pumping surface relation from experimental data, are very useful for transient base pressure evaluation.
8. The transient base pressure experimental tests verify that the analytical analysis gives a good prediction of base pressure-time history for simple, rapid, transient conditions.

Suggestions for Further Work

In light of the knowledge gained from this investigation, the following suggestions are made for further work:

1. Values of the jet spreading parameter, σ, should be found experimentally for axi-symmetric hypersonic jets.

2. The mechanism of blast wave interaction on the base region when encountering the wave front at an arbitrary orientation needs to be studied in order to modify this present analysis to be applicable to general cases.

3. In the present analysis, the very short-time pressure transients in the base due to wave reflections as the blast passes were neglected. For the aerodynamicist, this is admissible, since the effect on drag is small. The structural analyst, however, must know how the forces are applied no matter how short their duration. Thus, detailed knowledge of the wave patterns during the blast passage, leading to the quasi-steady condition "y", should be sought.

4. A similar analysis for laminar jet mixing flow seems to be advisable due to its occurrence in high altitude flight. Some suggestions for this are given in Reference 23.

5. $\mathcal{K}$ curves for Mach numbers other than two should be found by experiments similar to Phase II tests reported in Chapter IV.

FIGURES

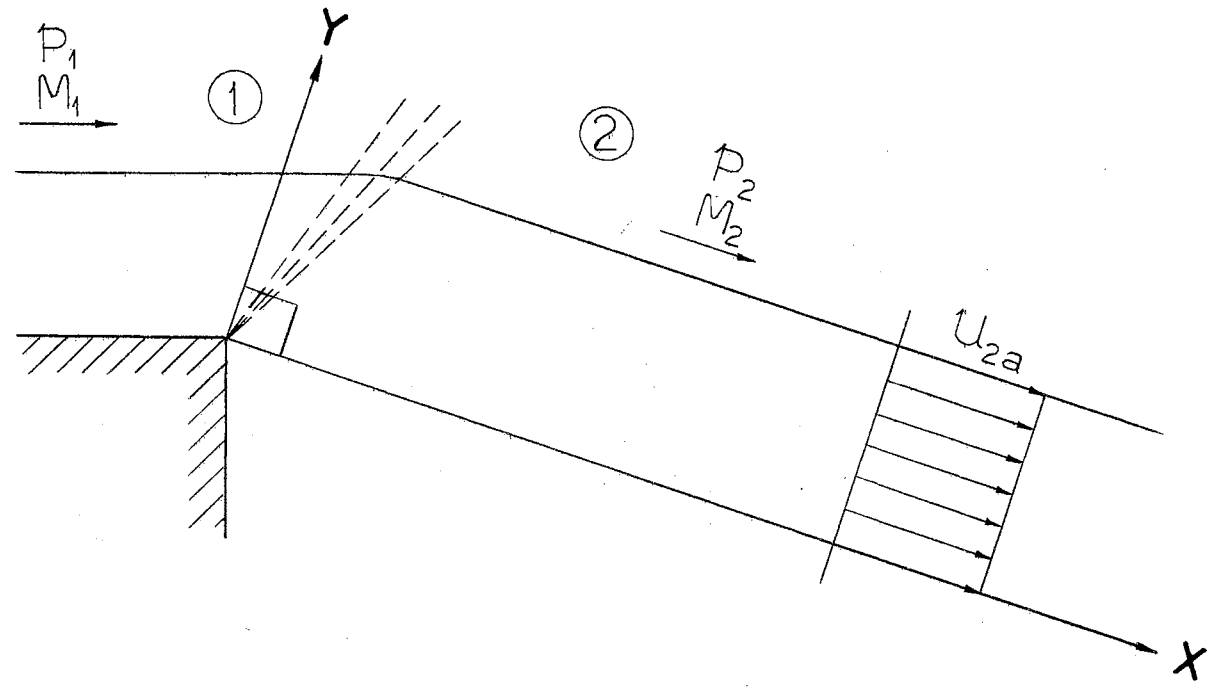

(a) Inviscid Jet

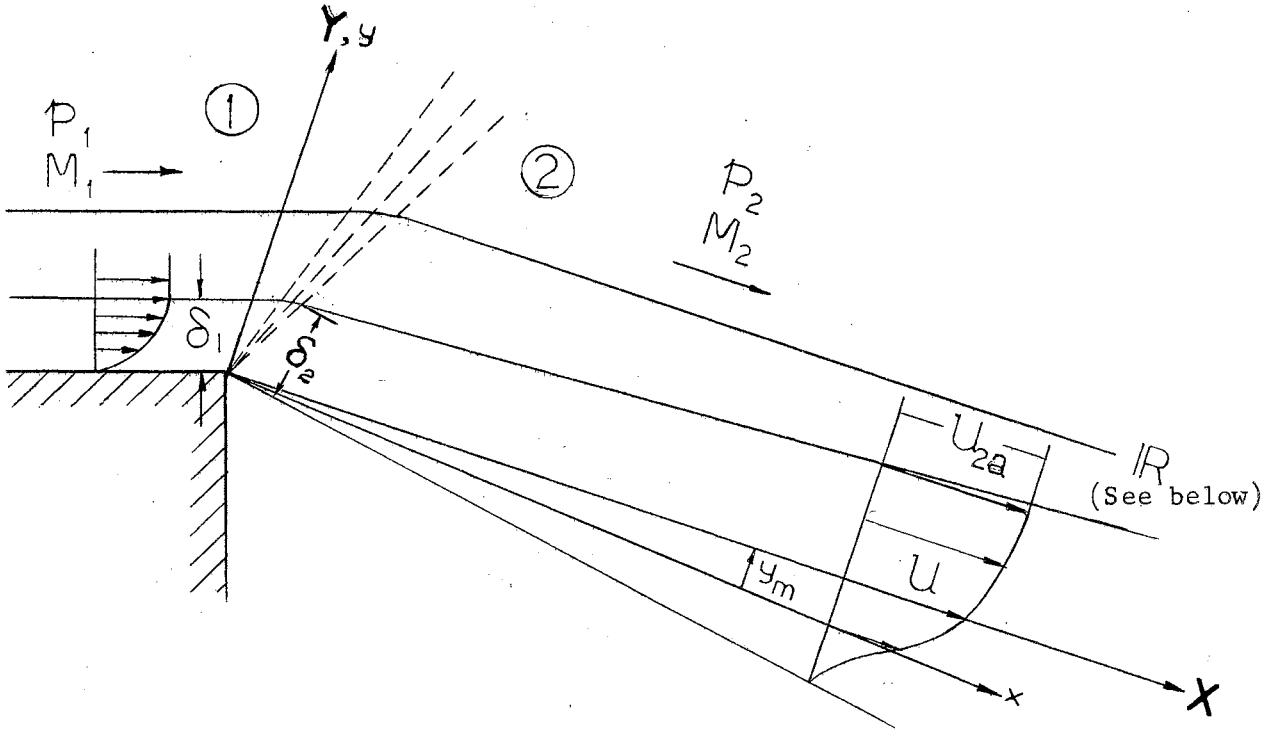

(b) Viscous Jet

(IR is a streamline outside the mixing region.)

Figure 1. Corresponding Inviscid and Viscous Jets.

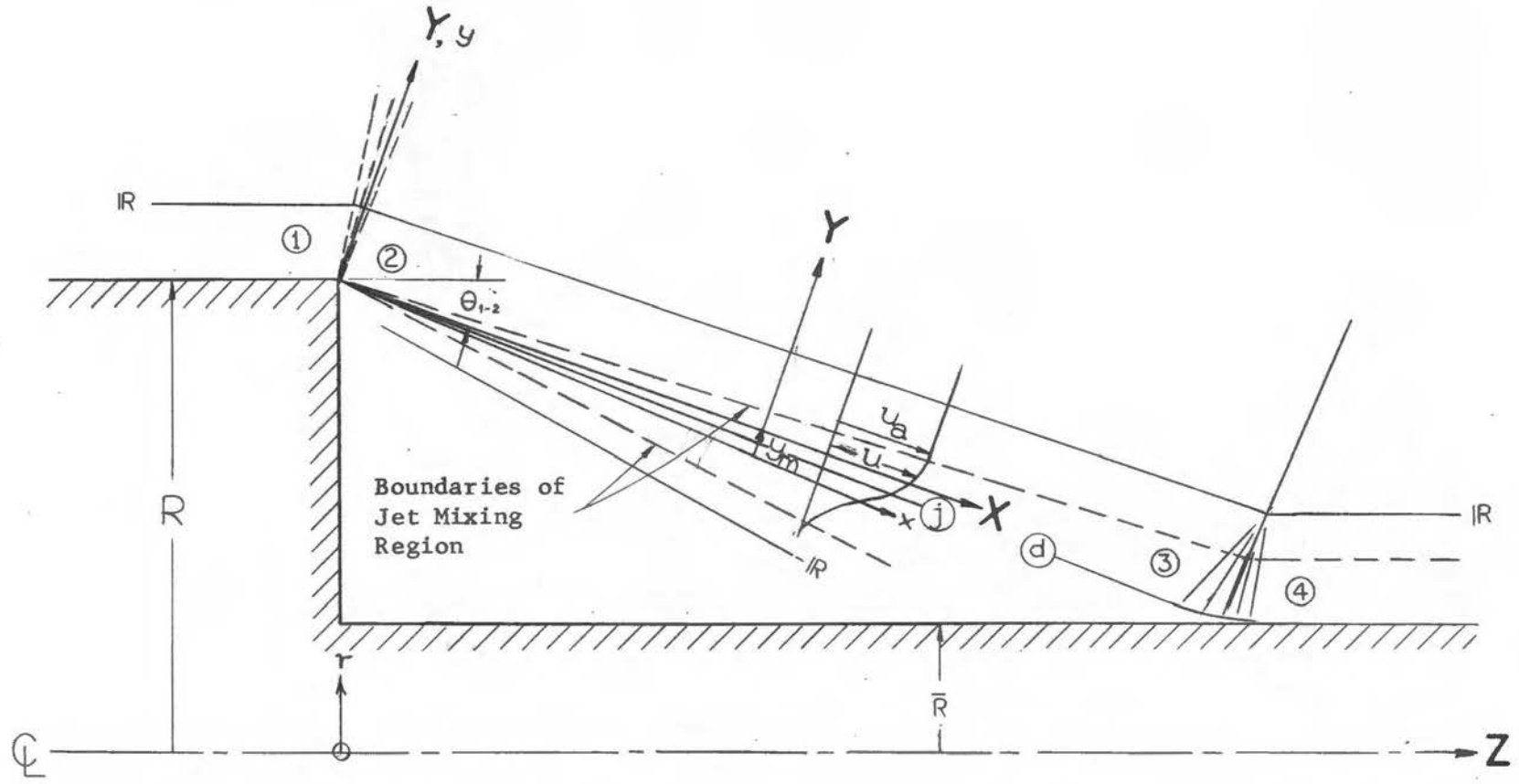

Figure 2. Flow Model for Use in the Analysis of a Conical Free Jet.

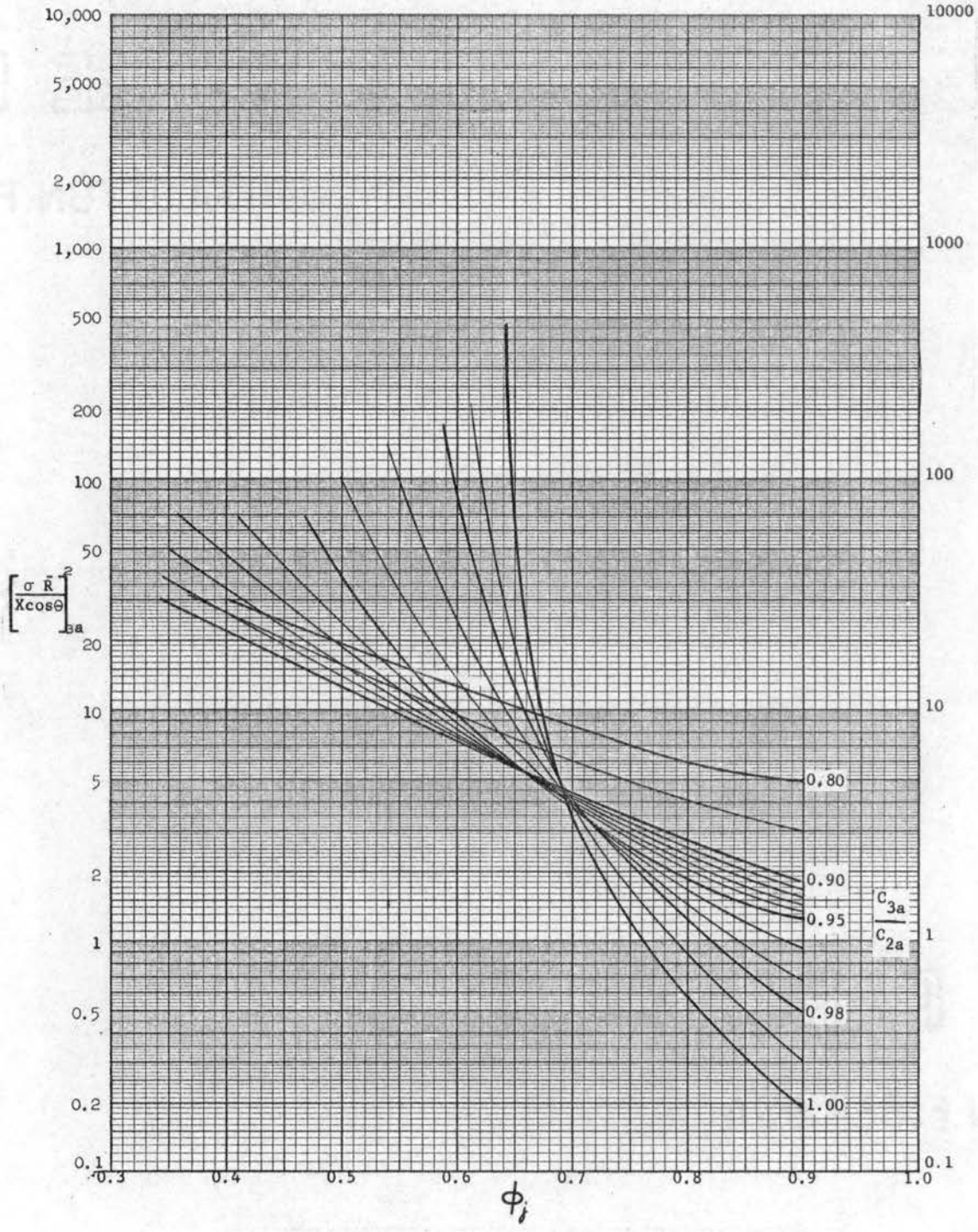

Figure 3. Auxiliary Curves $C^2_{3a} = 0.4$.

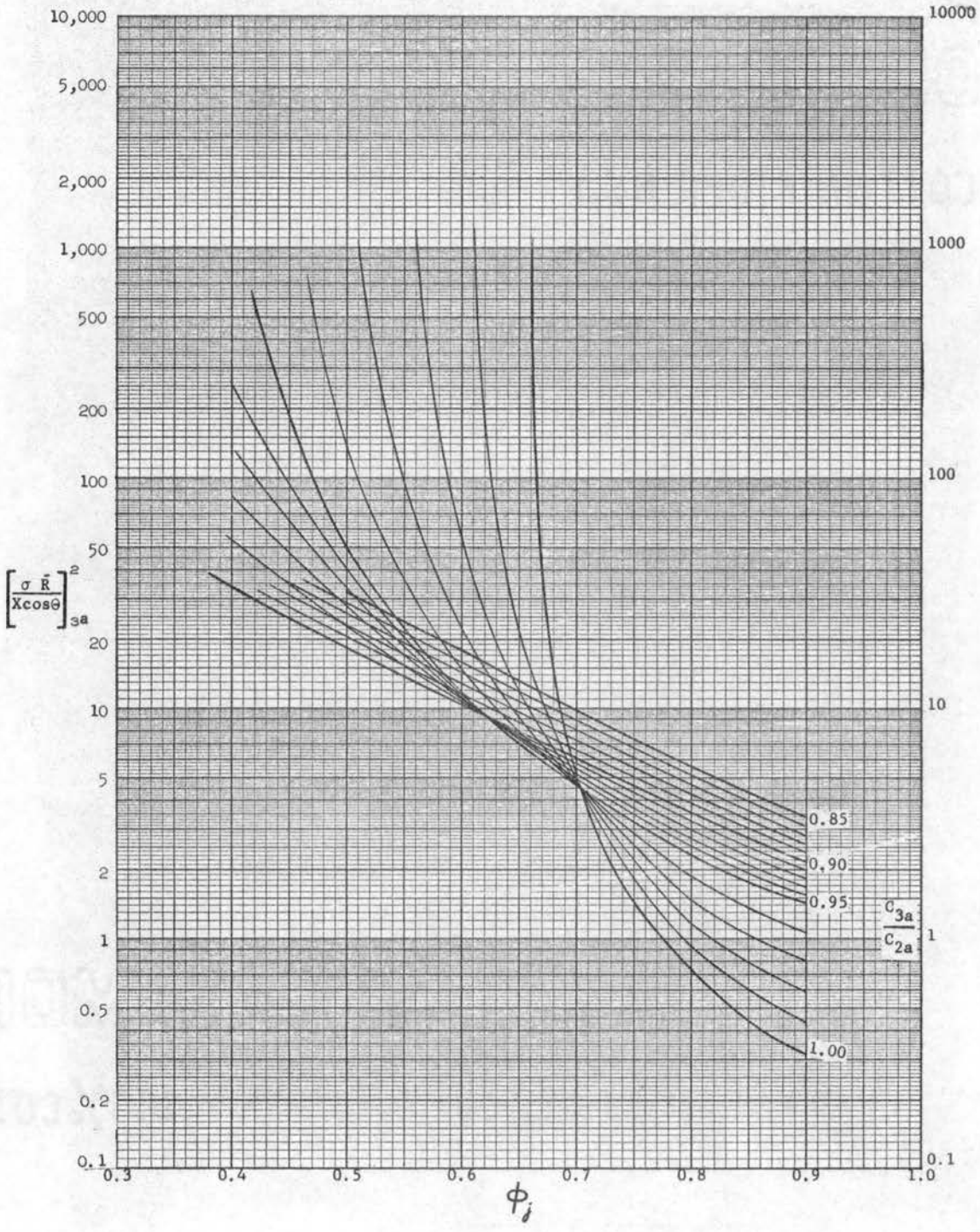

Figure 4. Auxiliary Curves $C_{3a} = 0.5$.

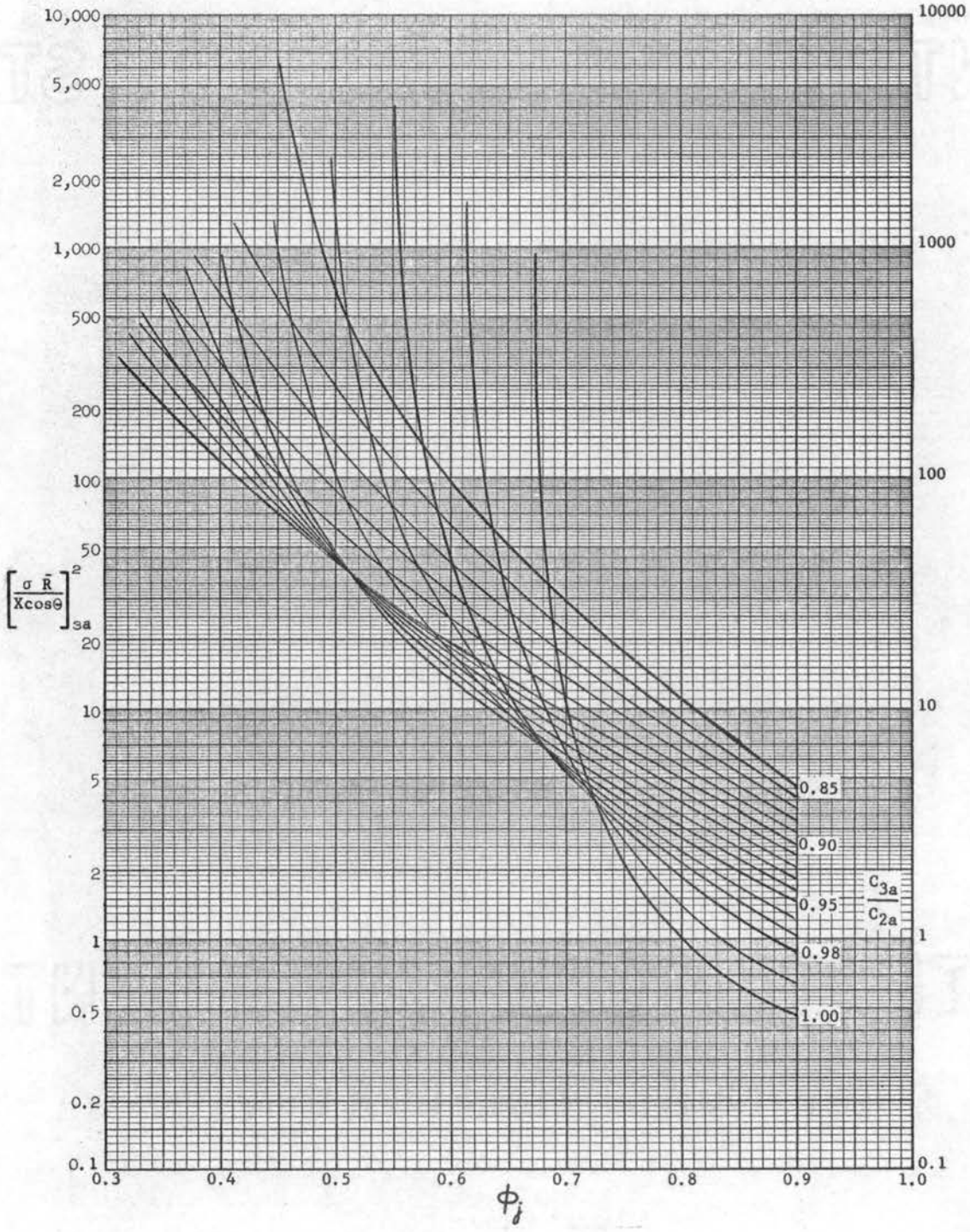

Figure 5. Auxiliary Curves $C_{3a}^2 = 0.6$.

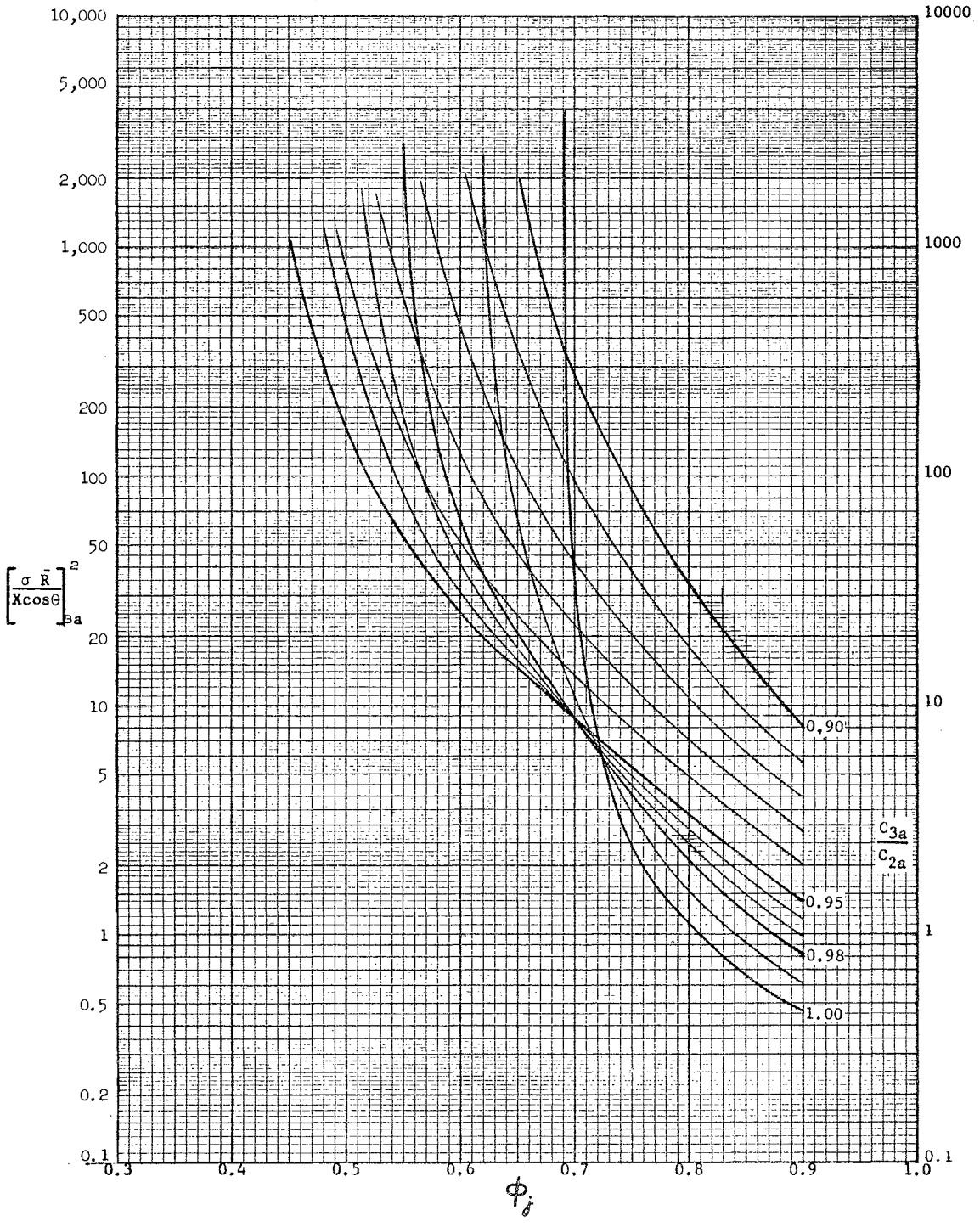

Figure 6. Auxiliary Curves $C^2_{Ba} = 0.7$.

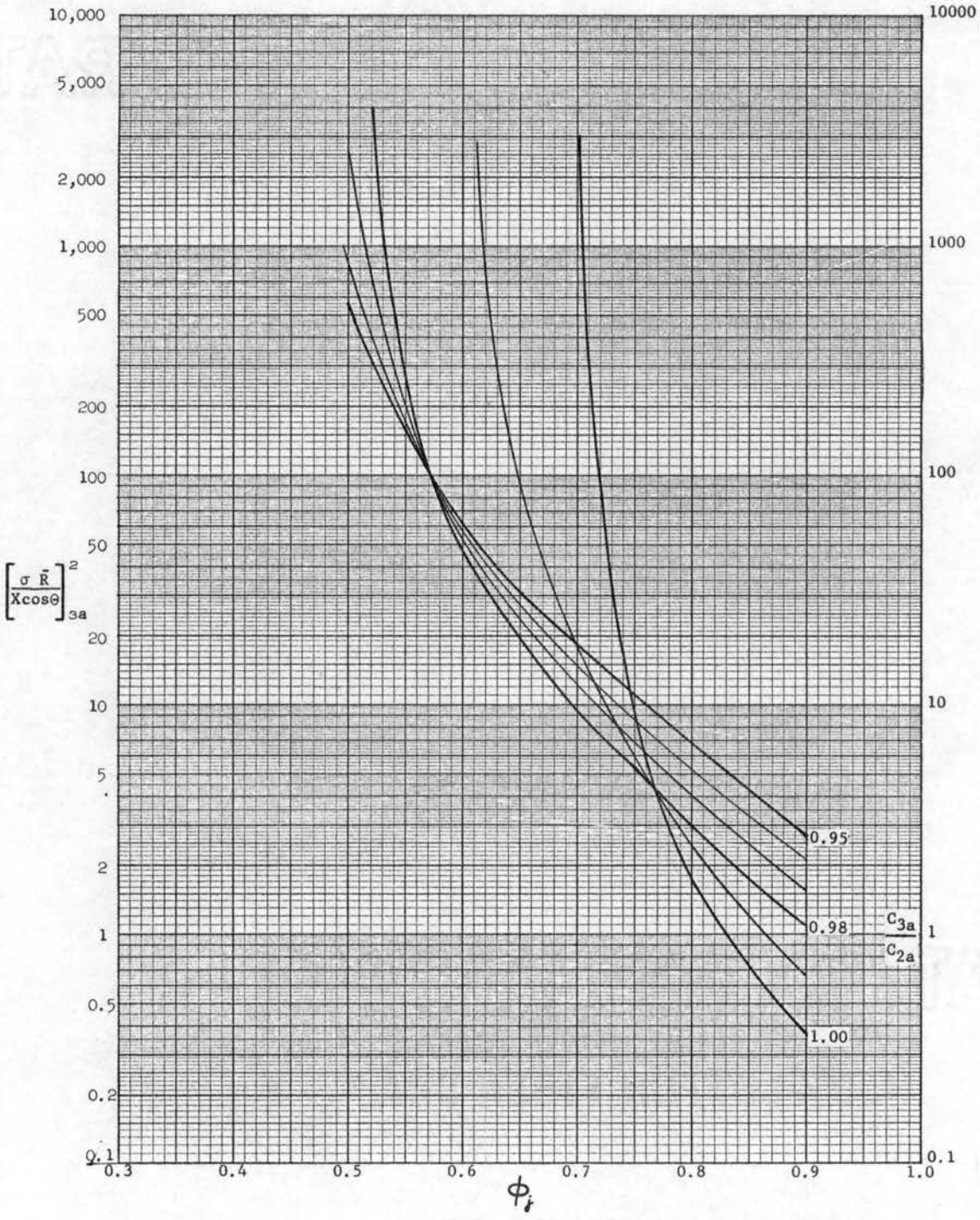

Figure 7. Auxiliary Curves $C_{3a}^2 = 0.8$.

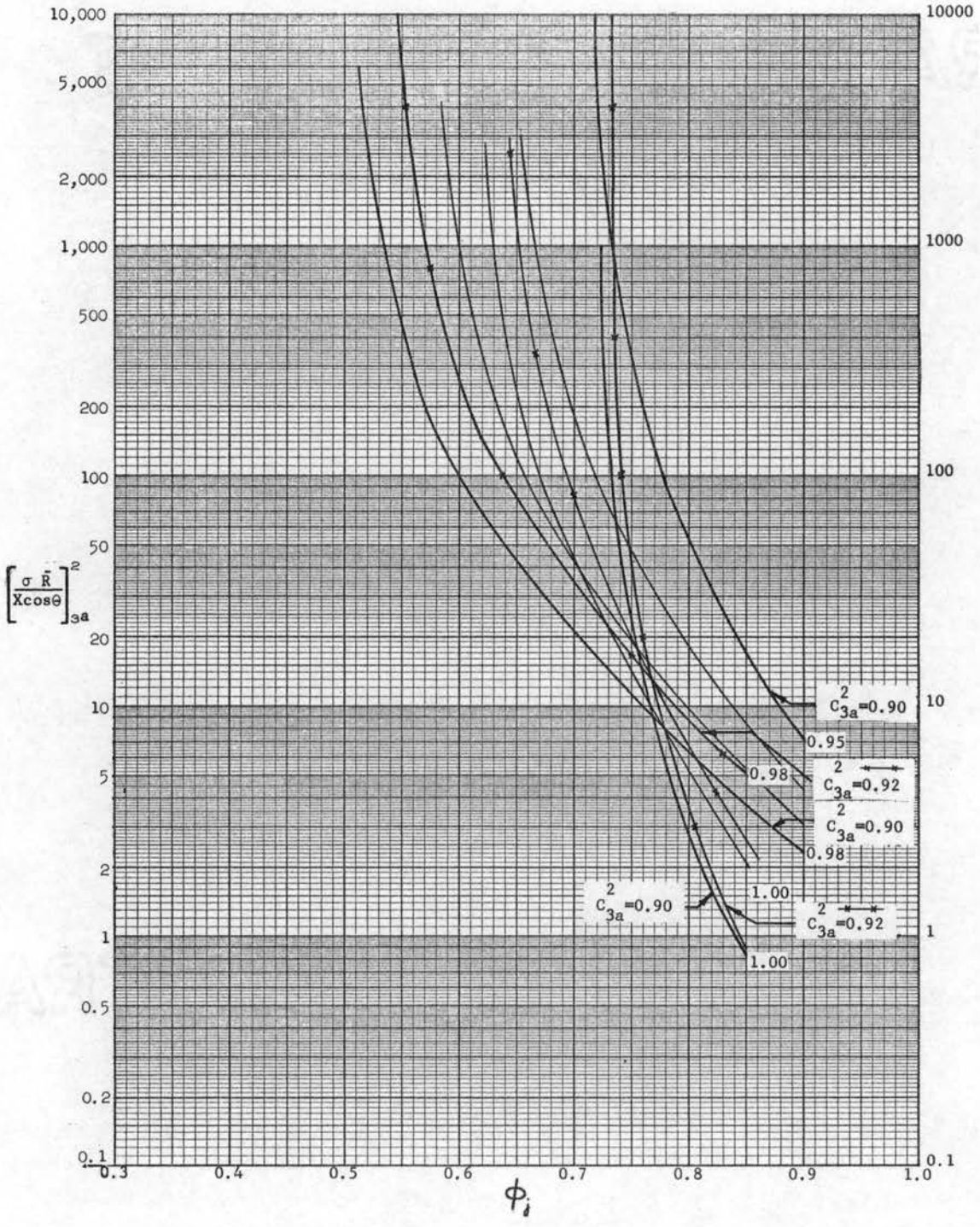

Figure 8. Auxiliary Curves C^2_{3a} = 0.9 and 0.92.

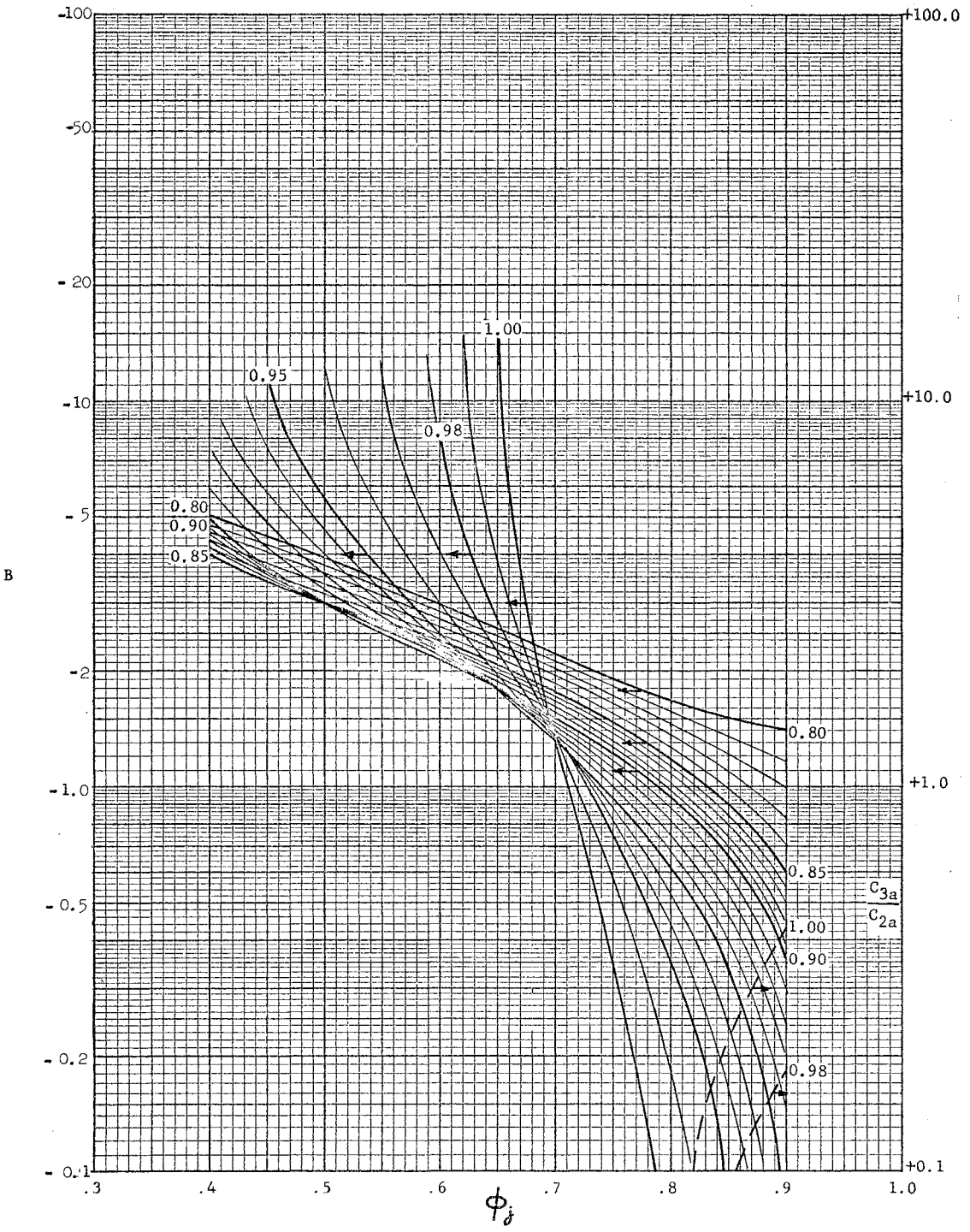

Figure 9. Auxiliary Curves $C_{3a}^2 = 0.4$.

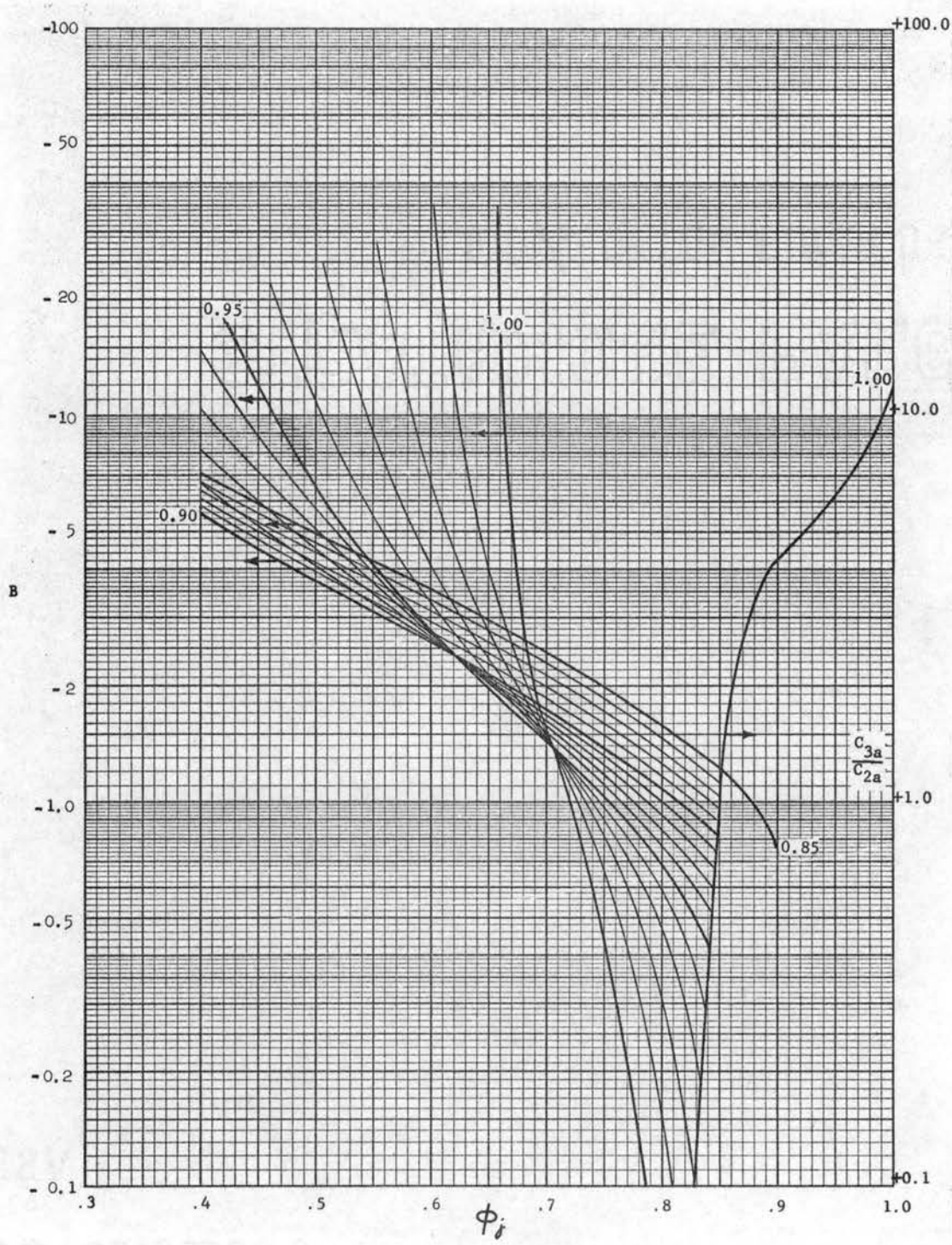

Figure 10. Auxiliary Curves $C_{3a}^2 = 0.5$.

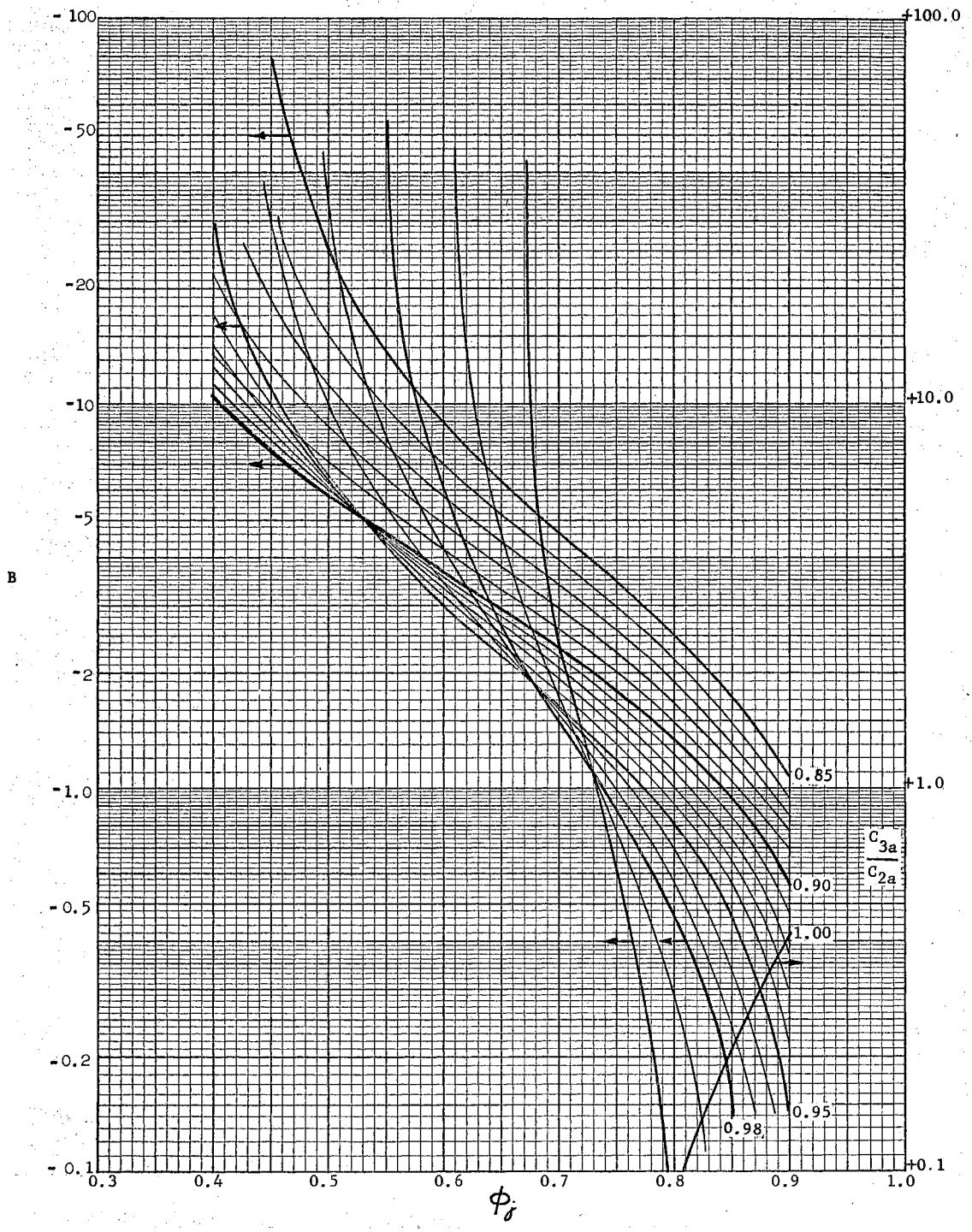

Figure 11. Auxiliary Curves $C_{3a}^2 = 0.6$.

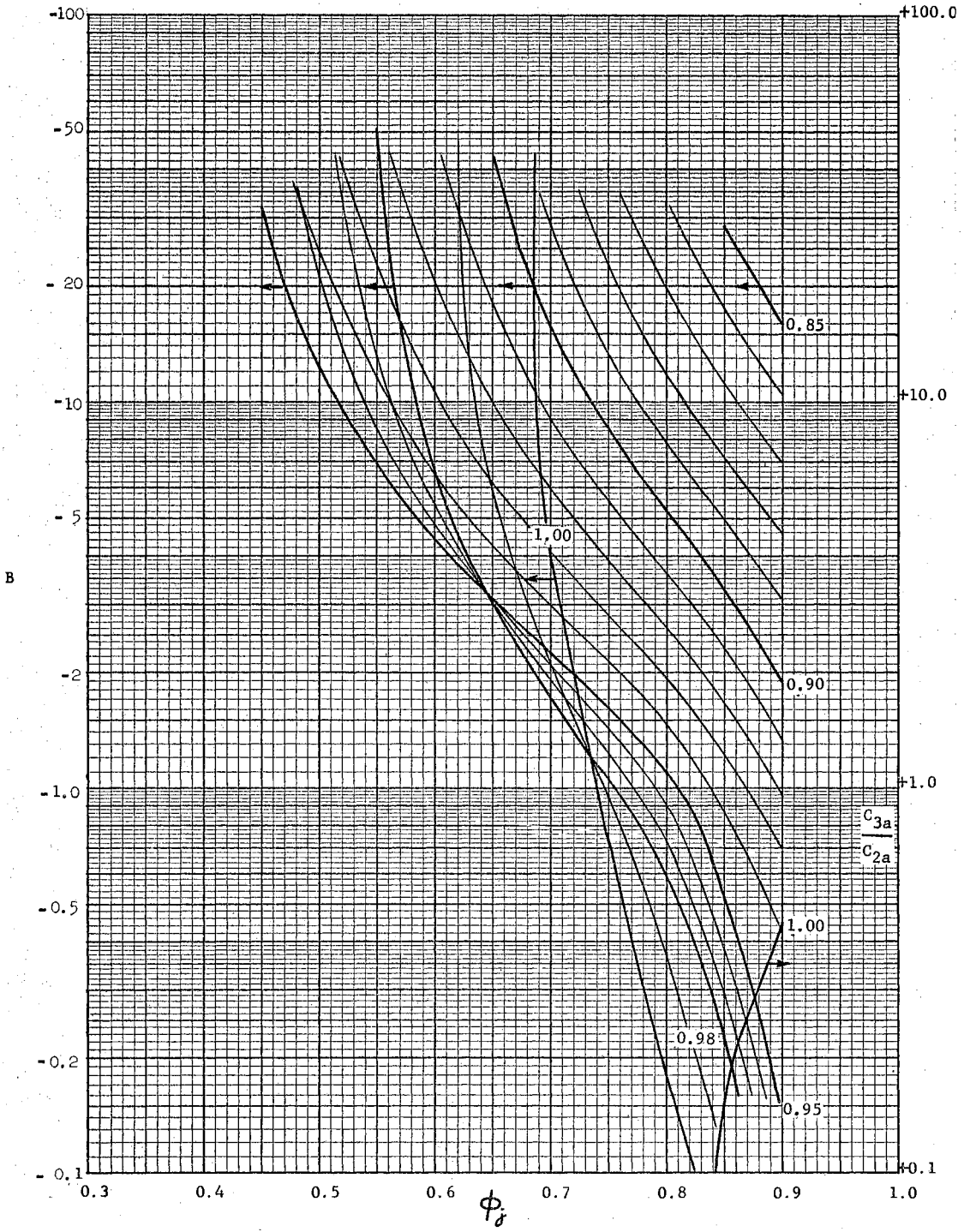

Figure 12. Auxiliary Curves $C_{3a}^{2} = 0.7$.

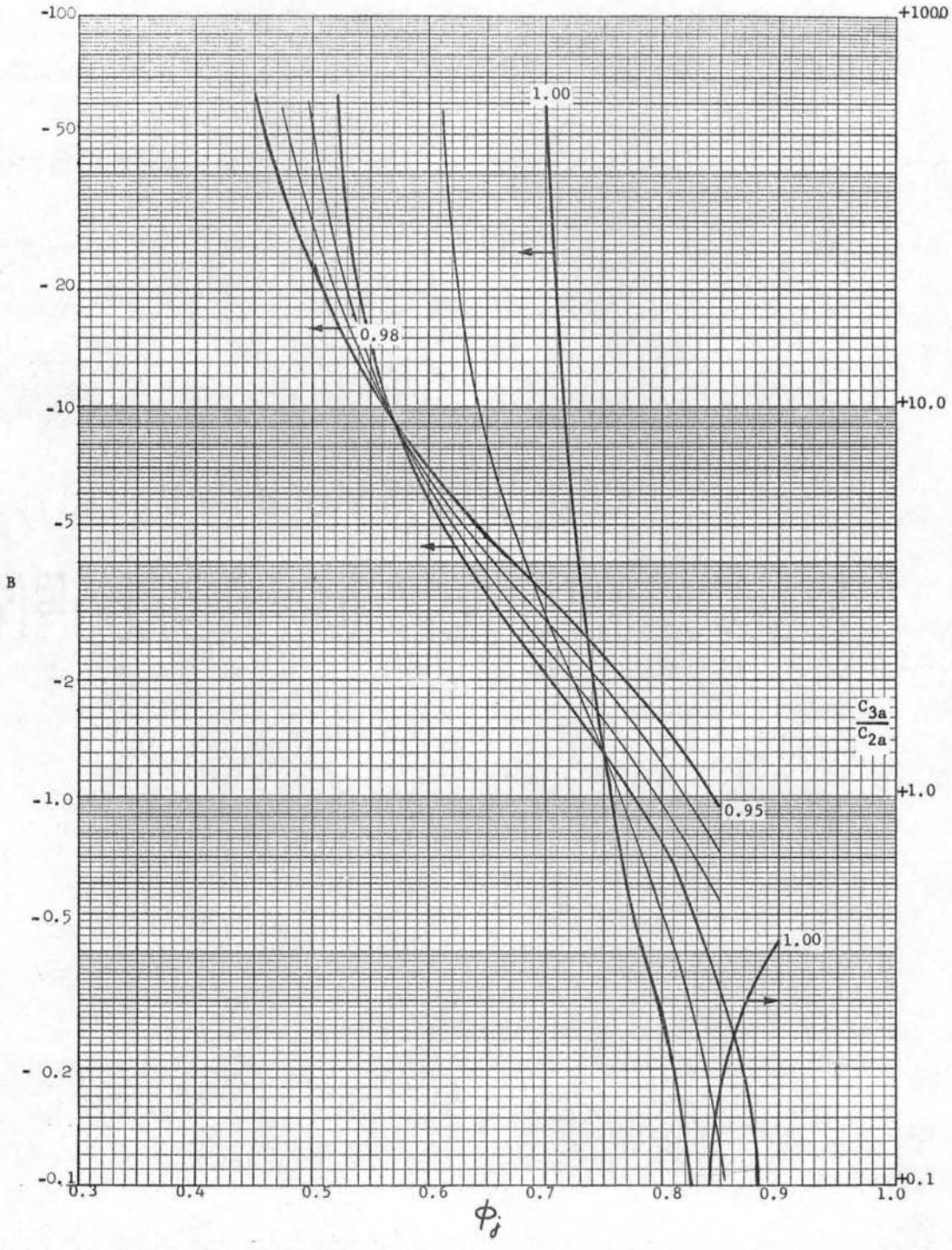

Figure 13. Auxiliary Curves $C_{3a}^2 = 0.8$.

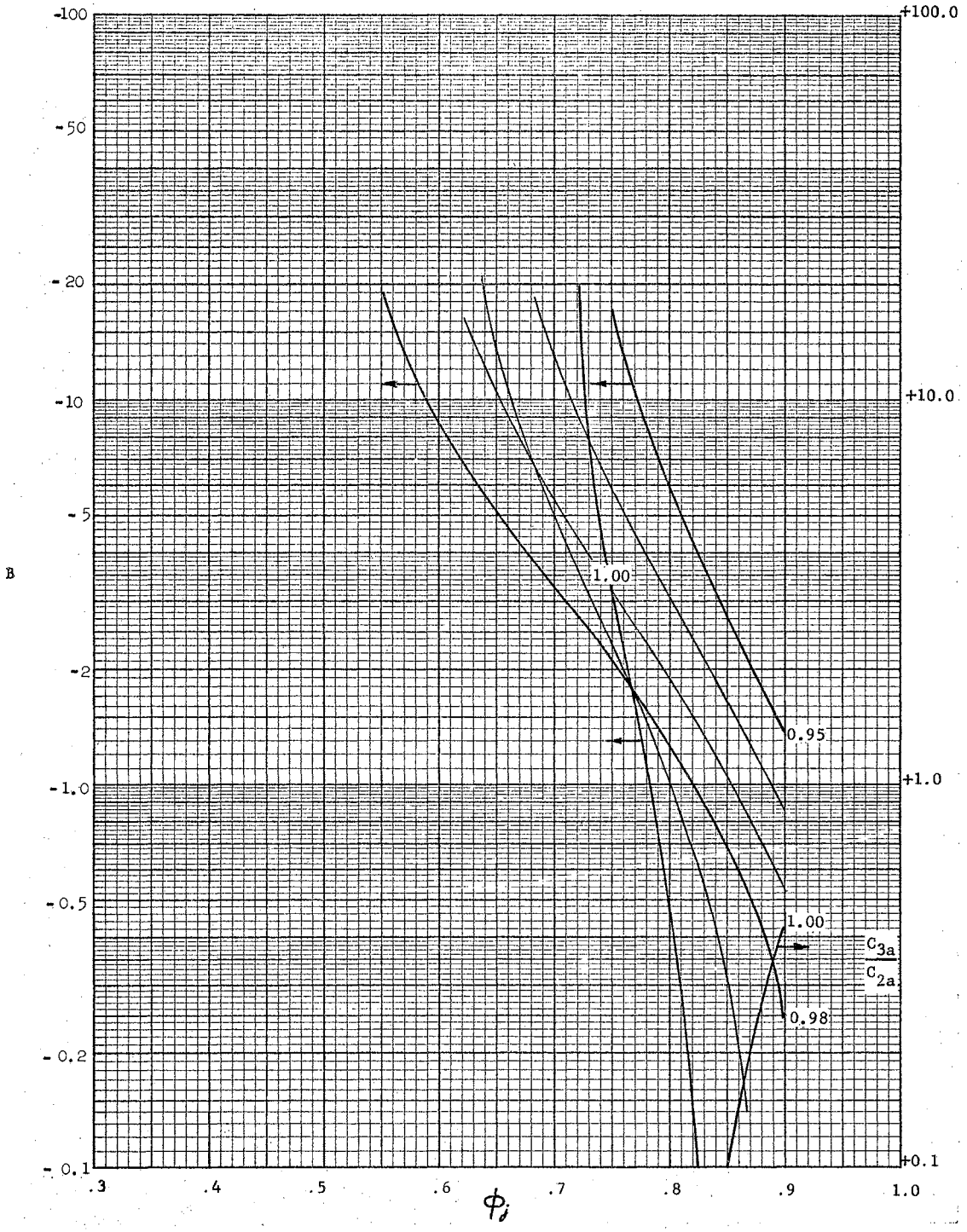

Figure 14. Auxiliary Curves $C_{3a}^{2} = 0.9$.

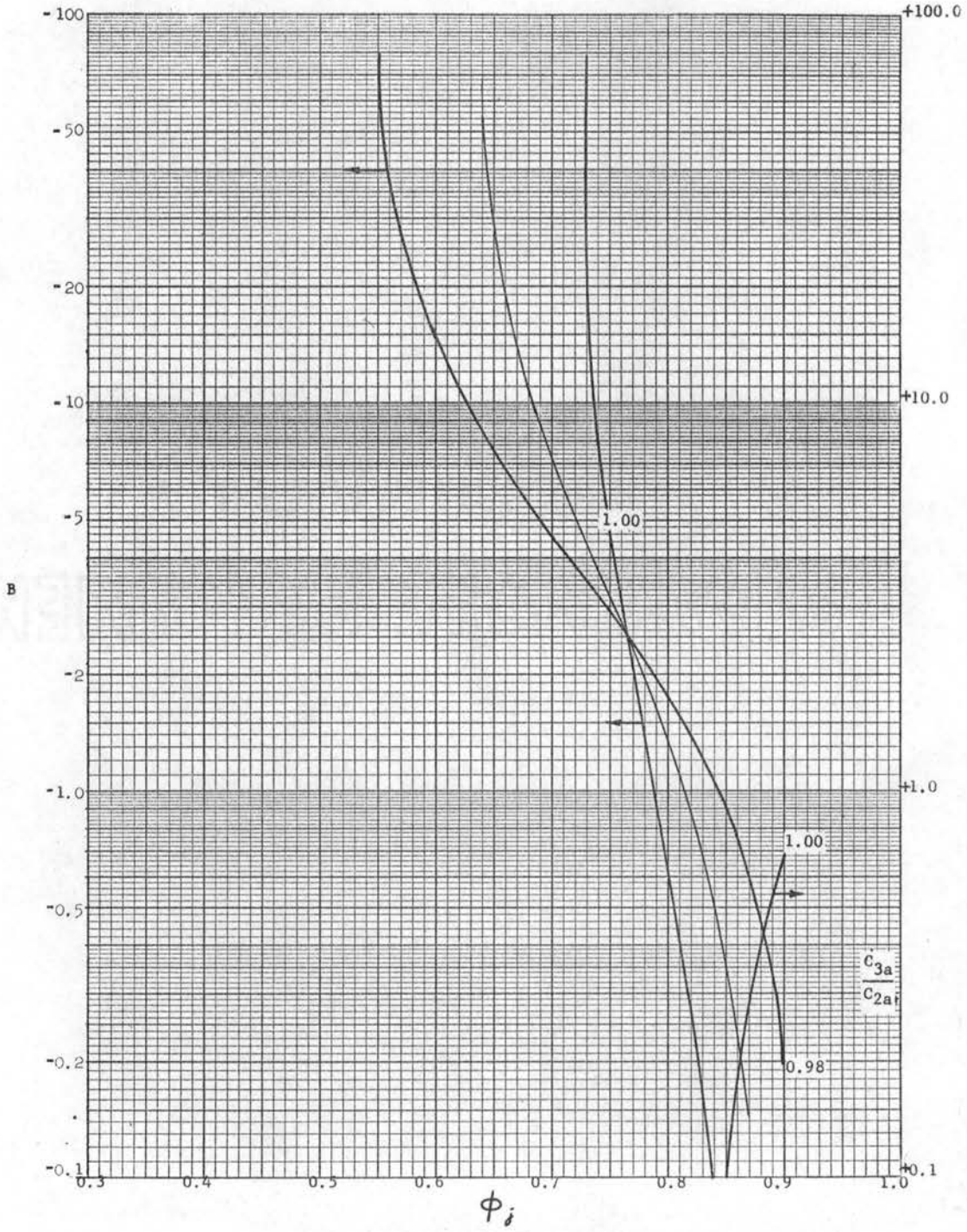

Figure 15. Auxiliary Curves $C_{\bar{3}a} = 0.92$.

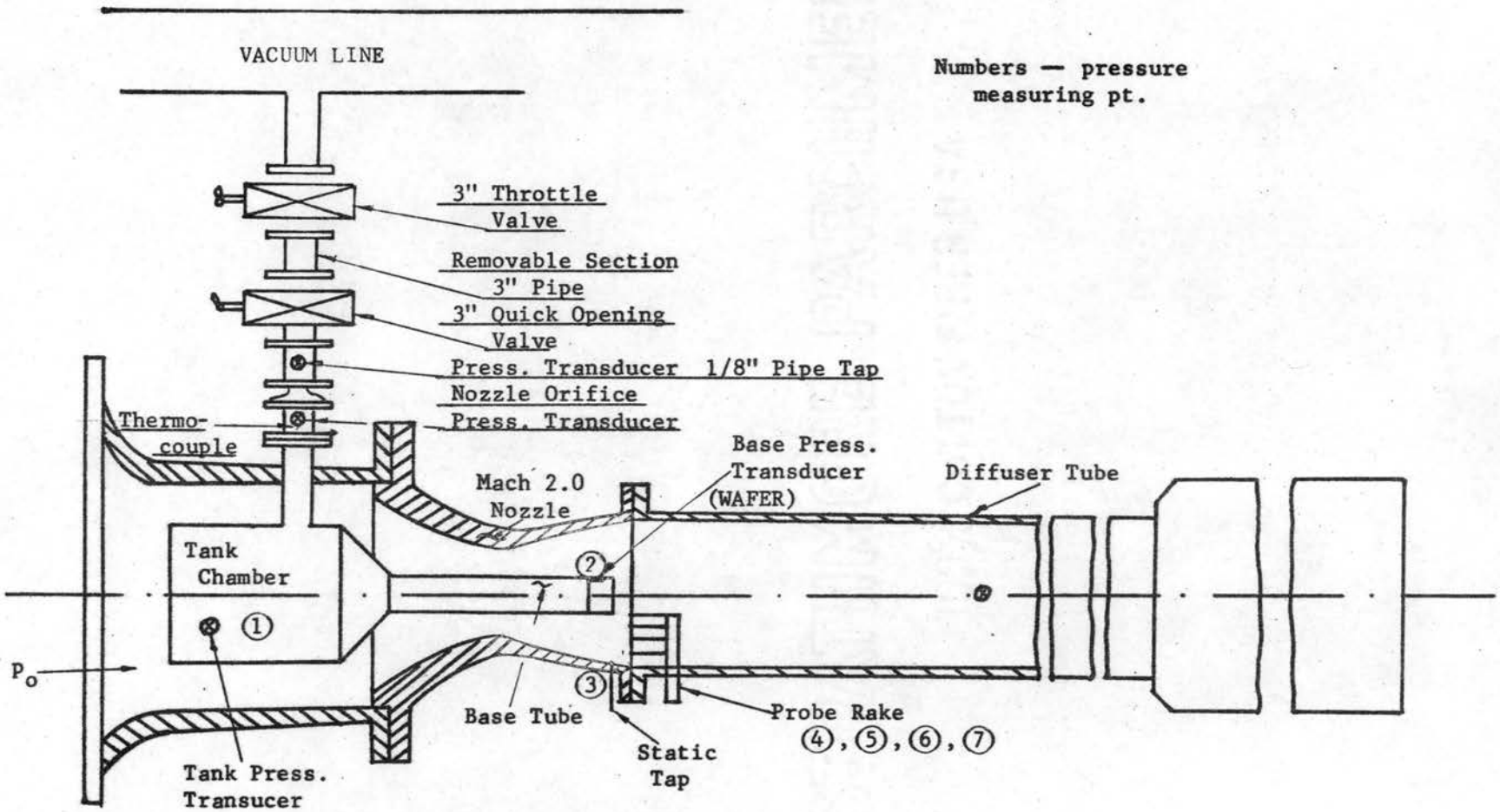

Figure 16. Schematic Diagram of the Experimental Equipment.

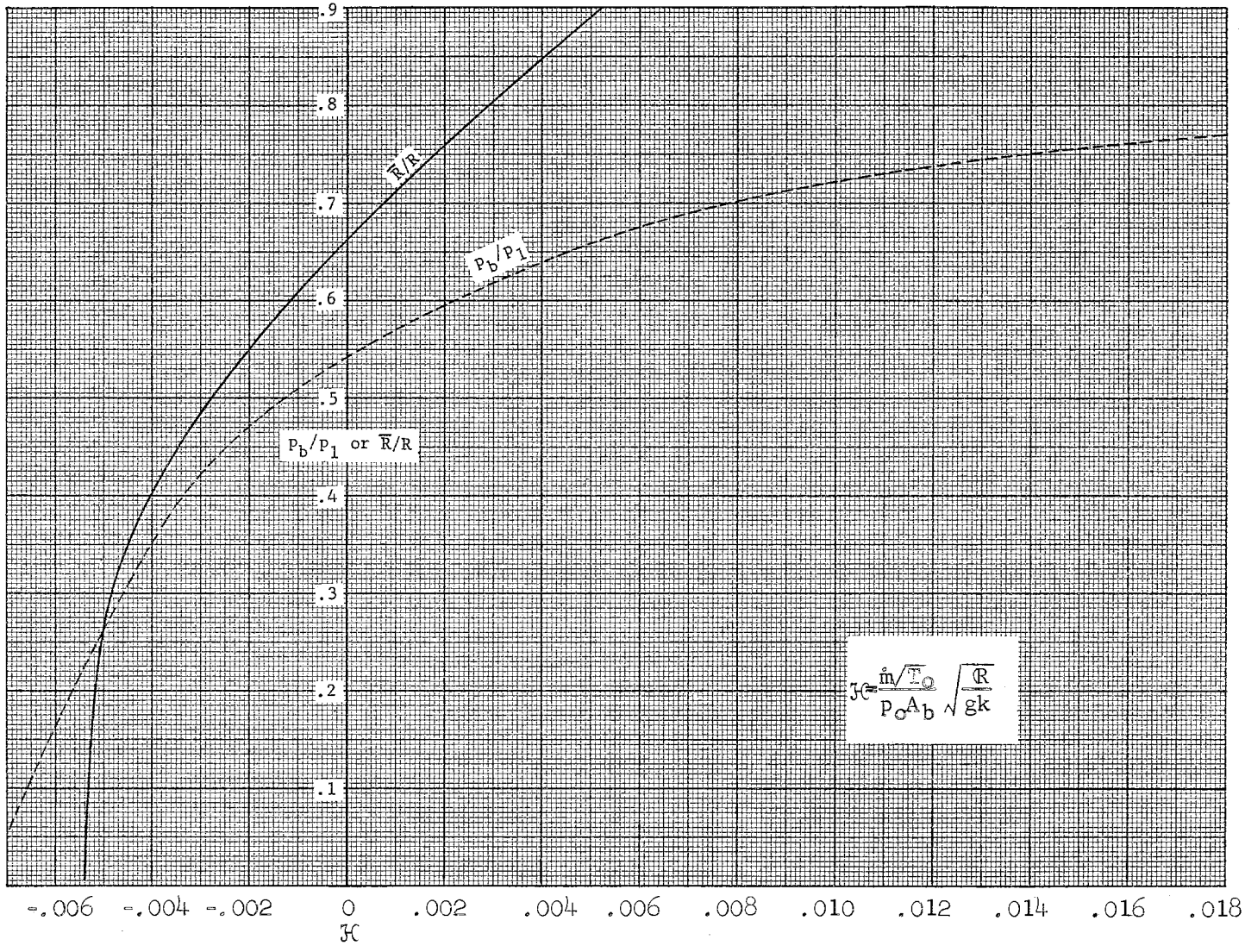

Figure 17. Effective Pumping Radius Ratio, $\bar{R}/R$, Versus Non-Dimensional Bleed Number, $\mathcal{H}$, for Conical Jet Mixing. (M_1 = 2.0.)

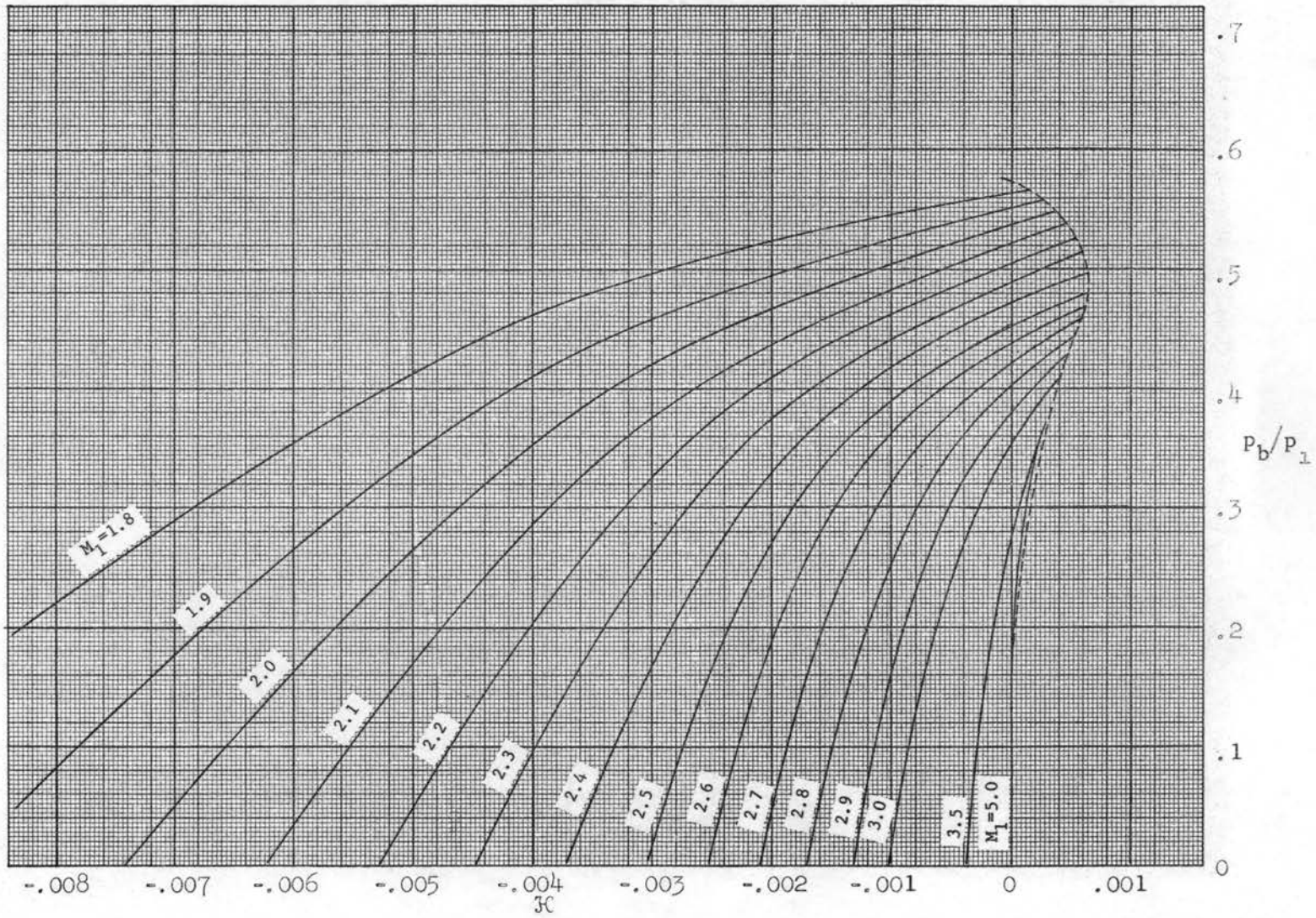

Figure 18. $\mathcal{K}$ Curves.

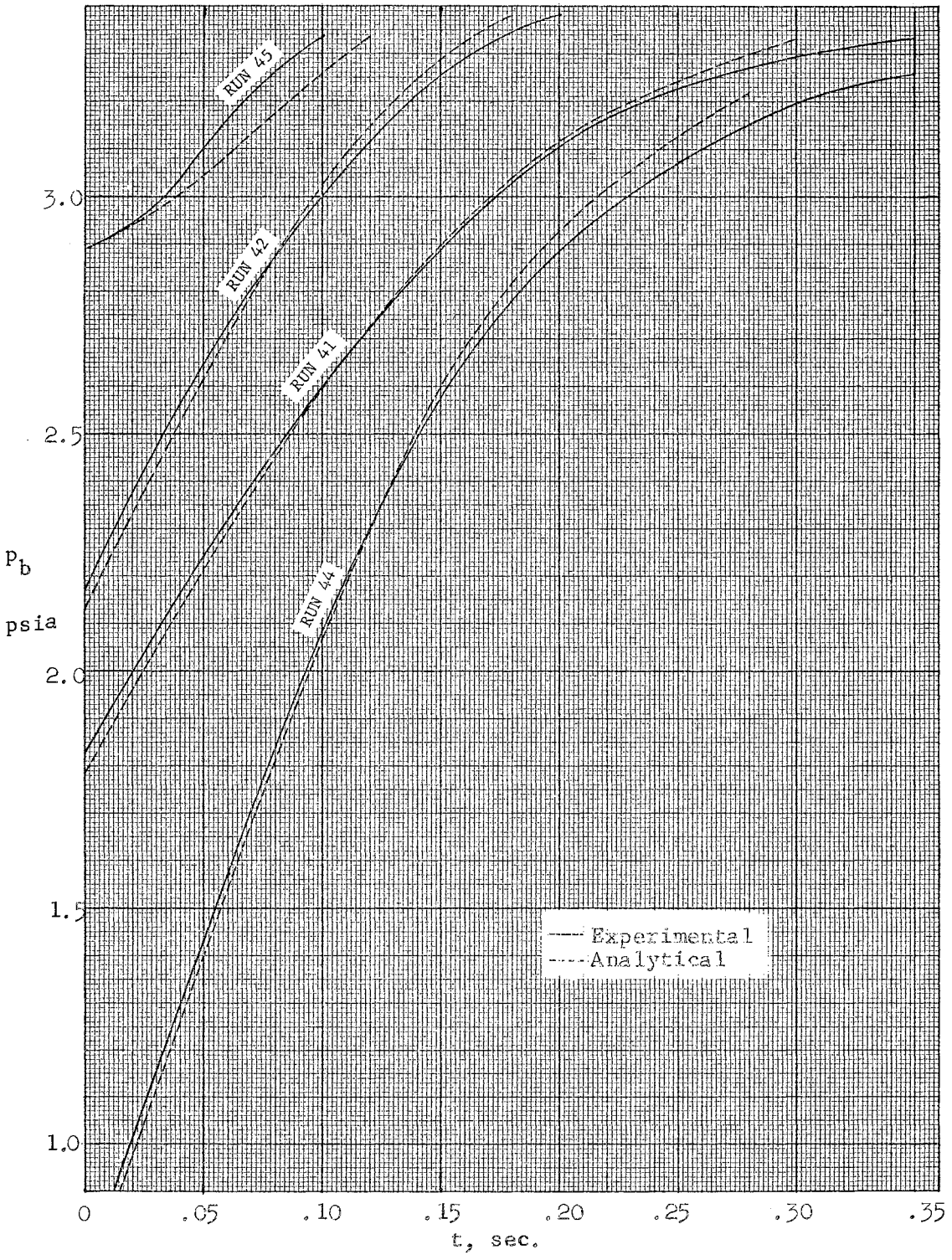

Figure 19. Comparison of the Analytical and Experimental Base Pressure-Time Histories for the Transient Wind Tunnel Tests.

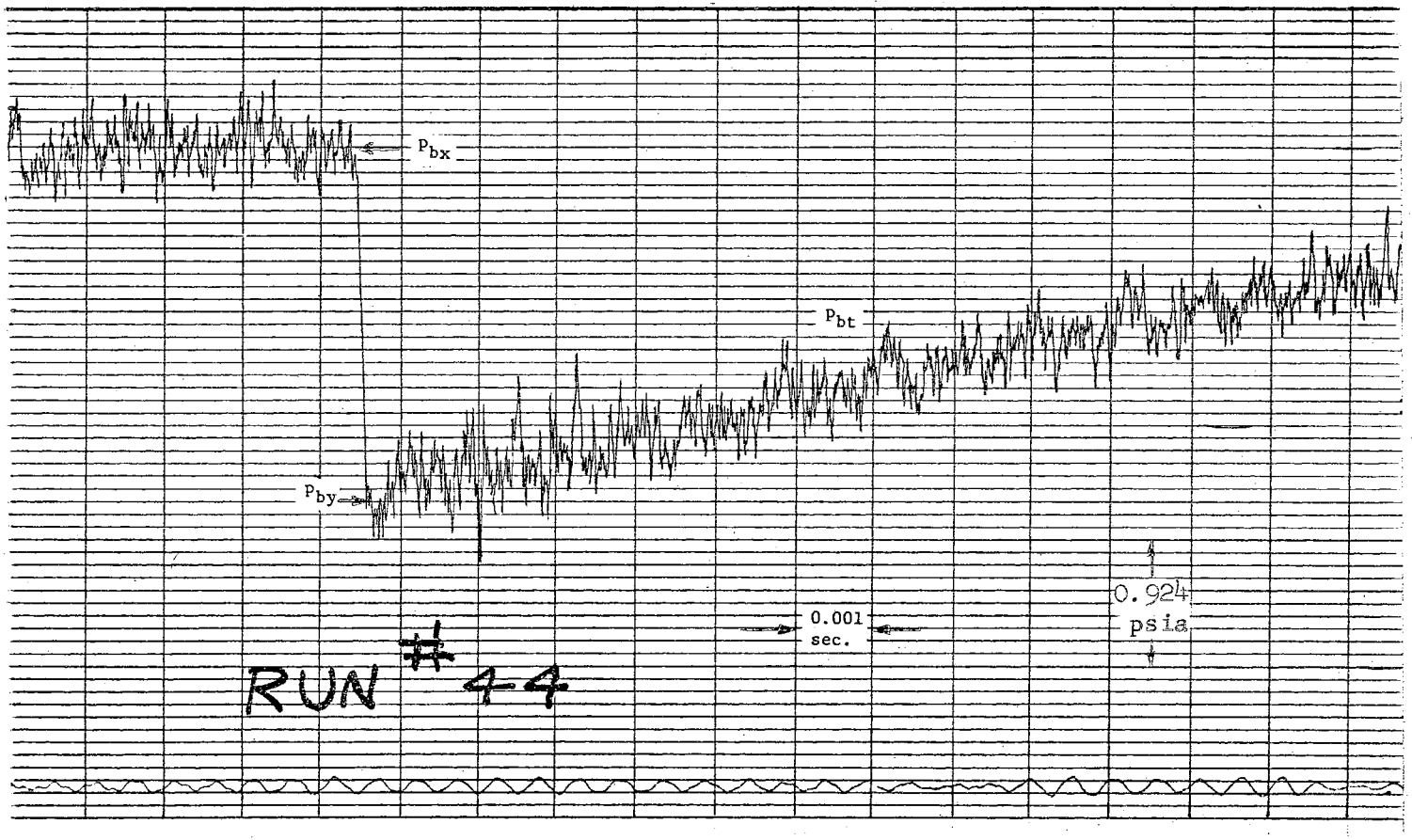

Figure 20. A Sample of the Transient Data Recording in the Base Pressure Tests.

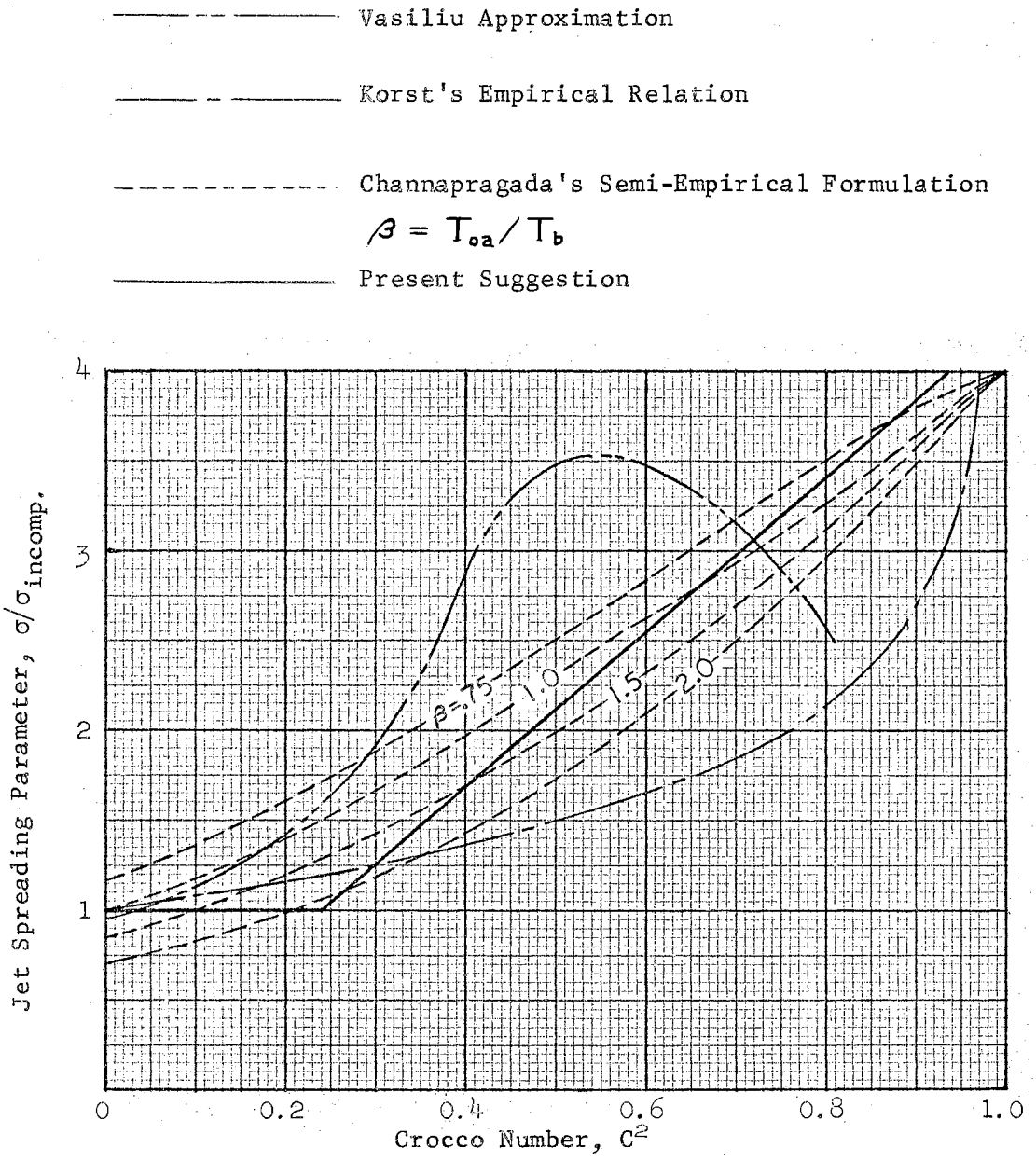

Figure 21. Variation of Jet Spreading Parameter with Crocco Number.

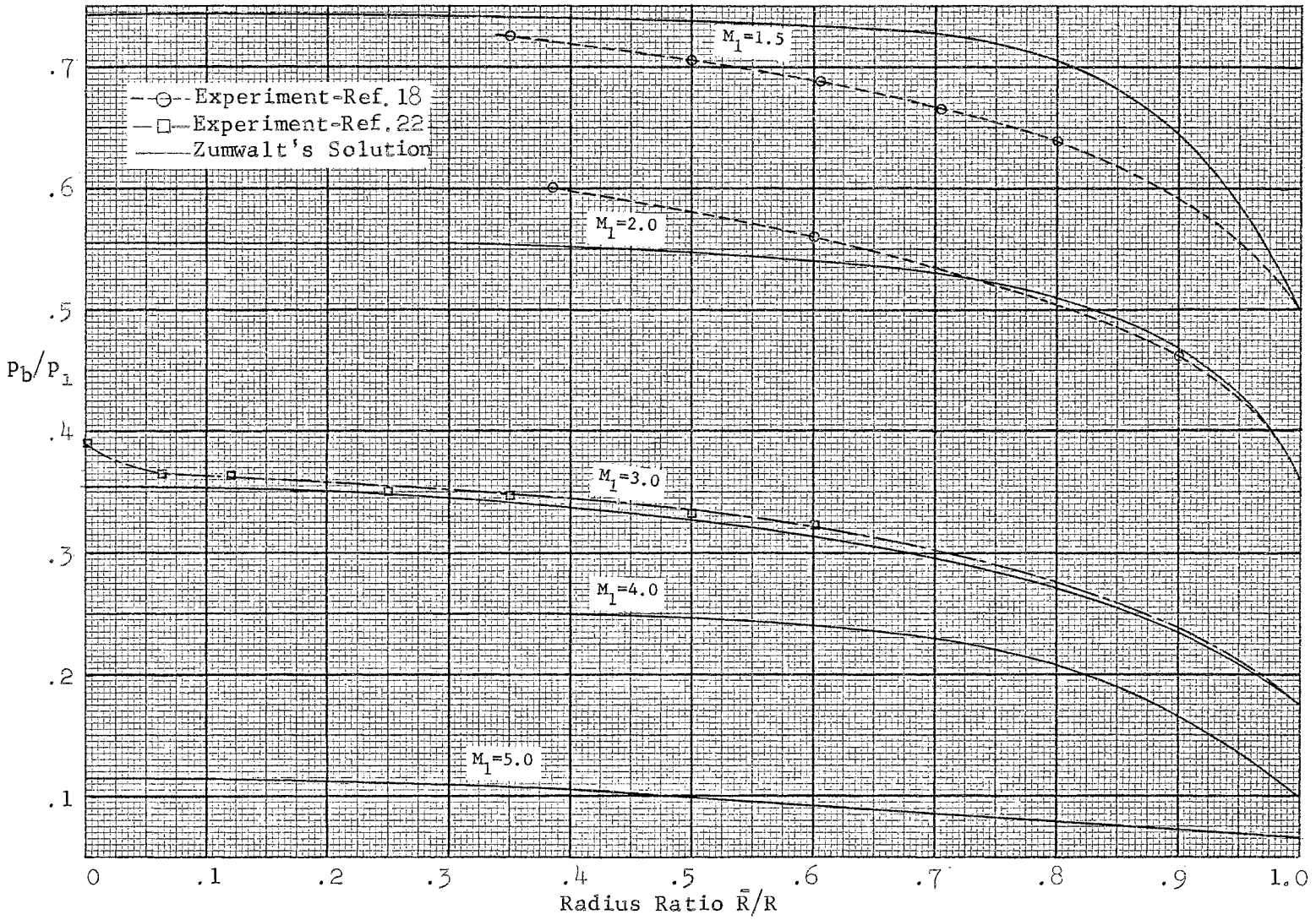

Figure 22. Comparison of the Conical Flow Theory with Experiment for Steady External Flow Past a Cylinder with Reduced Radius.

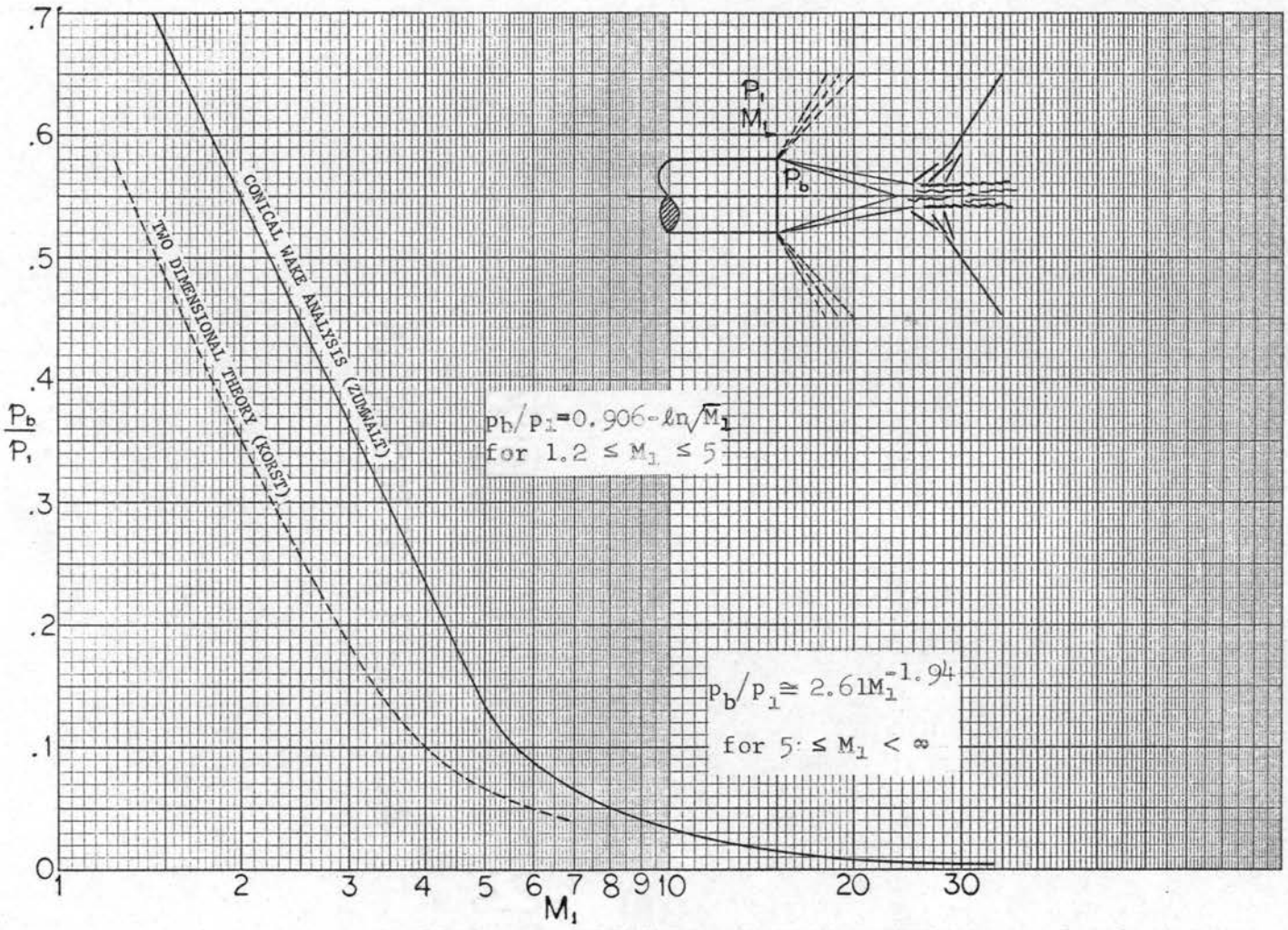

Figure 23. Steady, Non-Bleed, Base Pressure Solution by Using Zumwalt's Analysis.

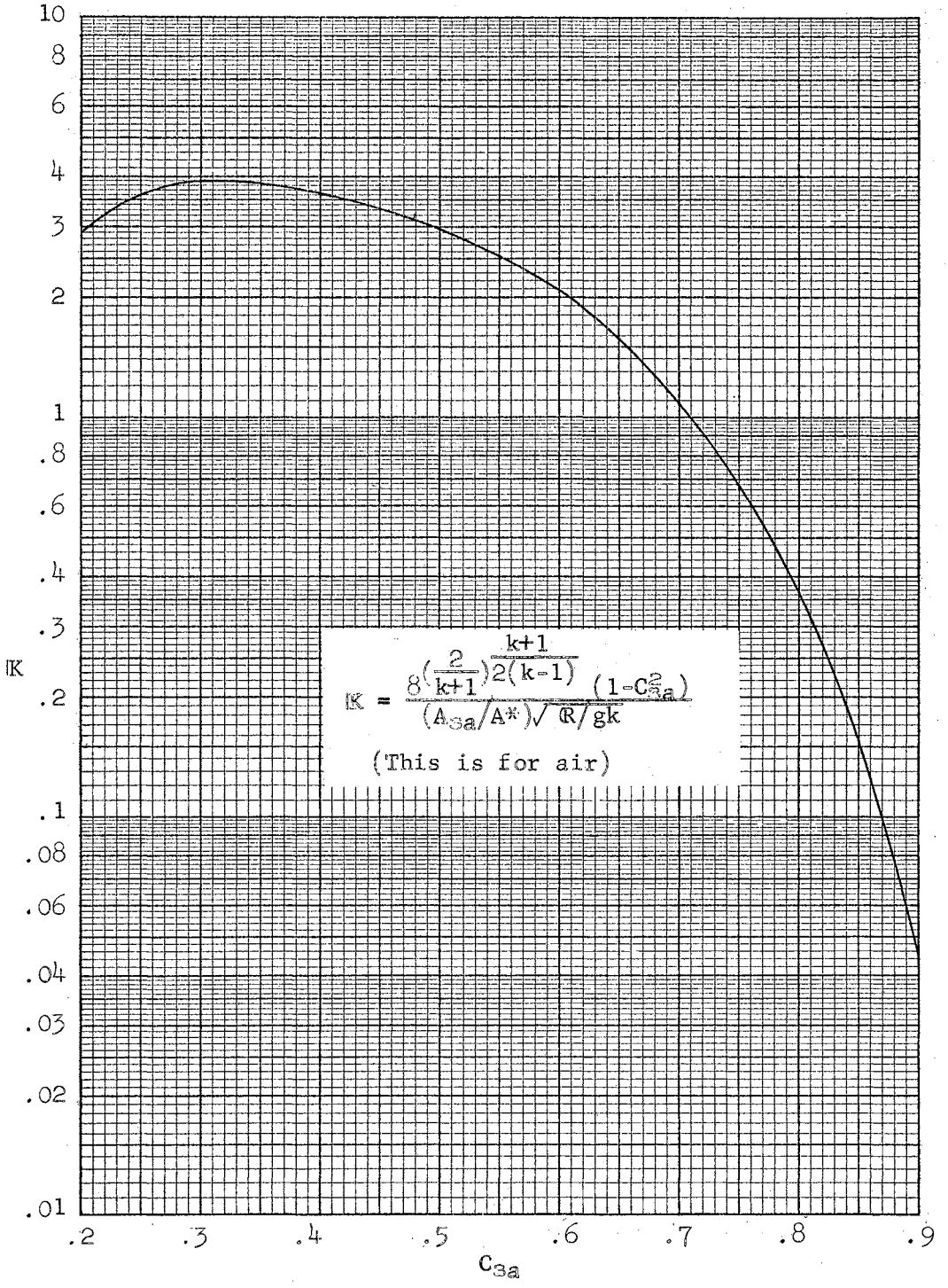

Figure 24. Plot of $\mathbb{K}$ Versus C_{3a} Curve for Use in Calculating G_d.

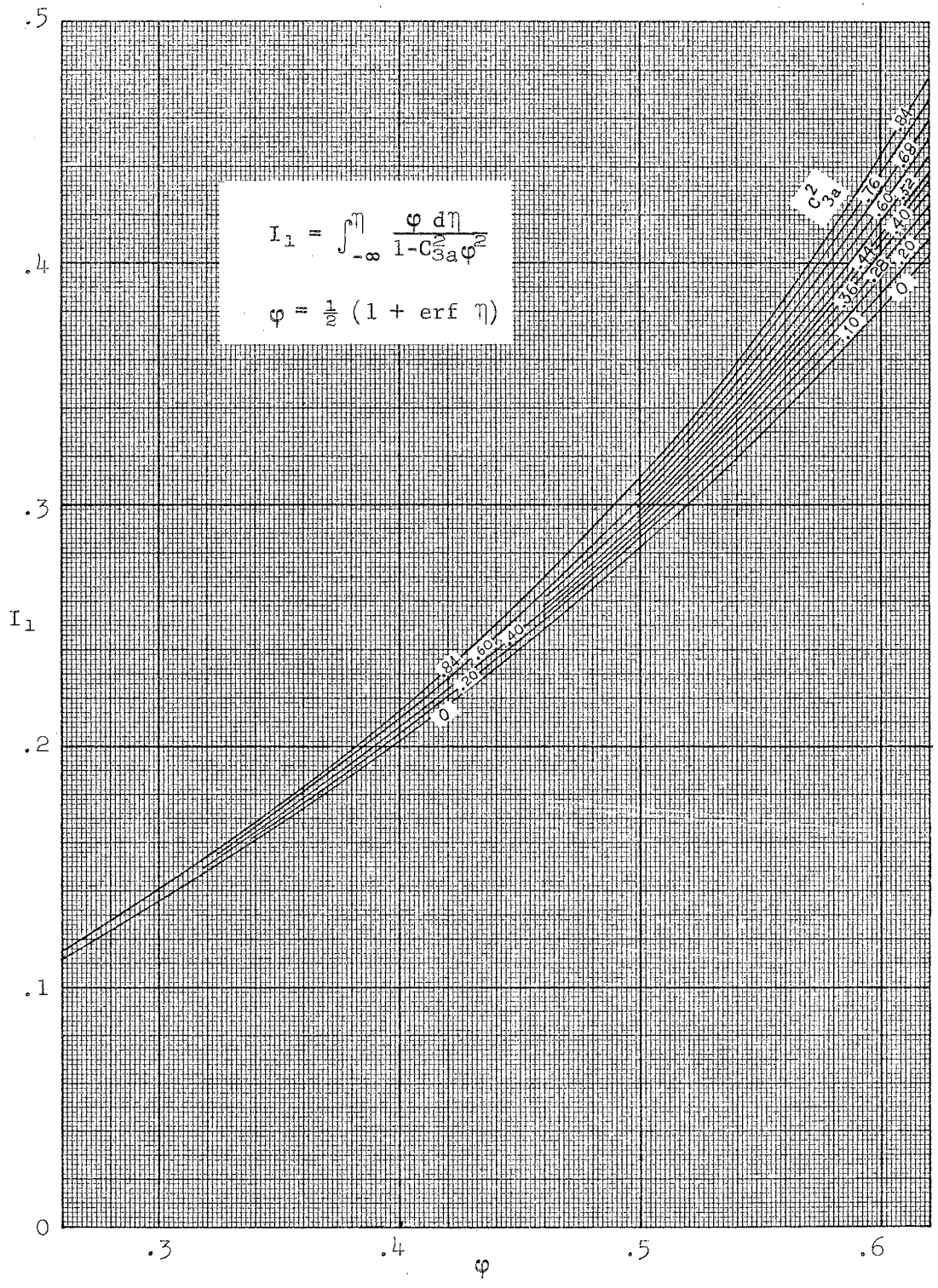

Figure 25(a). I_1 Integral for the Error Function Profile.

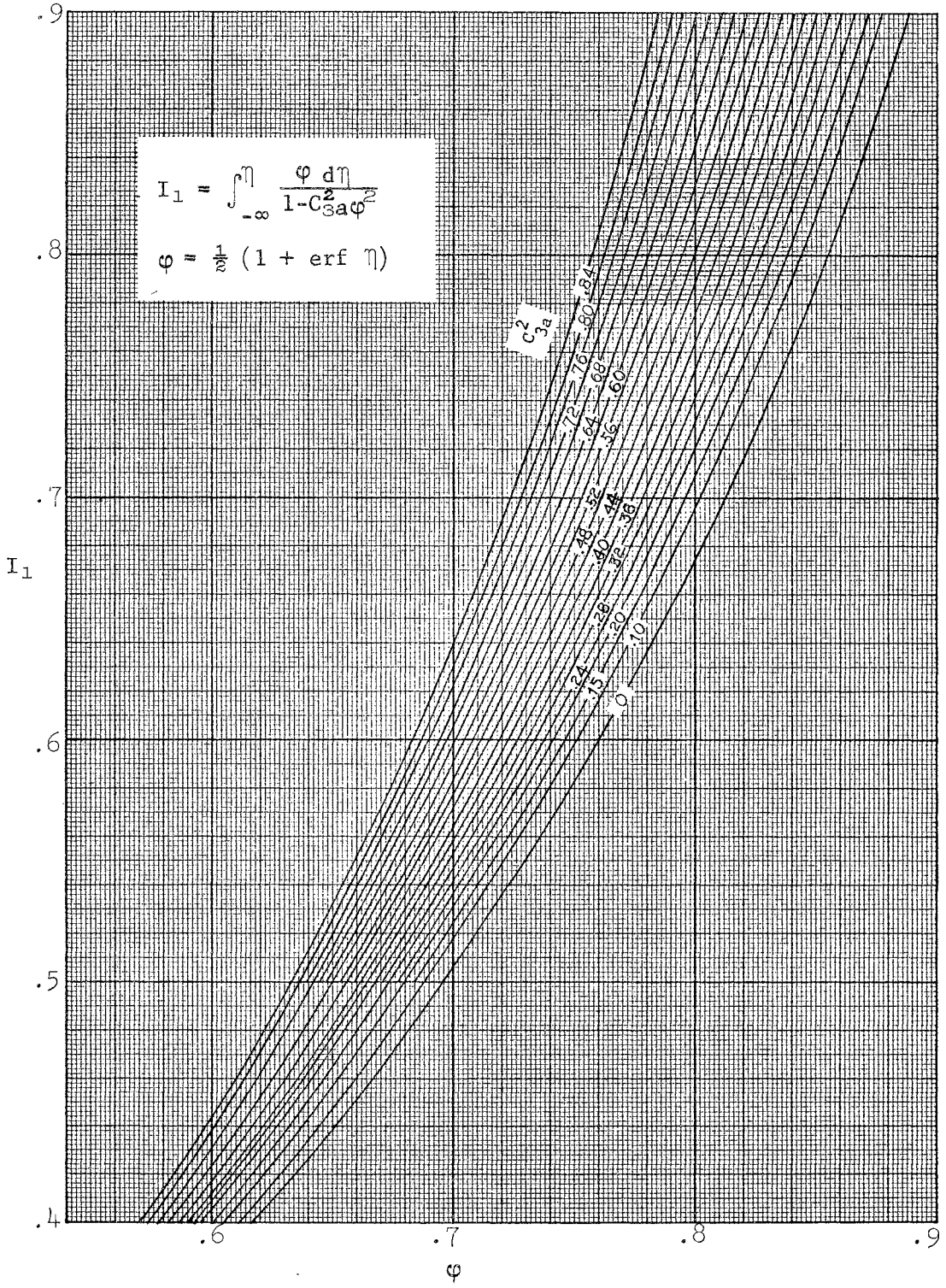

Figure 25(b). I_1 Integral for the Error Function Profile.

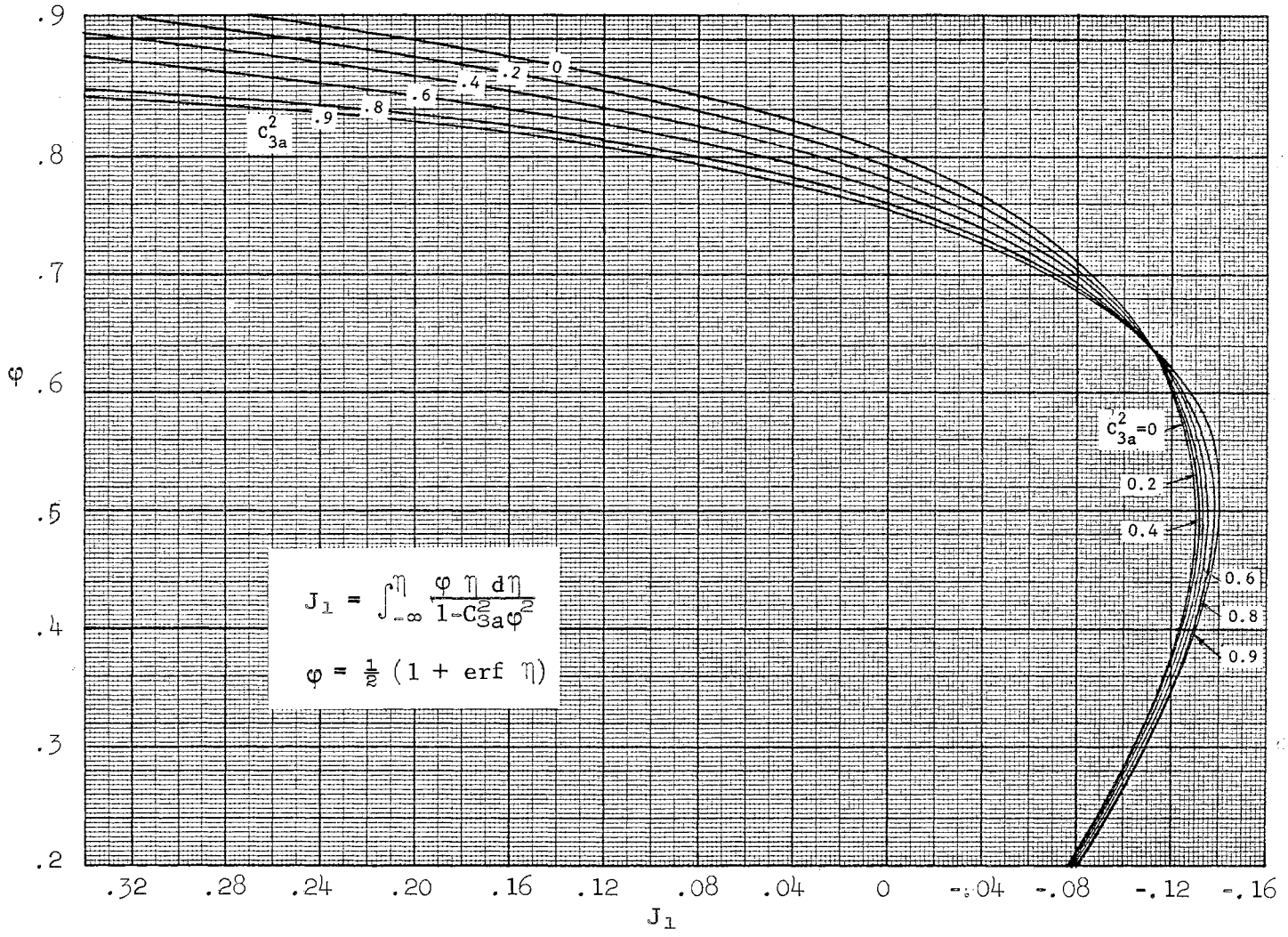

Figure 26. J_1 Integral for the Error Function Profile.

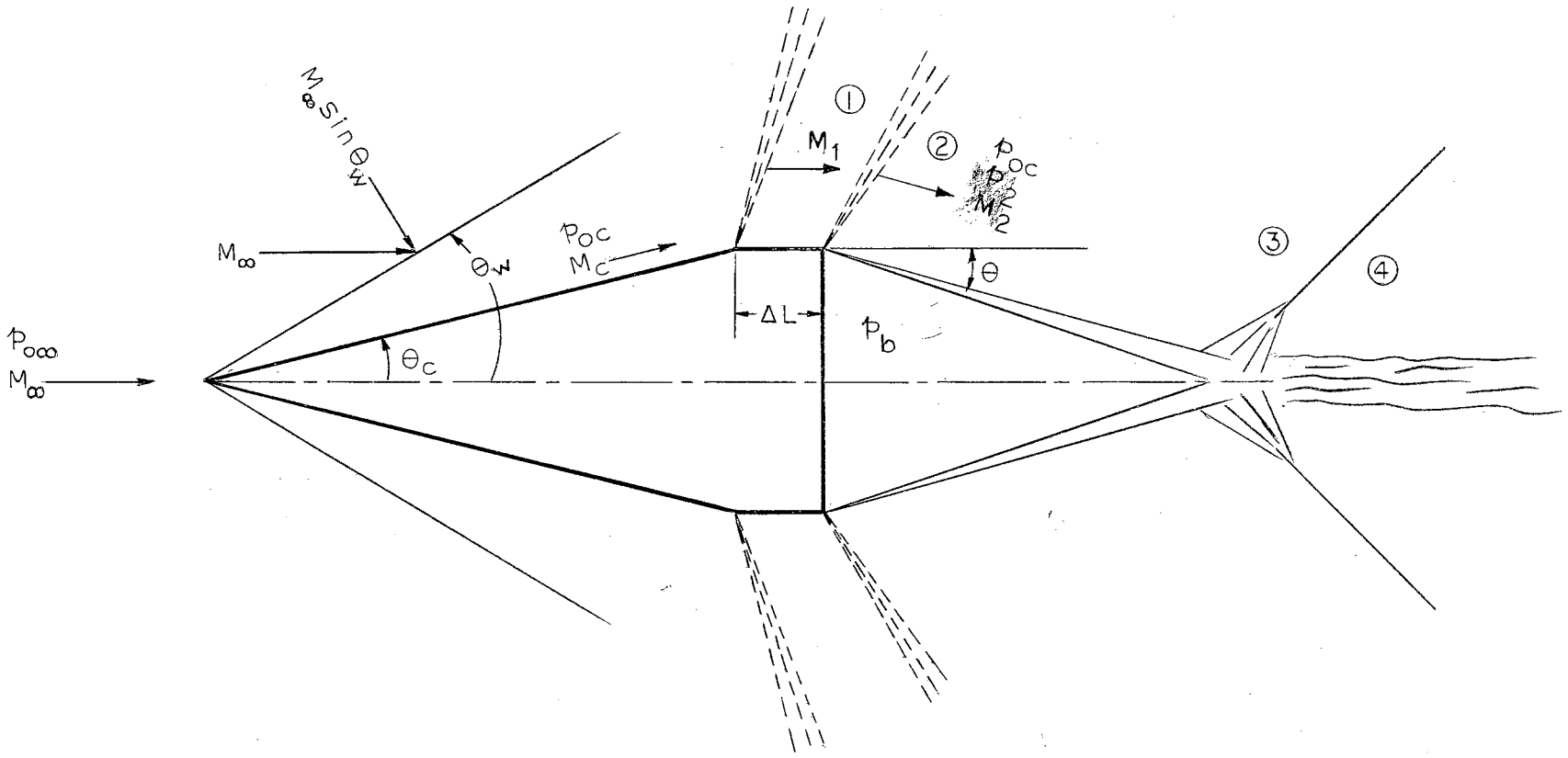

Subscript "x" is added to indicate conditions just before a blast wave intersects the cone head-on.
Subscript "y" is added to indicate conditions just after a blast wave has passed the position ④.

Figure 27. Flow Model for Appendix E.

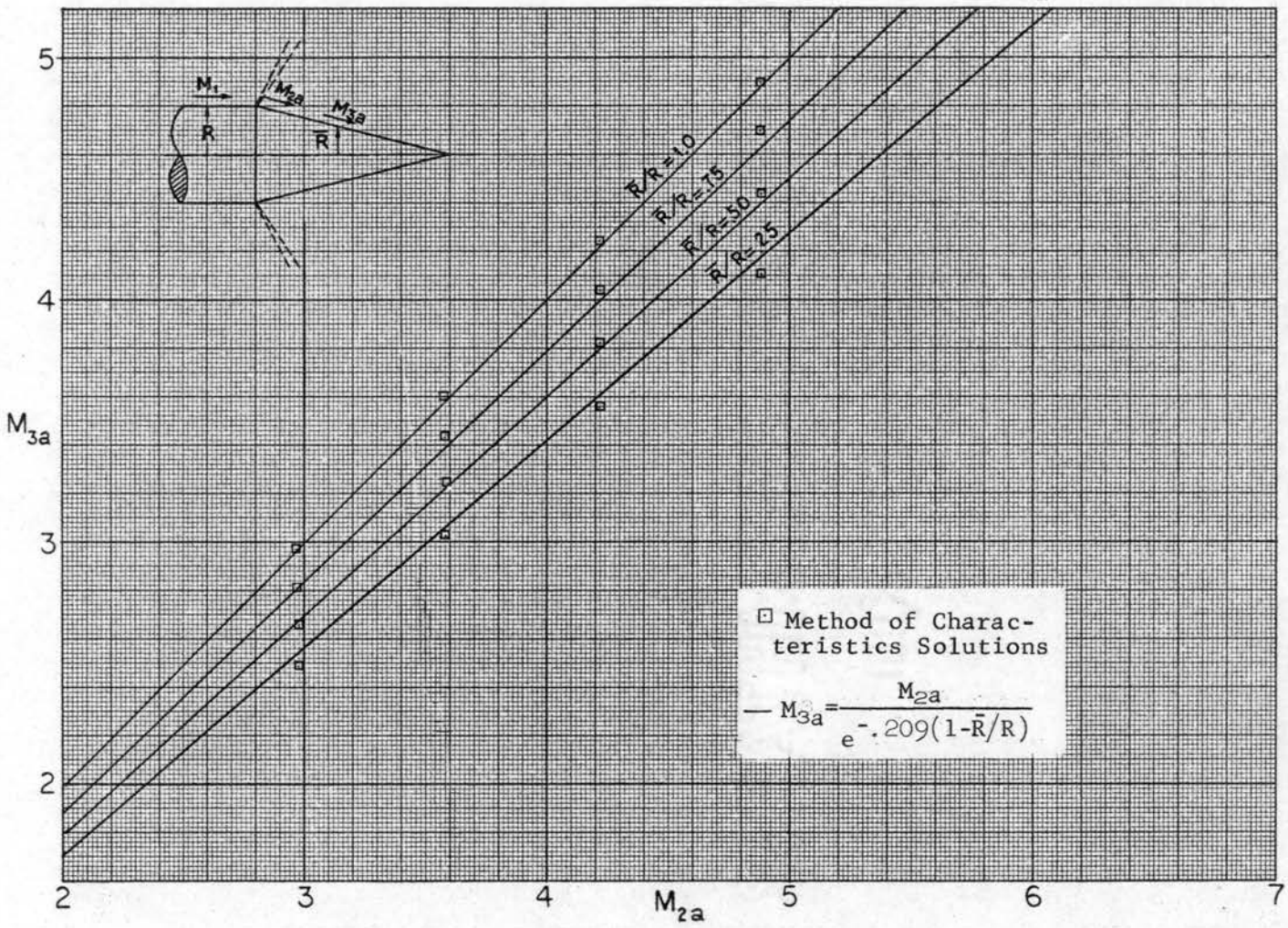

Figure 28. Comparison of Equation 11 and Exact Solution for Mach Number on a Conetail.

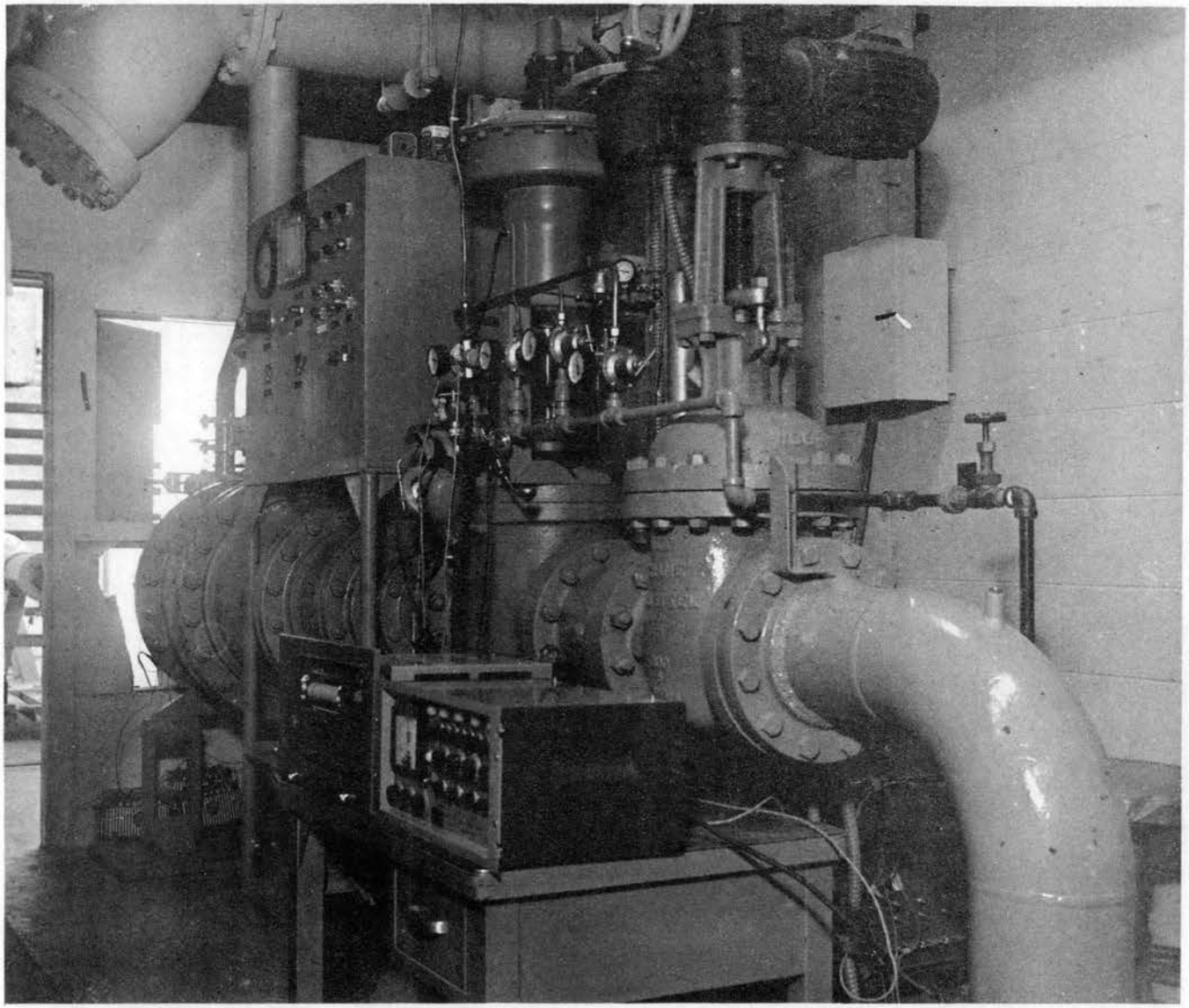

Figure 29. Wind Tunnel Unit with Supply Pressure Controls and Transient Phase Data Instrumentation.

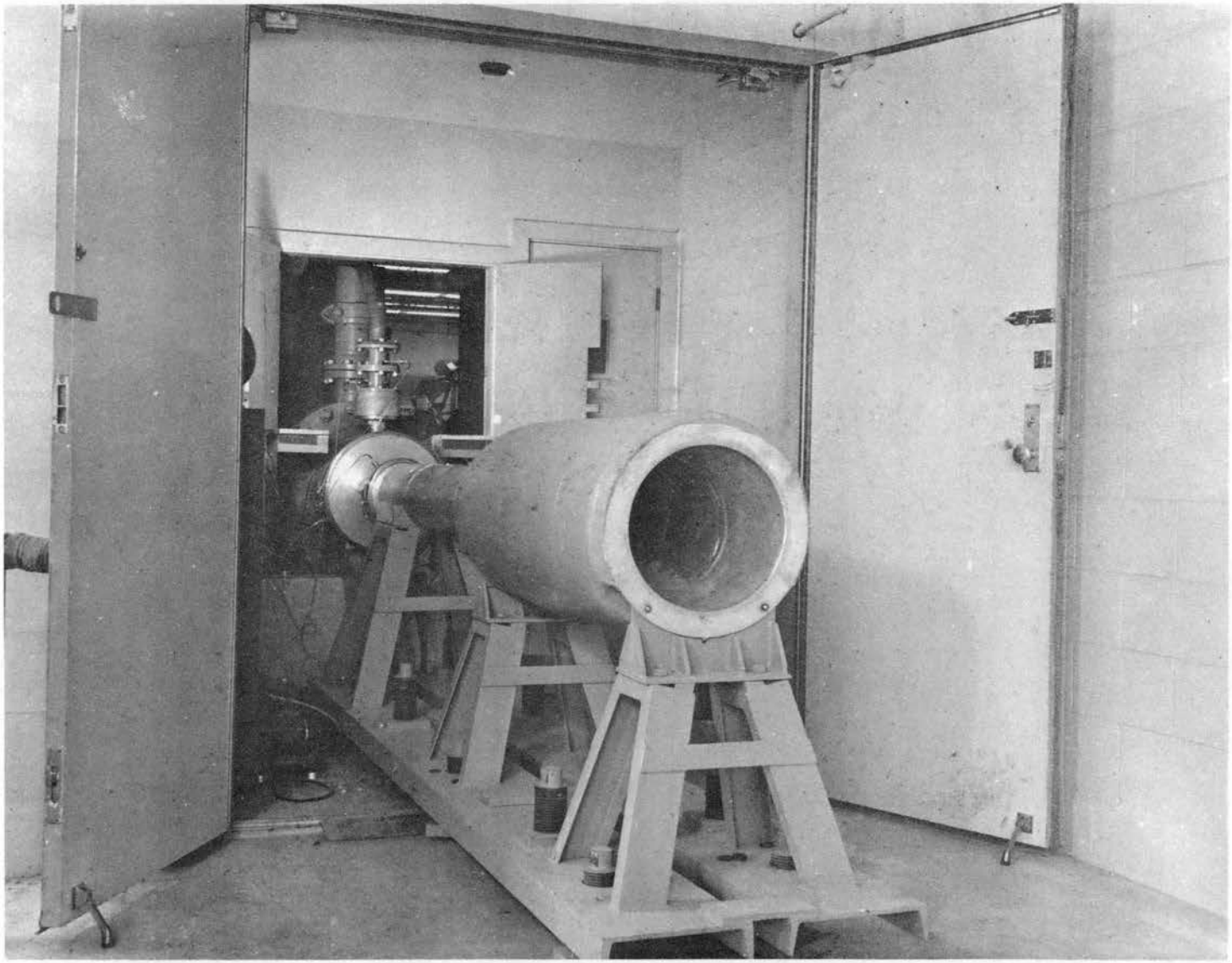

Figure 30. Mach 2 Annular Nozzle and the Outlet of Diffuser.

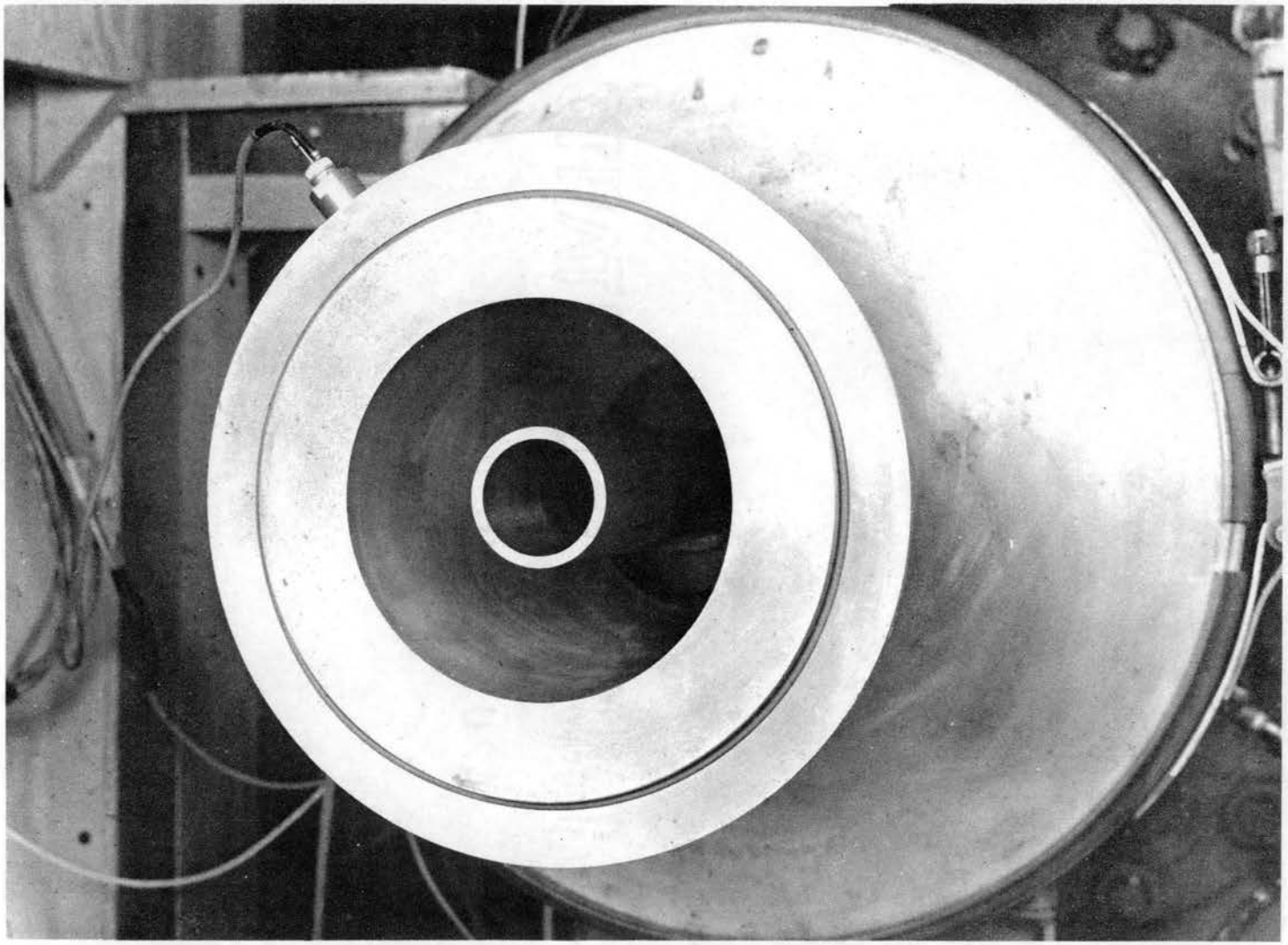

Figure 31. Extended Center Body Installed with Mach 2 Annular Nozzle for the Calibration Phase.

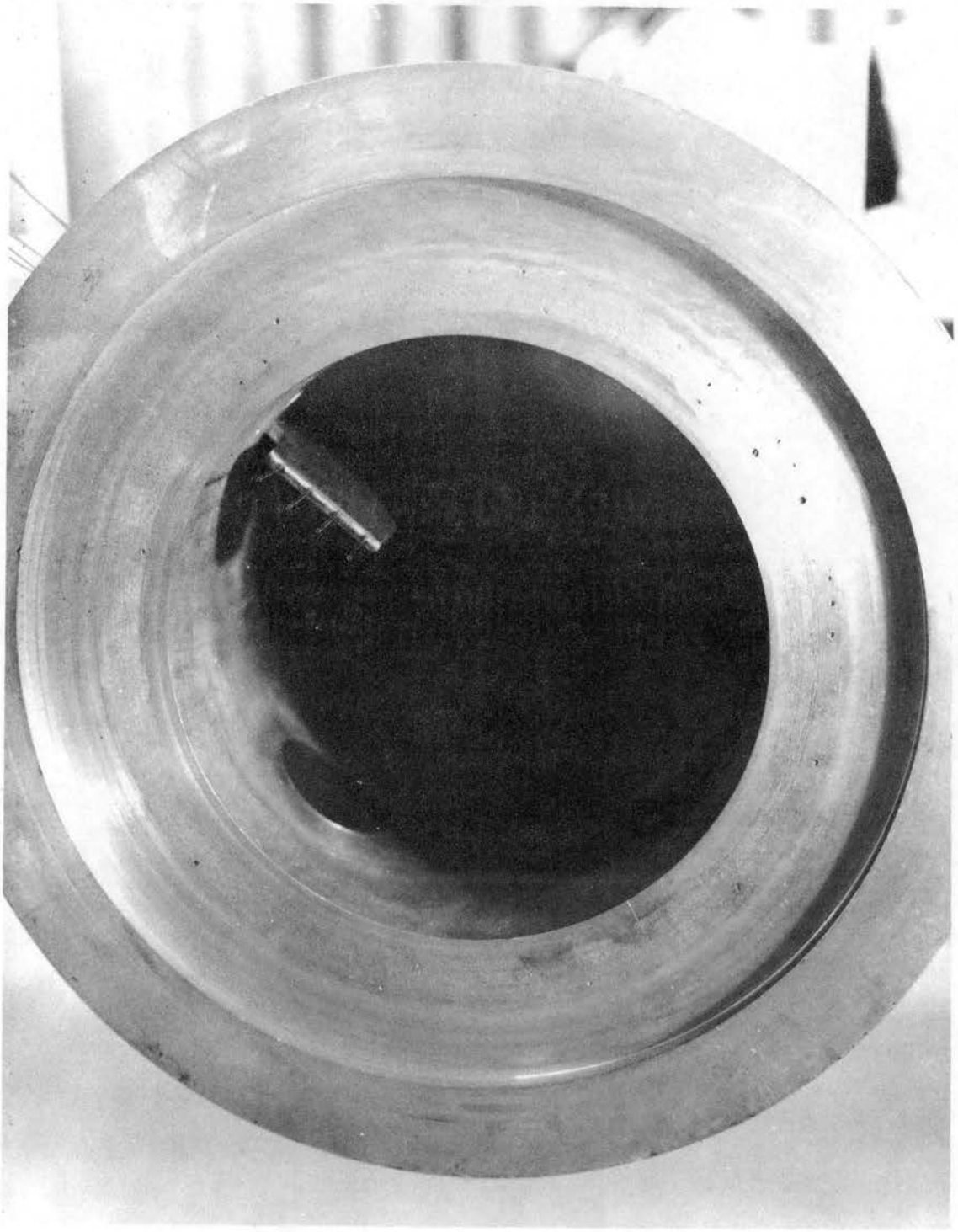

Figure 32. Rake Installed in the Diffuser Section for the Calibration Phase.

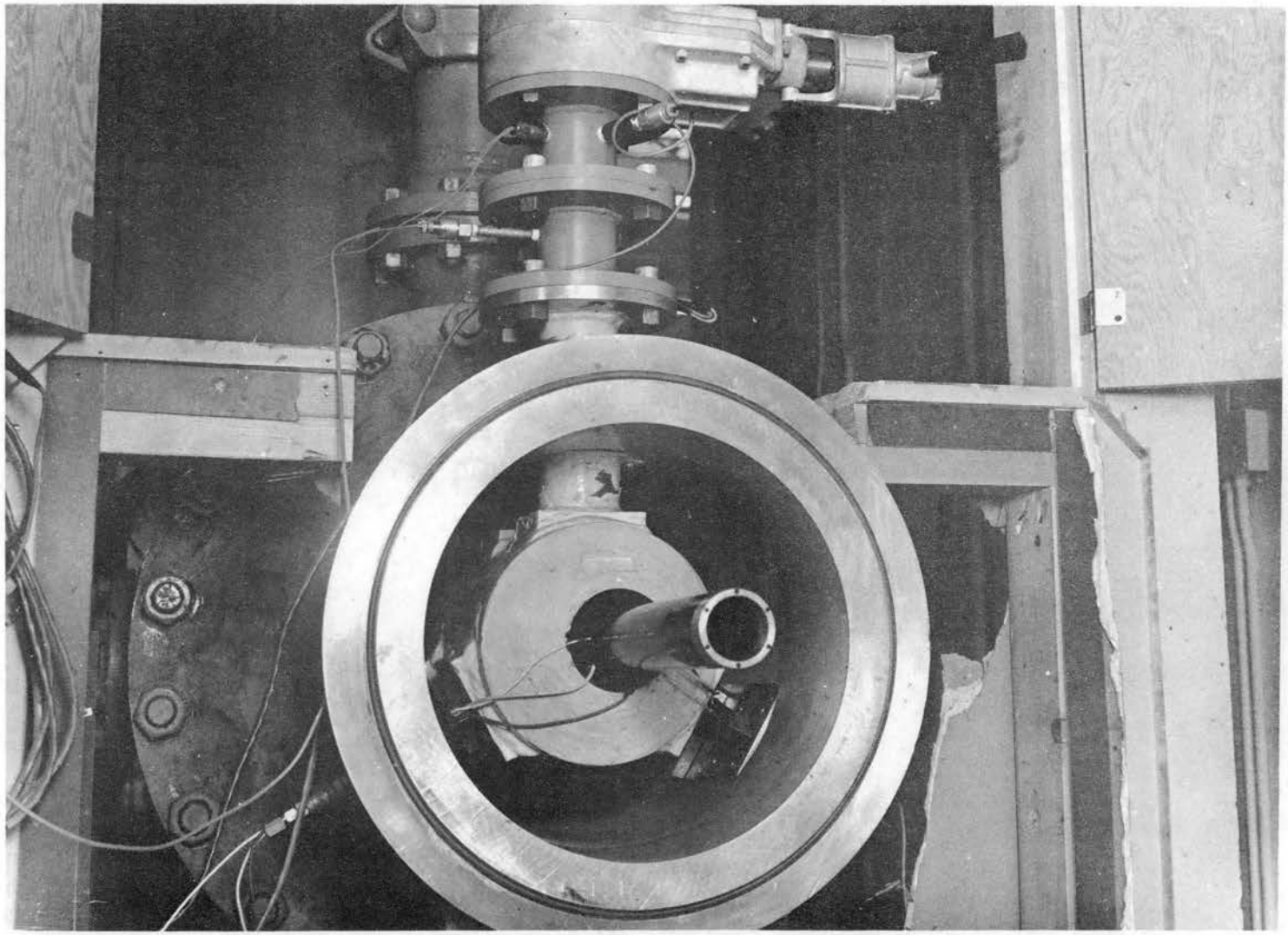

Figure 33. Base Tube with Nozzle Removed, Showing Base Tube Vented to Atmosphere When Valve is Opened.

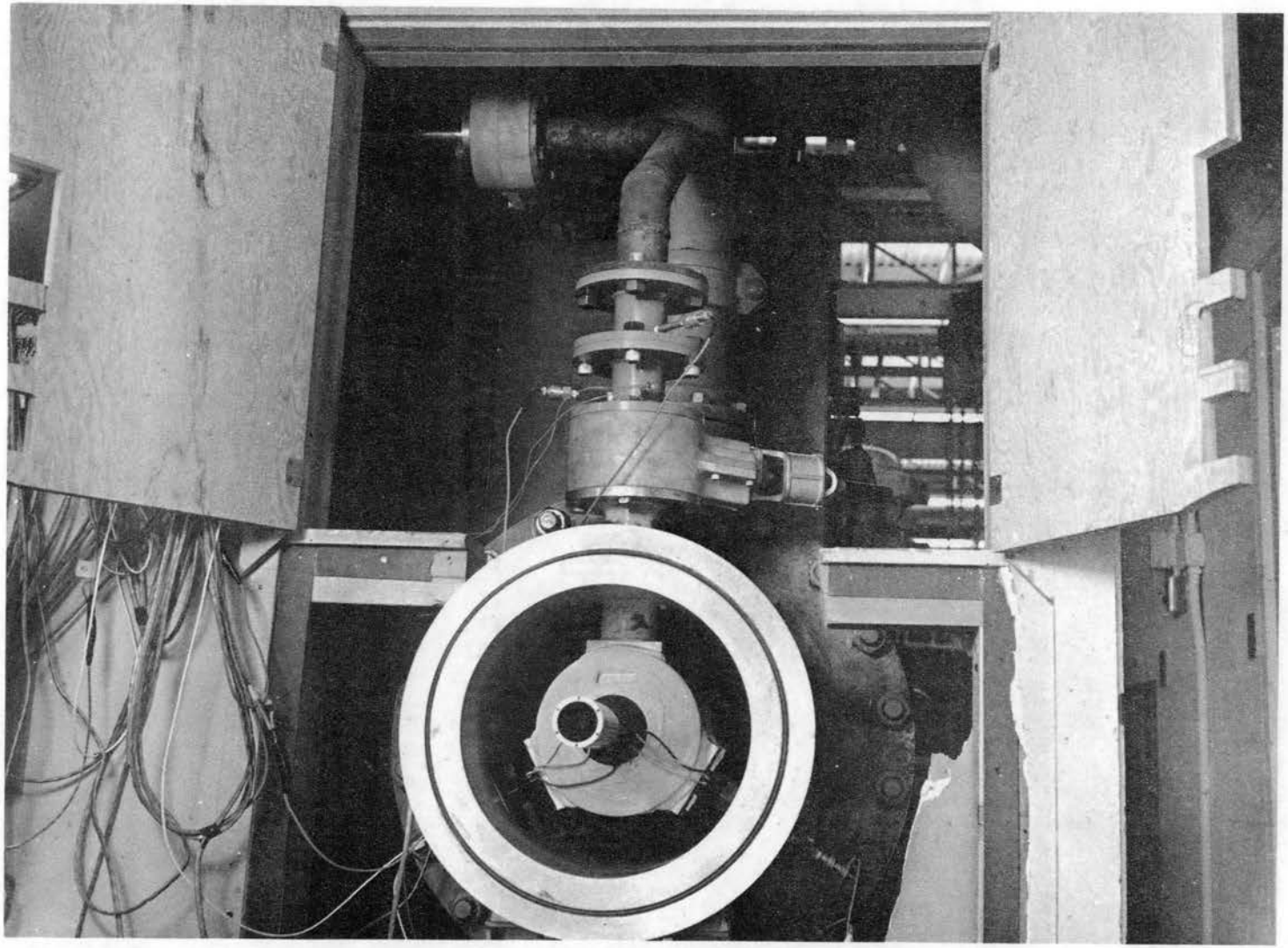

Figure 34. Base Tube with Nozzle Removed, Showing Base Tube Vented to Vacuum Source When Valve is Opened.

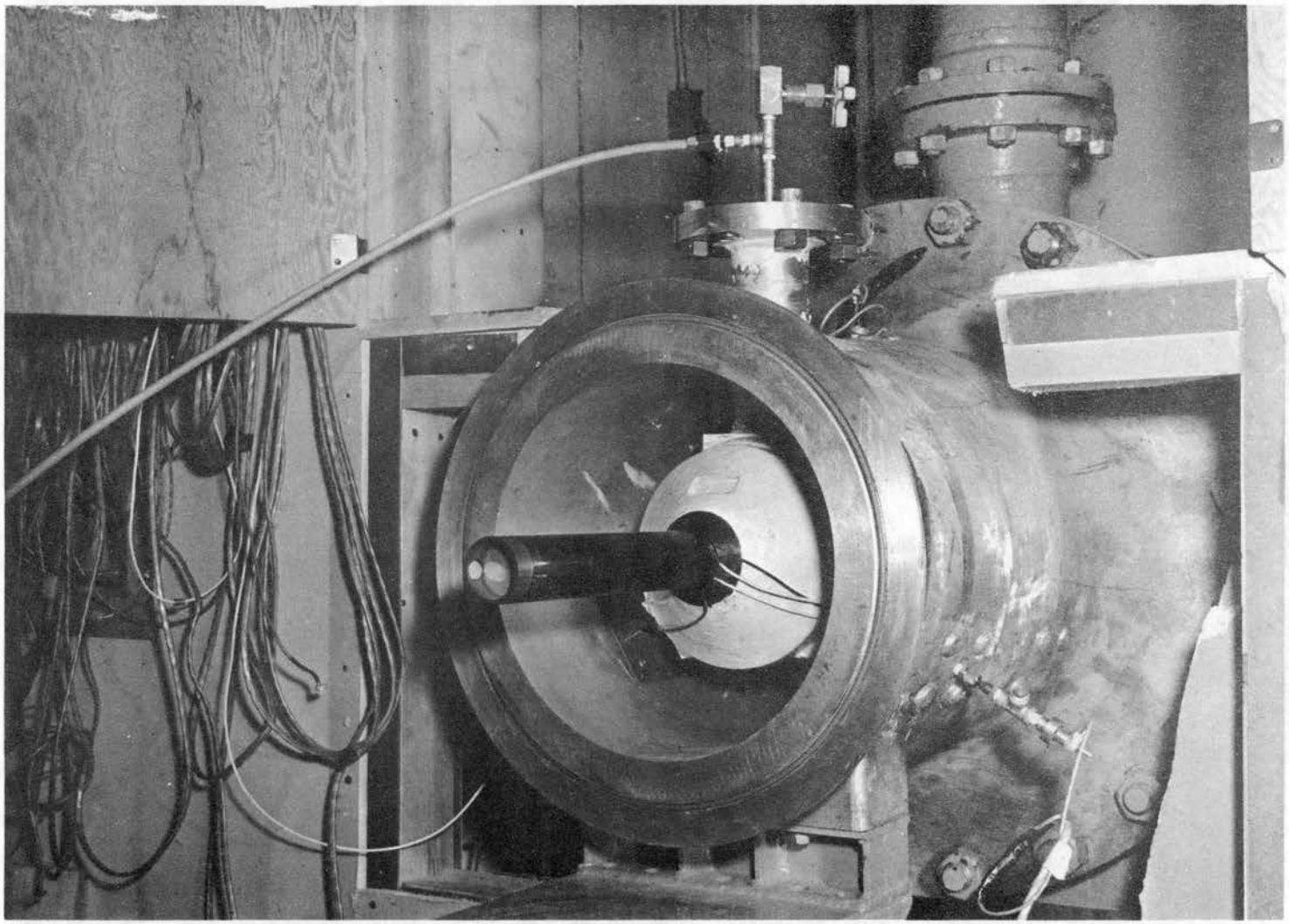

Figure 35. Base Tube for the Transient Phase, Showing Wafer Gage and Diaphragm Installed.

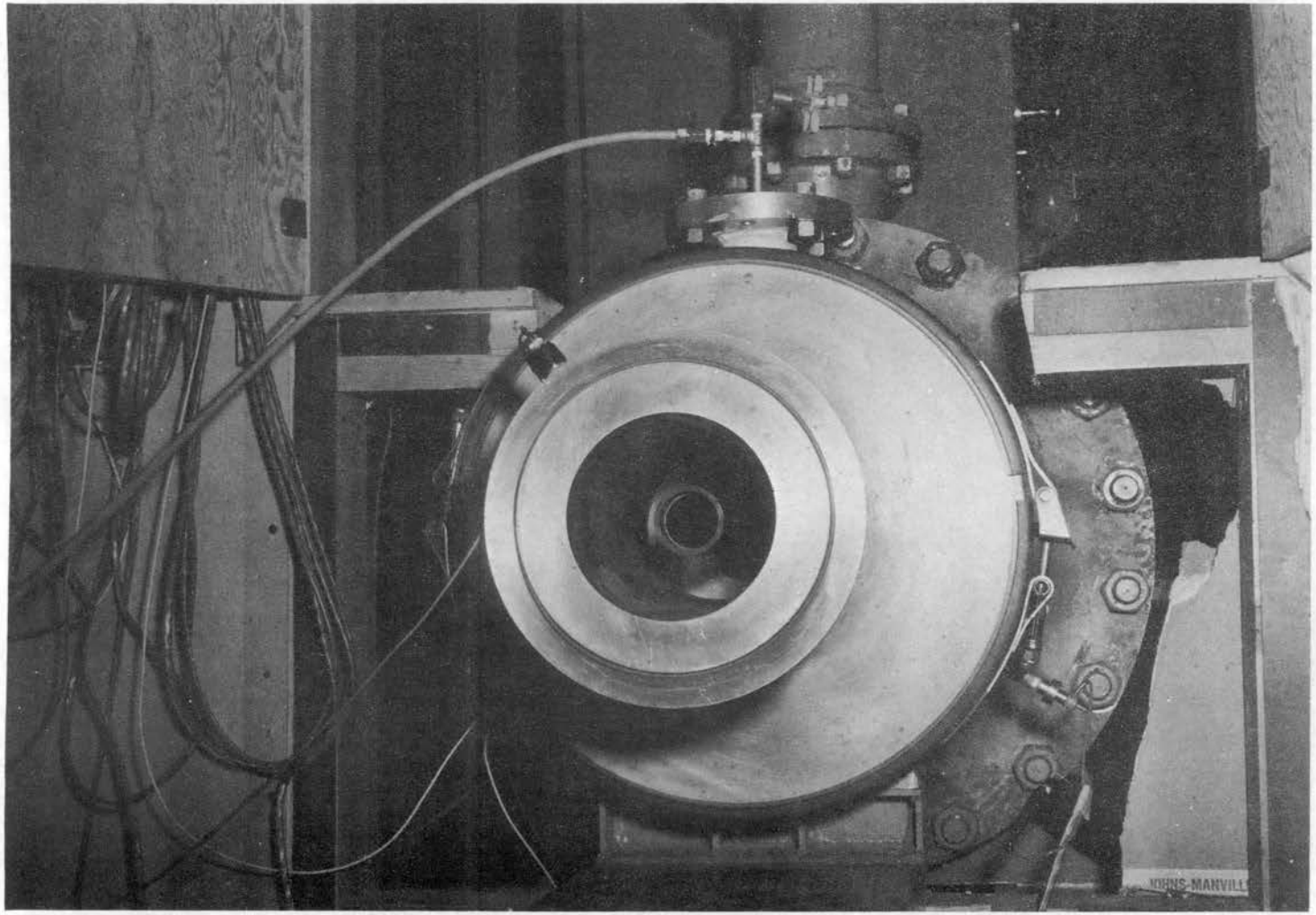

Figure 36. Base Tube with Annular Nozzle Installed, Showing the Diaphragm Burned Out Following a Transient Phase Test.

TABLES

TABLE I

CALIBRATION DATA OF MACH 2.0 NOZZLE (PHASE I)

Run No.	2	3	15
p_3, psia	6.230	4.892	6.562
p_o, psia	49.88	39.68	49.71
p_3/p_o	.1249	.1233	.1320
M_3	2.014	2.023	1.985
(pitot)p_{o4}, psia	35.59	28.34	35.79
p_{o4}/p_o	.7134	.7145	.7197
M_4	2.016	2.014	2.002
(pitot)p_{o5}, psia	35.56	28.32	35.67
p_{o5}/p_o	.7128	.7141	.7173
M_5	2.017	2.015	2.008
(pitot)p_{o6}, psia	35.79	28.49	35.91
p_{o6}/p_o	.7175	.7184	.7221
M_6	2.007	2.005	1.997
(pitot)p_{o7}, psia	35.90	28.50	35.83
p_{o7}/p_o	.7190	.7186	.7205
M_7	2.004	2.005	2.001

$M_{average}$ = 2.003 or p/p_o = 0.1270

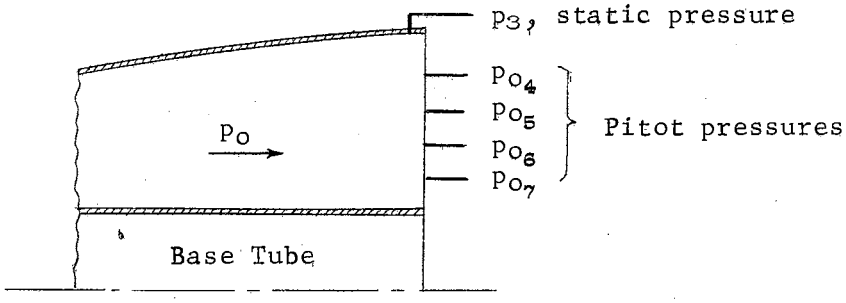

TABLE II

DATA ANALYSIS FOR STEADY, MASS-BLEED, BASE PRESSURE TESTS (PHASE II)
(all pressures in psia)

	Vented to Atmosphere				Vented to Vacuum			
Run No.	30	31	32	33	34	35	36	37
Orifice Dia.	1.0"	0.625"	0.5"	0.375"	0.625"	0.875"	1.5"	1.125"
Discharge Coeff.	1.0"	1.0"	0.60	0.60	1	1	1	1
Eff. Orifice Area	0.785in^2	0.3036	0.1178	0.0844	0.3066	0.6010	1.766in^2	0.9935
p_{atm}	12.14	12.15	12.14	12.14	12.14	12.14	12.13	12.12
p_{oo}, upstream of orif.	12.14	12.15	12.14	12.14	2.6617	1.8546	0.8050	1.1375
$\sqrt{T_o}$, $\sqrt{°R}$	23.38	23.29	23.28	23.27	23.27	23.23	23.22	23.21
p_o	49.58	50.12	49.85	50.11	50.24	49.85	49.90	49.96
*$\mathcal{K} = .2356\, Ap_{oo}/p_o$	.04528	.01751	.00675	.00481	-.00382	-.00526	-.00671	-.00532
p_b(Steady-Bleed)	5.138	4.876	4.532	4.162	2.351	1.544	0.558	0.820
p_o	49.58	50.12	49.85	50.11	50.24	49.85	49.90	49.96
$p_1 (=.127 p_o)$	6.297	6.365	6.330	6.364	6.381	6.330	6.338	6.345
p_b/p_1	0.816	0.766	0.716	0.654	0.368	0.244	0.088	0.129

*For Choked Orifice: $\mathcal{K} = 0.532 \dfrac{A_o p_{oo}}{A_b p_o} \sqrt{\dfrac{\mathcal{R}}{gk}}$

Note: p_{oo} means p_o supplied to orifice

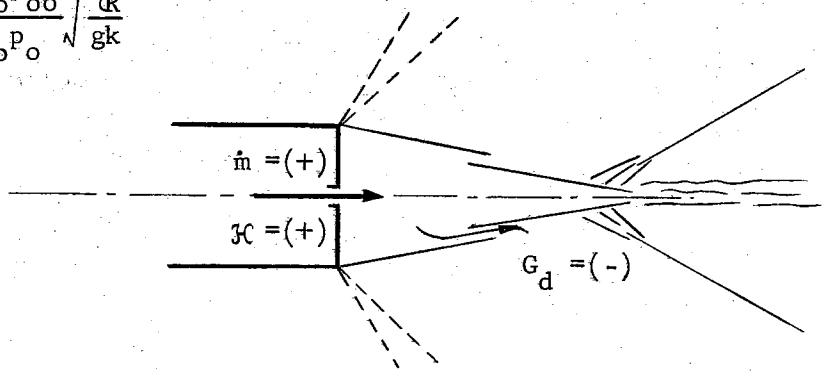

TABLE III

DATA ANALYSIS FOR STEADY, NON-BLEED, BASE PRESSURE TESTS (PHASE II)
(all pressure in psia)

Run No.	30	31	32	33	34	35	36	37
p_b	3.347	3.369	3.384	3.334	3.372	3.433	3.436	3.401
p_o	49.647	50.186	49.846	50.110	50.176	49.978	50.034	49.892
p_1	6.305	6.374	6.330	6.364	6.372	3.433	3.436	3.401
p_b/p_1	0.531	0.529	0.535	0.524	0.529	0.541	0.541	0.537

Average: $p_b/p_1 = 0.537$

TABLE IV

DATA ANALYSIS FOR TRANSIENT BASE PRESSURE TESTS (PHASE III)

Run	p_o	T_o	p_1	p_{bx}	p_c	p_a
41	50.32	543	6.391	3.334	1.52	12.09
42	50.33	551	6.392	3.393	2.05	12.10
44	49.64	539	6.304	3.300	0.89	12.13
45	50.15	540	6.369	3.334	2.68	12.11

Run 41 $\quad \dot{m} = \frac{p_o A_b}{\sqrt{T_o}} \sqrt{\frac{gk}{R}}(-\mathcal{K}) = 7.040(-\mathcal{K})$

t	0	0.05	0.10	0.15	0.20	0.25	0.30
p_b	1.833	2.281	2.595	2.890	3.103	3.228	3.297
p_b/p_1	0.2867	0.3568	0.4060	0.4523	0.4855	0.5050	0.5159
$-\mathcal{K}$	.00479	.00399	.00330	.00240	.00162	.00108	.00079
$\dot{m}$	0.0337	0.0281	0.0232	0.0169	0.0014	0.0076	0.0054

Run 42 $\quad \dot{m} = 6.971(-\mathcal{K})$

t	0	0.05	0.10	0.15	0.20	0.25
p_b	2.173	2.654	3.000	3.254	3.384	3.393
p_b/p_1	0.3400	0.4152	0.4693	0.5091	0.5294	0.5308
$-\mathcal{K}$	.00420	.00314	.00202	.00097	.00035	0
$\dot{m}$	0.0293	0.0219	0.0141	0.0068	0.0024	0

Run 44 $\quad \dot{m} = 7.959(-\mathcal{K})$

t	0	0.05	0.10	0.15	0.20	0.25	0.30	0.35	0.40
p_b	0.736	1.429	2.080	2.579	2.884	3.069	3.198	3.254	3.300
p_b/p_1	0.1167	0.2267	0.3300	0.4091	0.4575	0.4868	0.5073	0.5161	0.5400
$-\mathcal{K}$	.00642	.00541	.00431	.00325	.00229	.00159	.00103	.00075	0
$\dot{m}$	0.0447	0.0376	0.0299	0.0226	0.0159	0.0111	0.0072	0.0052	0

Run 45 $\quad \dot{m} = 7.018(-\mathcal{K})$

t	0	0.02	0.04	0.06	0.08	0.10
p_b	2.891	2.946	3.037	3.168	3.260	3.334
p_b/p_1	0.4538	0.4625	0.4767	0.4973	0.5118	0.5400
$-\mathcal{K}$	.00237	.00217	.00183	.00131	.00088	0
$\dot{m}$	0.0166	0.0152	0.0128	0.0092	0.0062	0

Units: T_o = °R
t = seconds
p = psia
$\dot{m}$ = lb_m/sec

SELECTED BIBLIOGRAPHY

1. Korst, H. H., R. H. Page, and M. E. Childs. "A Theory for Base Pressures in Transonic and Supersonic Flow." Univ. of Illinois, Engrg. Exper. Sta., ME-TN-392-2, OSR-TN-55-89, Contract No. AF 18(600)392, March 1955.

2. Chapman, D. R., "Laminar Mixing of a Compressible Fluid," NACA Report 958, 1950.

3. Pai, S. I., "Two-Dimensional Mixing of a Compressible Fluid," Journal of the Aero. Sci., V. 16., No. 8, pp. 463-469, 1949.

4. Pai, S. I., "Axially Symmetrical Jet Mixing of a Compressible Fluid," Quart. Applied Mathematics, 10 No. 2, July 1952, pp. 141-148.

5. Crane, L. J., "The Laminar and Turbulent Mixing of Jets of Compressible Fluids; Part II, The Mixing of Two Semi-Infinite Streams," Journal of Fluid Mechanics, Vol. 3, January 1958.

6. Zumwalt, G. W., "Analytical and Experimental Study of the Axially-Symmetric Supersonic Base Pressure Problem," Ph.D. Dissertation, Dept. of Mech. Engrg., Univ. of Illinois, 1959.

7. Maydew, R. C., and J. F. Reed, "Turbulent Mixing of Axisymmetric Compressible Jets (In the Half-Jet Region) with Quiescent Air," SC-4764(RR), Sandia Corporation, Albuquerque, N. M., March 1963.

8. Görtler, H., "Berechnung von Aufgaben der freien Turbulenz auf Grund eines neuen Naherungsansatzes," Z.A.M.M., V. 22, pp. 244-254, 1942.

9. Love, E. S., "Base Pressure at Supersonic Speeds on Two-Dimensional Airfoils and on Bodies of Revolution With and Without Fins Having Turbulent Boundary Layers," NACA TN-3819 Report, January 1957.

10. Beheim, M. A., "Flow in the Base Region of Axisymmetric and Two-Dimensional Configurations," Lewis Research Center, NASA-TR-R-77, 1960.

11. Channapragada, R. S., "Compressible Jet Spread Parameter for Mixing Zone Analysis," Journal of AIAA, Vol. 1, No. 9, September 1963, pp. 2188-2189.

12. "IBM Problem M Curves," Technical Memorandum SCTM 268-56-51, the Sandia Corporation, Reprinted June 1960.

13. Tripp, Wilson, "Analytical and Experimental Investigation of the Base Pressure Behind a Blunt Trailing Edge for Supersonic Two-Dimensional Flow. (Approaching streams have same stagnation temperatures, but different Mach numbers and stagnation pressures)," Ph.D. Thesis, Univ. of Illinois, June 1956.

14. Chrisman, C. C., and G. W. Zumwalt, "Evaluation of the Free Jet Spreading Rate Parameter for Axi-Symmetric Air Flow at M = 3." Research Report prepared for the Aero-Thermodynamics Dept. of Sandia Corporation, Albuquerque, N. M., by the Office of Engineering Research, Okla. State Univ., Stillwater, Okla., Report No. SBW-3, June 1962.

15. Golik, R. J., "On Dissipative Mechanisms Within Separated Flow Regions," Ph.D. Dissertation, Dept. of Mech. Engrg., Univ. of Illinois, 1962.

16. Zumwalt, G. W. and H. H. Tang, "Computation Curves for Axi-Symmetric Base Pressure Analysis," Research Report prepared for the Aero-Thermodynamics Dept. of Sandia Corporation, Albuquerque, N. M., by the Office of Engineering Research, Okla. State Univ., Stillwater, Okla. Report No. SBW-4, April 1963.

17. Reller, J. O., Jr. and F. M. Hamaker, "An Experimental Investigation of the Base Pressure Characteristics of Non-lifting Bodies of Revolution at Mach Numbers from 2.73 to 4.98," NACA-TN-3393, March 1955, (Supercedes RM A 52E20.)

18. Chapman, D. R., "An Analysis of Base Pressure at Supersonic Velocities and Comparison with Experiments," NACA Report 1051, 1951.

19. Korst, H. H., W. L. Chow, and G. W. Zumwalt, "Research on Transonic and Supersonic Flow of a Real Fluid at Abrupt Increases in Cross Section,"ME-TN-392, Engineering Experiment Station, Univ. of Illinois, December 1959.

20. Ames Research Staff, "Equations, Tables, and Charts for Compressible Flow," NACA Report 1135, 1953.

21. Zumwalt, G. W. and H. H. Tang, "Blast Wave Effect on Missile Base Pressure," Research Report SBW-1 for Sandia Corporation, P. O. 12-8012, Office of Engineering Research, Oklahoma State University, June 1961.

22. Sivier, K. R. and S. M. Bogdonoff, "The Effect of Support Interference on the Base Pressure of a Body of Revolution," Report No. 332, Princeton University, AFOSR RN-55-301, October 1955.

23. Tang, H. H., and G. W. Zumwalt, "Adaptation of Chapman's Laminar Jet Mixing Theory for Use in Non-Steady Base Pressure Problems," Research Report prepared for the Aero-Thermodynamics Dept. of Sandia Corporation, Albuquerque, N. M., by the Office of Engrg. Research, Okla. State Univ., Stillwater, Okla. Rpt. SWB-2, June 1962.

APPENDIX A

SOLUTION OF EQUATION 6, CHAPTER II

For Equation 6, $\frac{\partial \varphi}{\partial \xi} = \frac{\partial^2 \varphi}{\partial \zeta^2}$, $\varphi = \varphi(x, y)$.

The following initial and boundary conditions apply:

1. $\varphi(0,\zeta) \equiv 0$ for $-\infty < \zeta < 0$; i.e., velocity exists only for $y > 0$ at $x = 0$.

2. $\varphi(0,\zeta) \equiv \varphi_2(\zeta)$ for $0 < \zeta < 1$; i.e., for $x = 0$, velocity is a function of y within the boundary layer.

3. $\varphi(0,\zeta) \equiv 1$ for $1 < \zeta < +\infty$; i.e., for $x = 0$, velocity is constant outside the boundary layer.

4. $\varphi(\xi,-\infty) \to 0$ for $\xi > 0$; i.e., for all $x > 0$, velocity approaches zero as $y \to -\infty$.

5. $\varphi(\xi,+\infty) \to 1$ for $\xi > 0$; i.e., for all $x > 0$, velocity approaches u_{2a} as $y \to +\infty$.

φ is replaced to make an ordinary differential equation: $\varphi = \ell\, b$,

where $\ell \equiv \ell(\xi)$ and $b \equiv b(\zeta)$,

$$b \frac{d\ell}{d\xi} = \ell \frac{d^2 b}{d\zeta^2}.$$

Separating variables results in a "separation constant," $-\lambda^2$.

$$\frac{1}{\ell}\frac{d\ell}{d\xi} = \frac{1}{b}\frac{d^2 b}{d\zeta^2} = -\lambda^2$$

$$\frac{d\ell}{d\xi} + \lambda^2 \ell = 0; \quad \frac{d\ell}{\ell} = -\lambda^2 d\xi; \quad \ell = c_1 e^{-\lambda^2 \xi}$$

$$\frac{d^2 b}{d\zeta^2} + b\lambda^2 = 0; \quad \frac{1}{b}\frac{d^2 b}{d\zeta^2} = -\lambda^2; \quad b = c_2 \cos\lambda\zeta + c_3 \sin\lambda\zeta.$$

Therefore,

$$\varphi = e^{-\lambda^2\xi}\left[A\cos\lambda\zeta + B\sin\lambda\zeta\right].$$

The Fourier Integral for this, where f( ) represents boundary conditions, is , with ζ' as a dummy variable in the Fourier analysis:

$$f(x) = \frac{1}{\pi}\int_0^\infty\int_{-\infty}^\infty f(\zeta')\cos\lambda(\zeta'-\zeta)d\zeta'd\lambda$$

$$A = \frac{1}{\pi}\int_{-\infty}^\infty f(\zeta')\cos\lambda\zeta'd\zeta',$$

$$B = \frac{1}{\pi}\int_{-\infty}^\infty f(\zeta')\sin\lambda\zeta'd\zeta'.$$

$$\varphi = \frac{1}{\pi}\int_0^\infty e^{-\lambda^2\xi}\left\{\cos\lambda\zeta\int_{-\infty}^\infty f(\zeta')\cos\lambda\zeta'd\zeta' + \sin\lambda\zeta\int_{-\infty}^\infty f(\zeta')\sin\lambda\zeta'd\zeta'\right\}d\lambda$$

$$= \frac{1}{\pi}\int_0^\infty e^{-\lambda^2\xi}\left[\int_{-\infty}^\infty f(\zeta')(\cos\lambda\zeta\cos\lambda\zeta' + \sin\lambda\zeta\sin\lambda\zeta')d\zeta'\right]d\lambda$$

$$= \frac{1}{\pi}\int_0^\infty e^{-\lambda^2\xi}\left[\int_{-\infty}^\infty f(\zeta')\cos\lambda(\zeta'-\zeta)d\zeta'\right]d\lambda .$$

Inverting the order of integration:

$$\varphi = \frac{1}{\pi}\int_{-\infty}^\infty f(\zeta')\left[\int_0^\infty e^{-\lambda^2\xi}\cos\lambda(\zeta'-\zeta)d\lambda\right]d\zeta'.$$

Let $$Q = \int_0^\infty e^{-\lambda^2\xi}\cos\lambda(\zeta'-\zeta)d\lambda,$$

$$\frac{dQ}{d(\zeta'-\zeta)} = \int_0^\infty -\lambda e^{-\lambda^2\xi}\sin\lambda(\zeta'-\zeta)d\lambda$$

$$= \frac{\sin\lambda(\zeta'-\zeta)}{2\xi} e^{-\lambda^2\xi}\Big|_0^\infty - \frac{\zeta'-\zeta}{2\xi}\int_0^\infty e^{-\lambda^2\xi}\cos\lambda(\zeta'-\zeta)d\lambda$$

$$= 0 - \frac{\zeta'-\zeta}{2\xi}\, Q.$$

$$\frac{dQ}{Q} = -\frac{(\zeta'-\zeta)}{2\xi}\, d(\zeta'-\zeta),$$

$$\ell n\, Q = \frac{-(\zeta'-\zeta)^2}{4\xi} + K \text{ or } Q = Ke^{-\frac{(\zeta'-\zeta)^2}{4\xi}}.$$

Evaluating K, when $(\zeta'-\zeta) = 0$, $K = Q$.

$$Q_{(\zeta'-\zeta)=0} = K = \int_0^\infty e^{-\lambda^2\xi} d\lambda = \frac{\sqrt{\pi}}{2\sqrt{\xi}}$$

$$Q = \frac{\sqrt{\pi}}{2\sqrt{\xi}} e^{-\frac{(\zeta'-\zeta)^2}{4\xi}}.$$

Substituting in the φ equation:

$$\varphi = \frac{1}{\pi}\int_{-\infty}^{\infty} f(\zeta')\frac{\sqrt{\pi}}{2\sqrt{\xi}} e^{-\frac{(\zeta'-\zeta)^2}{4\xi}} d\zeta' = \frac{1}{2\sqrt{\pi}\sqrt{\xi}}\int_{-\infty}^{\infty} f(\zeta') e^{-\frac{(\zeta'-\zeta)^2}{4\xi}} d\zeta'$$

$$= \frac{1}{2\sqrt{\pi}\sqrt{\xi}}\left[\int_{-\infty}^{0} f(\zeta') e^{-\frac{(\zeta'-\zeta)^2}{4\xi}} d\zeta' + \int_0^1 f(\zeta') e^{-\frac{(\zeta'-\zeta)^2}{4\xi}} d\zeta'\right.$$

$$\left. + \int_1^\infty f(\zeta') e^{-\frac{(\zeta'-\zeta)^2}{4\xi}} d\zeta'\right].$$

Boundary condition 1 makes the first integral function: $f(\zeta') = 0$.

Boundary condition 2 makes the second integral function: $f(\zeta')=\varphi_2(\zeta')$

Boundary condition 3 makes the third integral function: $f(\zeta') = 1$.

$$\varphi = \frac{1}{2\sqrt{\pi}\sqrt{\xi}}\left[0 + \int_0^1 \varphi_2(\zeta')e^{-\frac{(\zeta'+\zeta)^2}{4\xi}}d\zeta' + \int_0^\infty e^{-\frac{(\zeta'-\zeta)^2}{4\xi}}d\zeta'\right]$$

Let: $\beta^2 = \frac{(\zeta'-\zeta)^2}{4\xi}$ and $\frac{1}{2\sqrt{\xi}} = \eta_p$; so then, $-\beta = \eta_p(\zeta'-\zeta)$.

Finally, boundary conditions 4 and 5 restrict ξ to positive values. Therefore, η_p is real.

Then:

$$\zeta' = \frac{-\beta}{\eta_p} + \zeta: \quad d\zeta' = -\frac{d\beta}{\eta_p}.$$

Further, let $\eta = \zeta\,\eta_p$, so that $\zeta' = \frac{\eta-\beta}{\eta_p}$,

$$\varphi = \frac{\eta_p}{\sqrt{\pi}}\left[\int_\eta^{\eta-\eta_p} \varphi_2\left(\frac{\eta-\beta}{\eta_p}\right)e^{-\beta^2}\left(-\frac{d\beta}{\eta_p}\right) + \int_{\eta-\eta_p}^{-\infty} e^{-\beta^2}\left(-\frac{d\beta}{\eta_p}\right)\right]$$

$$= \frac{1}{\sqrt{\pi}}\left[\int_{\eta-\eta_p}^{\eta} \varphi_2\left(\frac{\eta-\beta}{\eta_p}\right)e^{-\beta^2}d\beta + \int_{-\infty}^{\eta-\eta_p} e^{-\beta^2}d\beta\right].$$

The second integral can be written:

$$\int_{-\infty}^{\eta-\eta_p} e^{-\beta^2}d\beta = \int_{-\infty}^{0} e^{-\beta^2}d\beta + \int_0^{\eta-\eta_p} e^{-\beta^2}d\beta$$

$$= \int_0^\infty e^{-\beta^2}d\beta + \int_0^{\eta-\eta_p} e^{-\beta^2}d\beta$$

$$= \frac{\sqrt{\pi}}{2}\left[\operatorname{erf}\infty + \operatorname{erf}(\eta-\eta_p)\right]$$

$$= \frac{\sqrt{\pi}}{2} [1 + \text{erf } (\eta-\eta_p)].$$

Therefore:

$$\varphi = \frac{1}{2} [1 + \text{erf } (\eta-\eta_p)] + \frac{1}{\sqrt{\pi}} \int_{\eta-\eta_p}^{\eta} \varphi_2(\frac{\eta-\beta}{\eta_p}) e^{-\beta^2} d\beta.$$

This is Equation 7, page 9.

APPENDIX B

THE JET SPREADING PARAMETER σ

Recent Investigations

The jet spreading parameter σ, which is defined in $\eta = \sigma \frac{y}{x}$ as a similarity parameter to obtain the dimensionless velocity profile with transformed coordinate η for jet mixing problems, has been investigated by many scientists based on empirical or semi-empirical formulations. The empirical linear equation, $\sigma = 12 + 2.758M$, suggested by Korst and Tripp (13) has been shown to be good only for some specific regions, that is, for flows up to the neighborhood of Mach number 1.6. Recent experimental data are summarized as follows:

1. Maydew and Reed (7) $\sigma = 11$ for $M < 0.95$
   $\sigma = 15$ for $M = 1.5$
   $\sigma = 20$ for $M = 2.0$
2. Zumwalt (4) $\sigma \cong 30$ for $M = 3.0$
3. Channapragada (11) $\sigma = [\gamma \{1 + \beta (1-C^2)\}]^{-1} \sigma_{incomp.}$
4. Golik (15) $\sigma = \frac{12}{1-\varphi_b} + 2.76 M$ (two-streams)

The results of the first three sources are plotted in Figure 21 for comparison. Zumwalt and the author (16) suggested $\sigma = 47.1 C^2$ for $C^2 > 0.22$, which is based on the best agreement with recent experimental data for the compressible jets discharging into quiescent regions isoenergetically. This simple equation is used in this thesis.

Experimental Evaluation of the Jet Spreading Parameter

A free jet may be thought of as a boundary layer which has been separated from a guiding wall. The velocity profile in the viscous region is well approximated by the results of the theories of Gőrtler and Korst for both subsonic and supersonic jets:

u_a = velocity in the adjacent free stream

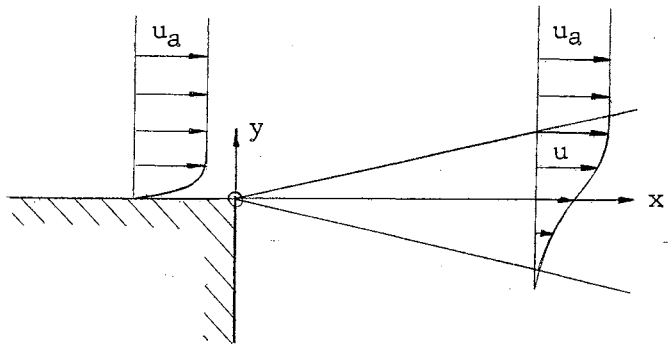

$$\varphi \equiv \frac{u}{u_a} = \frac{1}{2}(1 + \text{erf}\ \eta)$$

$\eta \equiv \sigma \frac{y}{x}$, where σ is the jet-spreading parameter.

$$\text{erf}\ \eta \equiv \frac{2}{\sqrt{\pi}} \int_o^{\eta} e^{-\beta^2} d\beta,$$ the Gaussian error function.

Experimental probing of the jet mixing region will give the velocity at each y'-station for a fixed x-station. This can be plotted thus:

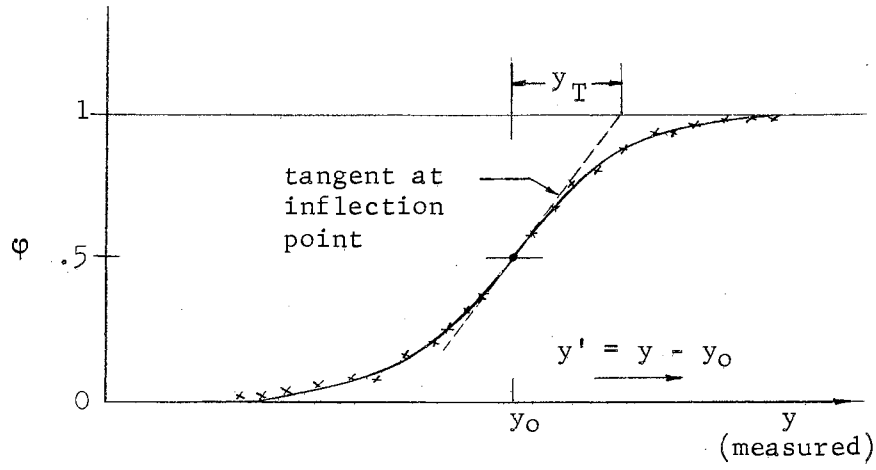

then σ can be found from the slope of the center of the profile:

$$\varphi = \frac{1}{2} + \frac{1}{\sqrt{\pi}} \int_0^{\frac{\sigma y}{x}} e^{-\beta^2} d\beta,$$

$$\frac{d\varphi}{dy} = \frac{1}{\sqrt{\pi}} \frac{\sigma}{x} e^{-\left(\frac{\sigma y}{x}\right)^2},$$

$$\frac{d^2\varphi}{dy^2} = \frac{-2y}{\sqrt{\pi}} \frac{\sigma^3}{x^3} e^{-\left(\frac{\sigma y}{x}\right)^2}.$$

For the inflection point, $\frac{d^2\varphi}{dy^2} = 0$, $\therefore y = 0$ is the inflection point.

$$\left.\frac{d\varphi}{dy}\right|_{y=0} = \frac{1}{\sqrt{\pi}} \frac{\sigma}{x},$$

$$\sigma = x\sqrt{\pi} \left.\frac{d\varphi}{dy}\right|_{y=0} = x\sqrt{\pi} \frac{\frac{1}{2}}{y_T} = \frac{x}{y_T} \frac{\sqrt{\pi}}{2}.$$

But, the determination of a tangent-slope from a plot is very inaccurate.

To determine σ more accurately and more easily, one may do as is done in turbulent boundary layer profile determination: plot on special paper. That is, for a boundary layer

$$\varphi \equiv \left(\frac{u}{u_a}\right) \cong \left(\frac{y}{\delta}\right)^{\frac{1}{n}}$$

$$\ell n \varphi = \frac{1}{n} \ell n \frac{y}{\delta}.$$

Plotting this on log-log paper gives a straight line with a slope of $\frac{1}{n}$.

Similarly, for $\varphi \cong \frac{1}{2}(1 + \text{erf}\eta)$, use of Gaussian Probability paper which will make the profile become a straight line if it follows this relationship. Then σ can be determined for $\eta = 1$ or $\eta = -1$.

For $\eta = 1$, $\varphi = 0.92135$; $\sigma = \left.\frac{x}{y'}\right|_{n=1}$

For $\eta = -1$, $\varphi = 0.07865$; $\sigma = \left.\frac{x}{-y'}\right|_{n=-1}$

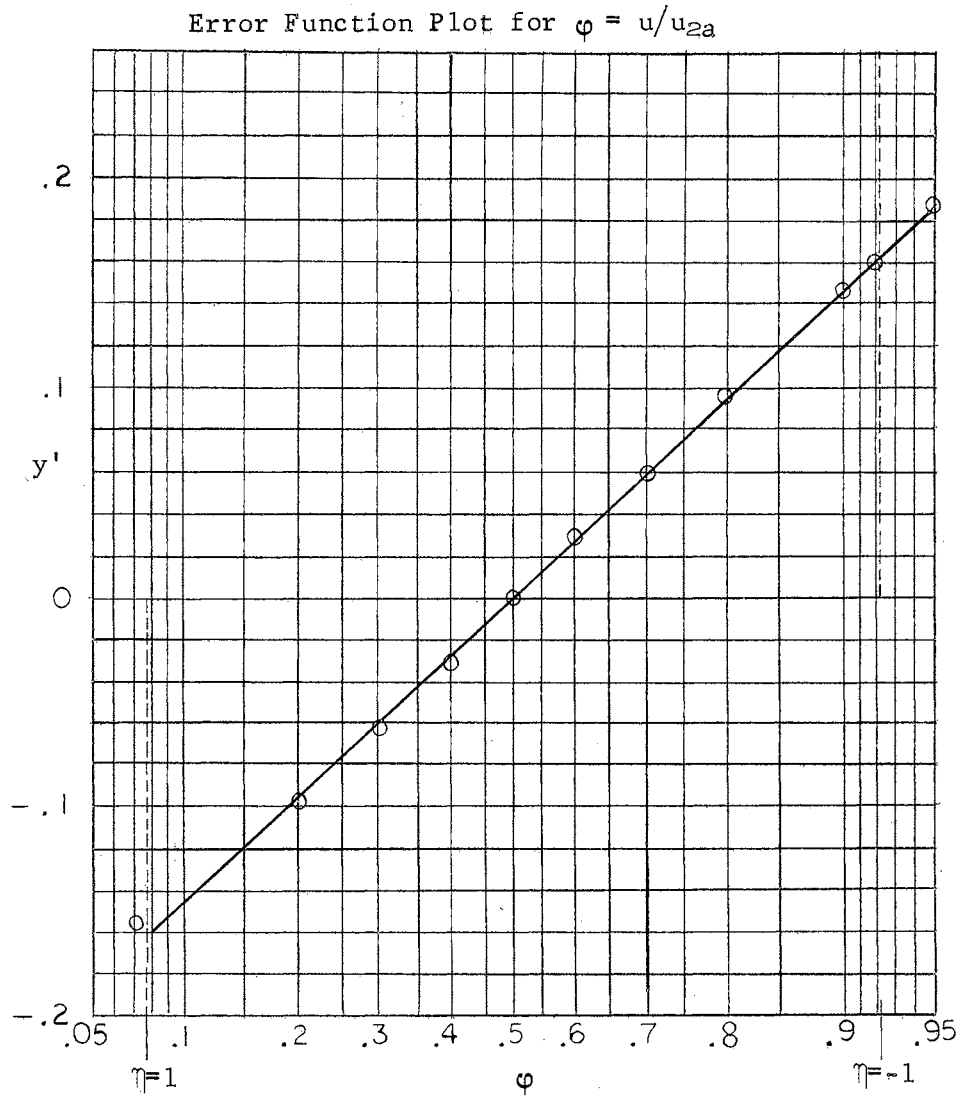

APPENDIX C

STEADY NON-BLEED AXI-SYMMETRIC BASE PRESSURE CALCULATION

For a given uniform M_1 flowing steadily near the end of a cylinder, the calculation for the pressure on the base of the cylinder is as follows. Picking a typical value of θ_{1-2}, one locates a proper $\bar{R}/R$ position by the trial and error method below. (Model is shown in Figure 2.)

1. M_{2a} or C_{2a} can be obtained when M_1 and θ_{1-2} are given by using Prandtl-Meyer expansion relations locally at the cylinder end.

2. Assume an $\bar{R}/R$ value, then Equation 11 based on conical after-body characteristic solutions yields M_{3a} or C_{3a} as

$$M_{3a} = \frac{M_{2a}}{e^{0.209(1-\bar{R}/R)}} .$$

Hence, for each assumed $\bar{R}/R$ value, M_{3a} can be obtained. Note that $C_{3a}^2 = M_{3a}^2 /(5 + M_{3a}^2)$ for air at moderate temperatures.

3. Calculate $\left[\frac{\bar{R}\,\sigma}{x\cos\theta}\right]_{3a}^2$:

a. Let $\theta_{3-4} = \theta_{1-2}$ (conical wake assumption)

b. $\sigma \cong 47.1\, C_{3a}^2$ by Equation 12

c. $$\left[\frac{\bar{R}\,\sigma}{x\cos\theta}\right]_{3a}^2 = \left[\frac{\sigma\tan\theta_{3-4}}{\frac{1}{\bar{R}/R} - 1}\right]_{3a}^2$$

4. Values of $\left[\frac{\bar{R}\,\sigma}{x\cos\theta}\right]_{3a}^2$, C_3^2, and C_{3a}/C_{2a} will allow one to find φ_j from Figures 3 to 8.

5. Since non-bleed wake prevails for steady flow, $\varphi_d = \varphi_j$, and $C_d = \varphi_d C_{3a}$.

6. But also, $C_d = \left[1 - \frac{1}{\left(\frac{p_4}{p_3}\right)^{\frac{k-1}{k}}}\right]^{\frac{1}{2}}$, since $p_{o_{3d}} = p_4$

where p_4/p_3 is the pressure ratio across an oblique shock of a stream flowing with velocity M_{3a} deflected through an angle θ_{3-4}.

If, for air, $\varphi_d C_{3a} \neq \left[1 - \frac{1}{\frac{p_4}{p_3}^{0.286}}\right]^{\frac{1}{2}}$, respect calculations from step 2.

7. With correct $\bar{R}/R$, M_{2a}, and θ_{1-2} values, p_b/p_1 at a specific position $\bar{R}/R$ can be obtained by the isentropic flow relation as:

$$\frac{p_b}{p_1} = \frac{p_2}{p_1} = \frac{\frac{p_2}{p_{o_2}} \Big| f(M_2)}{\frac{p_1}{p_{o_1}} \Big| f(M_1)} .$$

The base pressure is now known for a particular $\bar{R}/R$. A curve results similar to Figure 22.

Zumwalt's conical pressure rise analysis has been used to calculate the steady base pressures for Mach numbers 1.5, 2, 3, 4, and 5. The first three results check well with available experimental data (1), (16) (17). Results are plotted in Figure 22. The nearly constant value of p_b/p_1 in the region of small $\bar{R}/R$ values is the base pressure for a blunt base at M_1. Fortunately, they result in a simple empirical formula as

$$\frac{p_b}{p_1} = 0.906 - \ell n \sqrt{M_1} \qquad [21]$$

for $1.2 \leq M_1 \leq 5$. (See Figure 23.)

Evidently, this formula cannot be used when $M_1 > 5$. It is suggested to

obtain data for high Mach numbers so that an equation can be employed to form another simple relation which is valid in the region of hypersonic flows. Until this is done, an estimated value is shown for this region in Figure 23.

APPENDIX D

EVALUATION OF EFFECTIVE PUMPING SURFACE AS A FUNCTION OF DIMENSIONLESS BLEED NUMBER $\mathcal{K}$

Knowing p_b/p_1 versus $\mathcal{K}$ for a given Mach number M_1, one can proceed using the following outline to obtain $\bar{R}/R$ versus $\mathcal{K}$. (Arrow means "yields.")

1. $M_1 \rightarrow \nu_1$; also p_1/p_o.
2. Choose any $\mathcal{K}$, from the $\mathcal{K}$ curves (Figure 18)

$$\mathcal{K} \rightarrow \frac{p_b}{p_1} \rightarrow \frac{p_2}{p_o} \rightarrow \nu_{2a} \rightarrow \theta = (\nu_{2a} - \nu_1).$$
$$\searrow M_{2a},\ C_{2a}$$

3. Iterate $\bar{R}/R$, such that the $\mathcal{K}$ value calculated agrees with the $\mathcal{K}$ chosen at step 2.

The method to calculate $\mathcal{K}$ is outlined as follows:

$$\left.\begin{matrix} M_{2a} \\ \bar{R}/R \end{matrix}\right\} \rightarrow M_{3a} = e^{-0.209(1-\bar{R}/R)} M_{2a} \text{ by Equation 11}$$

$M_{3a} \rightarrow \mathbb{K}$ from Figure 24

$$M_{3a} \rightarrow C_{3a}^2 = \frac{M_{3a}^2}{5 + M_{3a}^2} \text{ for air.}$$

$$C_{3a}^2 \rightarrow \sigma_{3a} = 47.1\ C_{3a}^2 \text{ by Equation 12.}$$

$$\text{Calculate } \left[\frac{\sigma \tan\theta}{\frac{1}{\bar{R}/R} - 1}\right]^2 = \left[\frac{\sigma\ \bar{R}}{x\cos\theta}\right]^2$$

C_{3a}^2, $\frac{C_{3a}}{C_{2a}}$, and $\left[\frac{\sigma \tilde{R}}{x\cos\Theta}\right]^2 \rightarrow \varphi_j$ and B from Figures 3 to 15.

$\left.\begin{matrix}\varphi_j \\ C_{3a}^2\end{matrix}\right\} \rightarrow I_{1j}$ and J_{1j} from Figures 25 and 26.

$\left.\begin{matrix}M_{3a} \\ \Theta\end{matrix}\right\} \rightarrow \frac{p_4}{p_3}$ oblique shock chart

$\left.\begin{matrix}\frac{p_4}{p_3}\end{matrix}\right\} \rightarrow C_d^2 = 1 - \frac{1}{\left(\frac{p_4}{p_3}\right)^{0.286}}$

$\left.\begin{matrix}C_d \\ C_{3a}\end{matrix}\right\} \rightarrow \varphi_d = \frac{C_d}{C_{3a}}$

$\left.\begin{matrix}\varphi_d \\ C_{3a}^2\end{matrix}\right\} \rightarrow I_{1d}$ and J_{1d} from Figures 25 and 26.

Finally, $\mathcal{K} = -1.088 \frac{G_d\sqrt{T_o}}{P_o A_b}$

$$= -\frac{1.088\,\mathbb{K}}{\sigma_{3a}^2}\frac{\cot\Theta}{\sin\Theta}\left(1-\frac{\tilde{R}}{R}\right)^2\left[(J_{1d}-J_{1j})-B(I_{1d}-I_{1j})\right]$$

by Equation 16.

When $\mathcal{K}$ values from steps 2 and 3 agree, this is the solution.

APPENDIX E

This appendix serves as an example of the calculation method used to predict pressures on a high-velocity sharp-pointed cone before and immediately after it passes through a blast wave. The cone has zero yaw angle both before and after the blast intersection.

Referring to Figure 27, a cone is considered which has a plane base surface. The base pressure is determined by the upstream conditions, M_∞, p_∞, and θ_c (semi-cone angle). It has been assumed that a small cylindrical surface exists with an infinitesimal length, ΔL, in the limit, such that the flow will induce a conical shock and double Prandtl-Meyer expansions before it forms a free jet mixing layer in the base region. This imaginary infinitesimal flat surface technique employs the same concept as the "equivalent parallel flow" technique used by Korst (19).

For steady, non-bleed flow, Equation 21 gives p_b/p_1 value versus M_1, but only up to $M_1 = 5$, due to the lack of test data and information on jet spreading parameter values for hypersonic flows. Hence, for the time being, a curve (see Figure 23) has been extrapolated to $M_1 = 25$ on a log plot as well as possible. It can be seen that the error is insignificant since Newtonian-type flow appears for such high velocity, and the base pressure becomes practically zero.

For a small semi-apex angle cone, the boundary layer interaction and real-gas effects can be ignored. Values assumed to be known are: flight Mach number, M_∞; altitude; cone semi-apex angle, θ_c; base area,

A_b; and blast over-pressure, Δp_{max}.

Condition x: before intersecting the blast wave.

free stream conditions;

1. Altitude $\rightarrow p_{\infty x}$, $T_{\infty x}$, $a_{\infty x}$, $u_{\infty x} = M_{\infty x} a_{\infty x}$.

2. $$p_{o\infty x} = \frac{p_{\infty x}}{\left.\frac{p_{\infty x}}{p_{o\infty x}}\right|_{M_{\infty x}}} .$$

conditions behind the nose shock;

3. $$\left.\begin{matrix} M_{\infty x} \\ \theta_c \end{matrix}\right\} \left(\begin{matrix}\text{conical} \\ \text{shock}\end{matrix}\right) \rightarrow \theta_{wx} \rightarrow M_{\infty x} \sin\theta_{wx} \left(\begin{matrix}\text{normal} \\ \text{shock}\end{matrix}\right) \rightarrow \frac{p_{ocx}}{p_{o\infty x}} \rightarrow p_{ocx} .$$

4. $$\left.\begin{matrix} M_{\infty x} \\ \theta_c \end{matrix}\right\} \left(\begin{matrix}\text{conical} \\ \text{shock}\end{matrix}\right) \rightarrow p_{cx} = p_{\infty x}\left(1 + \frac{k}{2} M_{\infty x}^2 C_{px}\right)$$

C_{px} from p. 50, NACA Report 1135 (20).

5. $$\frac{p_{cx}}{p_{ocx}} \left(\begin{matrix}\text{isen.} \\ \text{rel.}\end{matrix}\right) \rightarrow M_{cx} \rightarrow \nu_{cx}.$$

conditions on the cylindrical section;

6. $$\nu_{1x} = (\nu_{cx} + \theta_c) \rightarrow M_{1x} \left(\begin{matrix}\text{isen.} \\ \text{rel.}\end{matrix}\right) \rightarrow \frac{p_{1x}}{p_{ocx}} \rightarrow p_{1x}.$$

base flow conditions;

7. $$M_{1x} \text{-(Fig. 23)} \rightarrow \frac{p_{bx}}{p_{1x}} \rightarrow p_{bx}.$$

8. $$\frac{p_{bx}}{p_{ocx}} \left(\begin{matrix}\text{P.M.} \\ \text{turn}\end{matrix}\right) \rightarrow \nu_{2x} \rightarrow \theta_{2x} = (\nu_{2x} - \nu_{1x}) \rightarrow \tan\theta_{2x}.$$

Condition y: immediately after passing through the blast wave.

free stream conditions:

1. $p_{\infty y} = p_{\infty x} + \Delta p_{max}$.

2. $\frac{p_{\infty y}}{p_{\infty x}} \rightarrow u_{sh} = a_{\infty x}\sqrt{\frac{1}{7}\left(6\frac{p_{\infty y}}{p_{\infty x}} + 1\right)} \equiv$ (velocity of the blast wave).

3. $\frac{p_{\infty y}}{p_{\infty x}} \rightarrow \left(\begin{matrix}\text{normal}\\ \text{shock}\end{matrix}\right) \rightarrow M'_y \rightarrow \frac{p_{\infty y}}{p'_{o\infty y}} \rightarrow p'_{o\infty y}$.

4. $\frac{p_{\infty y}}{p_{\infty x}} \rightarrow \left(\begin{matrix}\text{normal}\\ \text{shock}\end{matrix}\right) \rightarrow \frac{T_{\infty y}}{T_{\infty x}} = \left(\frac{a_{\infty y}}{a_{\infty x}}\right)^2 \rightarrow a_{\infty y}$ and $T_{\infty y}$.

5. $u'_y = M'_y\, a_{\infty y}$ (velocity of atmosphere behind the blast wave, relative to the blast wave)

6. $u_{\infty y} = u_{\infty x} + u_{sh} - u'_y$ (velocity of atmosphere behind the blast wave, relative to the missile)

7. $\frac{u_{\infty y}}{a_{\infty y}} = M_{\infty y} \rightarrow \left(\begin{matrix}\text{isen.}\\ \text{rel.}\end{matrix}\right) \rightarrow \frac{p_{\infty y}}{p_{o\infty y}}$; $p_{o\infty y} = \left.\frac{p_{\infty y}}{\frac{p_{\infty y}}{p_{o\infty y}}}\right|_{M_{\infty y}}$

$\rightarrow \frac{T_{\infty y}}{T_{o\infty y}}$; $T_{o\infty y} = \left.\frac{T_{\infty y}}{\left(T_{\infty y}/T_{o\infty y}\right)}\right|_{M_{\infty y}}$

conditions behind the nose shock:

8. $\left.\begin{matrix}M_{\infty y}\\ \theta_c\end{matrix}\right\} \rightarrow \left(\begin{matrix}\text{conical}\\ \text{shock}\end{matrix}\right) \rightarrow \theta_{wy} \rightarrow M_{\infty y}\sin\theta_{wy} \rightarrow \left(\begin{matrix}\text{normal}\\ \text{shock}\end{matrix}\right) \rightarrow \frac{p_{ocy}}{p_{o\infty y}} \rightarrow p_{ocy}$

9. $\left.\begin{matrix}M_{\infty y}\\ \theta_c\end{matrix}\right\} \rightarrow \left(\begin{matrix}\text{conical}\\ \text{shock}\end{matrix}\right) \rightarrow p_{cy}$.

10. $\frac{p_{cy}}{p_{ocy}} \rightarrow \begin{pmatrix} \text{isen.} \\ \text{rel.} \end{pmatrix} \rightarrow M_{cy} \rightarrow \nu_{cy}$,

conditions on the cylindrical section:

11. $\nu_{1y} = (\nu_{cy} + \theta_c) \rightarrow M_{1y} \rightarrow \begin{pmatrix} \text{isen.} \\ \text{rel.} \end{pmatrix} \rightarrow \frac{p_{1y}}{p_{ocy}} \rightarrow p_{1y}$.

12. $M_{1y} \xrightarrow{\text{(Figure 23)}} \frac{p_{by}}{p_{1y}} \rightarrow p_{bys}$ (stable).

This is the steady-state base pressure which would result from a steady application of $M_{\infty y}$ and $p_{\infty y}$. The actual base pressure, p_{by}, immediately after the blast wave passage, would asymptotically approach this value if $M_{\infty y}$ and $p_{\infty y}$ were maintained constant, i.e., the blast wave were a step function.

13. To find p_{by}, assume θ_{2y}.

$$\nu_{2y} = (\nu_{1y} + \theta_{2y}) \rightarrow \begin{pmatrix} \text{P.M.} \\ \text{turn} \end{pmatrix} \rightarrow \frac{p_{2y}}{p_{ocy}} \rightarrow p_{2y}$$

For adiabatic compression of the air trapped behind the base,

$$\tan\theta_{2y} \rightarrow p_{bx}\left(\frac{\tan\theta_{2y}}{\tan\theta_{2x}}\right)^k = p_{by}.$$

If $p_{2y} \neq p_{by}$, choose a new θ_{2y}, until $p_{2y} = p_{by}$.

14. M_{1y} and $\frac{p_{by}}{p_{1y}} \rightarrow \mathcal{K}$ from Figure 18.

15. The rate of mass being added to the base region at $t = 0^+$ (y condition) is

$$\dot{m} = -\mathcal{K}\frac{p_{ocy}A_b}{\sqrt{\frac{\mathcal{R}}{gk}T_{o\infty y}}} = -\mathcal{K}\frac{p_{ocy}A_b}{1.088\sqrt{T_{o\infty y}}} \quad .$$

16. The mass contained in the base region, i.e., the dead air mass, is

$$m_{by} = (\rho V)_{by} = \frac{p_{by}}{\mathcal{R}\,T_{o\infty y}}\left(\frac{1}{3}\pi R^2 \ell\right) = \frac{\pi R^3}{3\mathcal{R}}\,\frac{p_{by}}{T_{o\infty y}\tan\Theta_{2y}}$$

For a time later than y, due to the base region mass addition and the blast wave decay, conditions at time t can be calculated from the conditions at the previous time, t-Δt.

1. $(m_b)_t = (m_b)_{t-\Delta t} + \dot{m}\Delta t$

$$= \frac{\pi R^3}{3\mathcal{R}}\left(\frac{p_b}{T_{o\infty}\tan\Theta_2}\right)_{t-\Delta t} - \left(\mathcal{K}\frac{p_{oc}}{\sqrt{T_{o\infty}}1.088}\right)_{t-\Delta t} A_b\Delta t$$

2. $p'_{\infty t} = p_{\infty x} + \Delta p_t = p_{\infty t}$

where $\Delta p_t = \Delta p_{max}\left(1 + \frac{t}{t^+}\right)e^{t/t^+}$

$\frac{p'_{\infty t}}{p'_{o\infty t}} \rightarrow M'_{\infty t}$; note that $p'_{o\infty t} = p'_{o\infty y}$.

3. $a_{\infty t} = a_{\infty y}\left(\frac{p_{\infty t}}{p'_{\infty y}}\right)^{\frac{k-1}{2k}}$

4. $u'_{\infty t} = a_{\infty t}M'_{\infty t}$ since $a'_{\infty t} = a_{\infty t}$.

5. $u_{\infty t} = u_{\infty x} + u_{sh} - u'_{\infty t}$

6. $\frac{u_{\infty t}}{a_{\infty t}} = M_{\infty t}$.

Knowing $M_{\infty t}$, one can follow steps 7 to 12 as for condition "y" (all notations are the same except subscript t replaces y) to obtain the p_{bs} value. The base pressure can be obtained from Equation 20 by iterating θ_2 such that p_2, obtained by Prandtl-Meyer relation, agrees with p_b by Equation 20.

If desired, instantaneous values of stagnation pressure and temperature can also be obtained from knowledge of $M_{\infty t}$, $p_{\infty t} = p'_{\infty t}$, and

$$T_{\infty t} = T_{\infty y}\left(\frac{p_{\infty t}}{p_{\infty y}}\right)^{\frac{k-1}{k}} .$$

APPENDIX F

The assumption of isoenergetic jet mixing during the transient phase following the passing of a blast wave needs to be justified (p.31). The term "isoenergetic" means that the temperature of the base region gas equals the entraining free stream stagnation temperature. This has been shown to be so in Reference 19 for steady flows. In case of blast wave interaction, the free stream conditions immediately after the wave front are those resulting from a plane moving shock, while the fluid in the base region undergoes a sudden adiabatic compression; thus, different temperature changes are possible.

In Reference 21, several cases of M_∞, Δp_{max} and altitude combination have been evaluated, some typical results are listed below:

M_∞	2	2	2	2	2	5	5	5
alti.	5,000'	10,000'	20,000'	20,000'	20,000'	20,000'	20,000'	20,000'
Δp_{max}	3	15	3	5	8	3	8	15
T_{oa}	1063	1345	961	1050	1170	2900	3365	3800
T_b	929	980	843	874	886	2970	3350	3770
T_{oa}/T_b	1.145	1.372	1.140	1.200	1.320	0.977	1.004	1.006

It has been shown in Reference 19 that the steady base pressure solution is almost independent of T_{oa}/T_b until the temperature ratio is greater than 2. Since in the above listed cases, which represent a considerable range of likely conditions, the T_{oa}/T_b ratios are lower

than 2, it is permissible to use an isoenergetic jet mixing assumption for the present analysis.

VITA

Homer Ho Tang

Candidate for the Degree of

Doctor of Philosophy

Thesis: ANALYTICAL AND EXPERIMENTAL STUDY OF THE TRANSIENT BASE PRESSURES RESULTING WHEN AN AXI-SYMMETRIC SUPERSONIC MISSILE FLIES HEAD-ON THROUGH A BLAST WAVE

Major Field: Mechanical Engineering (Aerospace)

Biographical:

Personal Data: Born in Swatow, Kwangtung, China, April 4, 1934, the son of Jen and Shuh-Teh Tang; Admitted as immigrant in the United States on September 5, 1963.

Education: Attended public school in Kwangtung, China; graduated from Taiwan Provincial Pingtung High School, China, 1952; received the Bachelor of Science Degree in Mechanical Engineering in 1956 from Taiwan Provincial Cheng-Kung University; received the Master of Science Degree in 1961 from the Oklahoma State University; completed requirements for the Doctor of Philosophy Degree at Oklahoma State University in October, 1963.

Professional Experience: Served two years as a Second Lieutenant with the Chinese Air Force, 1956-58; employed as Junior Engineer at Taiwan Power Company, 1959-60; worked as Graduate Assistant and Instructor at Oklahoma State University, 1960-1963.

Professional Organizations: The author is a member of Phi Kappa Phi, Pi Mu Epsilon and AIAA.